METAL-OXIDE THIN FILMS DEPOSITED FROM AQUEOUS SOLUTIONS: THE ROLE OF CATION/WATER INTERACTIONS

by

PAUL N. PLASSMEYER

A DISSERTATION

Presented to the Department of Chemistry and Biochemistry
and the Graduate School of the University of Oregon
in partial fulfillment of the requirements
for the degree of
Doctor of Philosophy

December 2016

DISSERTATION APPROVAL PAGE

Student: Paul N. Plassmeyer

Title: Metal-Oxide Thin Films Deposited from Aqueous Solutions: The Role of Cation/Water Interactions

This dissertation has been accepted and approved in partial fulfillment of the requirements for the Doctor of Philosophy degree in the Department of Chemistry and Biochemistry by:

Mark C. Lonergan	Chairperson
Catherine J. Page	Advisor
Shannon W. Boettcher	Core Member
Richard P. Taylor	Institutional Representative

and

Scott L. Pratt	Dean of the Graduate School

Original approval signatures are on file with the University of Oregon Graduate School.

Degree awarded December 2016

DISSERTATION ABSTRACT

Paul N. Plassmeyer

Doctor of Philosophy

Department of Chemistry and Biochemistry

December 2016

Title: Metal-Oxide Thin Films Deposited from Aqueous Solutions: The Role of Cation/Water Interactions

Metal-oxide thin films are used in a wide variety of electronic devices. Although many techniques have been developed to deposit thin films of metal oxides, a need for alternative cost- and energy-effective deposition methods exists. Deposition of metal oxide thin films from aqueous solutions of all-inorganic metal salts provides a method that meets these needs. Although many aqueous-deposited metal-oxide thin films have been successfully incorporated into functioning devices, the mechanisms that occur as precursors transition to metal oxides are not well understood.

The work presented in this dissertation is primarily concerned with examining the processes that occur as metal oxide thin films form from spin-deposited aqueous precursor solutions with a particular focus on the role of H_2O in these processes. Chapter I summarizes methods for thin film deposition, and describes the use of aqueous metal salt solutions as precursors for the deposition of metal oxide thin films. Chapter II investigates the precursor chemistry, film-formation processes and properties of $LaAlO_3$ thin films deposited from aqueous precursors. This chapter also serves as general guide to the processes that occur as metal-oxide thin films form from aqueous precursors. Chapters III and IV focus on the effects of $H_2O(g)$ during spin-deposition of precursor thin films and

during the annealing process in which precursors are converted to metal oxides, respectively. The presence of $H_2O(g)$ during spin-deposition has a striking effect on the thickness of the thin films and affects the elemental gradient and density profiles. During annealing, $H_2O(g)$ reduces the temperatures at which counterions are expelled and influences the metal-hydroxide framework formation and its condensation to a metal oxide. The data also indicate that $H_2O(g)$ enhances diffusion of gaseous byproducts from within the films. Chapter V focuses on precursor concentration and its impact on the thermal evolution of thin films. The processes involved in the conversion of precursors to metal oxide thin films occur at lower temperatures as precursor concentration decreases. Although partially due to thickness effects, concentration-dependent precursor speciation may also be involved in lowering the film densification temperatures.

This dissertation includes previously published and unpublished coauthored material.

CURRICULUM VITAE

NAME OF AUTHOR: Paul N. Plassmeyer

GRADUATE AND UNDERGRADUATE SCHOOLS ATTENDED:

University of Oregon, Eugene, OR
Colorado State University, Fort Collins, CO
University of Northern Colorado, Greeley, CO

DEGREES AWARDED:

Doctor of Philosophy, Chemistry, 2016, University of Oregon
Bachelor of Science, Chemistry, 2007, Colorado State University

AREAS OF SPECIAL INTEREST:

Materials Chemistry
Inorganic Chemistry

PROFESSIONAL EXPERIENCE:

Research Assistant, Page Research Group, University of Oregon 2011-2016. Research in materials chemistry focused on studying the formation of thin-film metal oxides from precursors spin-deposited from aqueous solutions.

Research Scientist, Eltron Research and Development, 2008-2010. Research in thermoelectrics, conversion of diesel fuel to synthesis gas, and zeolite gas-separation membranes.

PUBLICATIONS:

Richter, P.; Plassmeyer, P. N.; Harzdorf, H.; Ruffer, T.; Lang, H.; Kalbacova, J.; Johrmann, N.; Schulze, S.; Hietschold, M.; Arekapudi, S. S. P. K.; Albrecht, M.; Zahn, D. R. T.; Page, C. J.; Salvan, G. High Quality Magnetic Oxide Thin Films Prepared

Norelli, K. M.; Plassmeyer, P. N.; Woods, K. N.; Glassy, B. A.; Knutson, C. C.; Beekamn, M.; Page, C. J. Influence of composition and processing parameters on the properties of solution-deposited aluminum phosphate oxide (AlPO) thin films. Solid State

Plassmeyer, P. N.; Archila, K.; Wager, J. F.; Page, C. J. Lanthanum Aluminum Oxide Thin-Film Dielectrics from Aqueous Solution. ACS Appl. Mater. Interfaces. 2015, 7, 1678-1684.

Wiedle, R. A.; Warner, M.; Tate, J.; Plassmeyer, P. N.; Page C. J. Thermal conductivity of thin-film Al-P-O on silicon. Thin Solid Films, 2013, 548, 225-229.

ACKNOWLEDGMENTS

I wish to express my appreciation for the Center for Sustainable Materials Chemistry (CSMC) which was funded through the National Science Foundation (CCI CHE-1102637). The CSMC provided funding for my research and facilitated the many collaborations that I've had the honor to be a part of. I thank the staff of CAMCOR, especially Stephen Gollege, Kurt Langworthy Steve Wiemholt, for their help with various instruments. I also thank the Technical Science Administration's machine shop and Kris Johnson and John Boosinger in particular.

I wish to express my thanks to the many collaborators and colleagues that I've worked with over the years. In particular, I'd like to thank my lab-mates: Keenan Woods and Devin McBain; and my collaborators: Hans Chiang, Kevin Archila, Deok-Hie Park, Gavin Mitchson, Peter Richter, Blake Hammann, Susannah Wood and Donald Clayton. Thanks for listening to my input and offering your input on the many projects that we've worked on together. Also, to those that have created a generally engaging environment: Adam Smith, Andy Ritenour, Fuding Lin, Lena Trotochaud, Annie Greenaway and many others. I'll miss the unique blend of personalities that resulted in so many philosophical and scientific discussions and arguments. Also, I'd like to thank Matt Kast for taking the time to help me think through my often intuitive leaps and for frequently delving into the realm of pure speculation with me.

I'd also like to express my gratitude to my committee who helped me develop as a scientist. Specifically, I thank my advisor Dr. Catherine Page, for taking me as her first graduate student in several years and honing my presentation skills.

I’d like to express my gratitude to my parents. Mom, you nurtured my scientific curiosity from an early age through your general interests in subjects like astronomy, geology and meteorology (you were always so concerned with the weather…). Dad, you nurtured my philosophical and analytical sides, both were essential for my development as a scientist.

Lastly, I’d like to thank my wife Amanda and daughter Elise. You’ve kept me happy and put up with a lot over the last few years.

To my friends and family

TABLE OF CONTENTS

Chapter Page

LIST OF FIGURES

Figure Page

Figure Page

LIST OF SCHEMES

Scheme Page

CHAPTER I

INTRODUCTION

The work presented in this thesis is focused on the deposition of metal-oxide thin films from aqueous precursor solutions. Particular emphasis is placed on understanding the impacts of precursor composition, concentration, spin deposition conditions, and subsequent annealing parameters (temperature ramp parameters and atmosphere) on the chemistry and densification that occur as the spin cast precursor solutions convert to metal oxide thin films. The impacts of these processing parameters on the properties of the resulting metal-oxide thin films are also investigated and correlated with the film chemistry, density and morphology. Although most of the work reported herein is focused on insulators, the processes discussed in the majority of this work, especially in chapters III, IV and V, are likely generally applicable to all metal-oxide thin films deposited from aqueous solutions.

Metal Oxides: Properties and Applications

Metal oxides have a wide variety of properties that make them useful in numerous electronic devices. Metal oxides continue to play important roles in the development of computers and many of the portable electronic devices and display technologies that have become ubiquitous over the last two decades rely heavily on metal-oxide components.

Metal oxides span the entire spectrum of electronic conductivity. Insulating metal oxides are commonly employed as the gate dielectrics in transistors and the dielectrics in capacitors found in integrated circuits.[1–5] They are also used in more exotic electronic

components such as resistive switches, memristors and charge-trapping memory devices.[4,6–13] Semiconducting metal oxides are used for transistors and photovoltaics.[14–18] Some high bandgap metal oxides can be heavily doped to yield highly conductive and transparent materials known as transparent conductive oxides (TCOs).[19–22] In 1986 a new class of ternary copper oxide high temperature superconductors was discovered which opened new interest in metal oxide research.[23]

Metal oxides can also support ionic conductivity and display redox chemistry. Lithium (and other mobile cations) can be reversibly incorporated into various redox-active metal oxides making them ideal cathode materials for secondary lithium batteries.[24–27] Other, redox-inactive metal oxides can achieve high lithium conductivities.[25,28,29] Such versatile properties allow for potentially all-solid-state metal-oxide batteries. Metal oxides also serve as oxygen-ion conductors and cathode materials in solid-oxide fuel cells.[30–32] Redox-active metal oxides can also be used as electrochromic materials in 'smart' windows if they have a significant light-absorption difference between oxidized and reduced states.[33–35]

Finally, transition metal and rare-earth oxides also commonly display magnetic properties. Transition metal oxides have been used to store memory magnetically.[36] Metal-oxide thin film laminates that display giant magento-resistance can be used to read magnetically stored memory.[37,38] Magnetic oxides have also been used in spintronic devices which could allow for spin-aligned electron currents.[39–41] Such devices have the potential to increase the power and speed of many electronic devices.

Deposition of Metal-Oxide Thin Films

In most of the applications mentioned above, the metal oxides are implemented in thin-film form, generally as one layer in a multilayered device. Many deposition techniques have been developed to meet the various challenges presented by the layered architectures and the interactions between adjacent layers in these devices. These deposition techniques can generally be fit to one of two categories: vapor-phase deposition and solution-phase deposition.

In vapor-phase deposition, gaseous precursors are used to deposit thin films on a substrate. These deposition techniques typically require expensive and complex tools, low pressures, specialized gases and unique precursor materials. In physical vapor deposition, precursor materials are thermally evaporated under low pressures and are ballistically transported to the substrate.[42,43] Pulsed laser deposition and sputtering are similar, but reactive gasses (such as O_2) can be present in the deposition chamber to control oxygen stoichiometry in the resulting metal-oxide thin film.[44–48] Chemical vapor deposition (CVD) methods transport vapor phase precursors to the substrate where they decompose to the desired material. These techniques can be used to deposit epitaxial, heteroepitaxial and amorphous thin film metal-oxides.[34,49–52] Furthermore, CVD growth allows for minimal defects between substrate and film in epitaxial cases, and can be used to deposit continuous films on somewhat complex substrate architectures.[53,54] A related technique, atomic layer deposition (ALD), uses similar principles, but the deposition process is more complex. Using alternating pulses of different reactants which deposit via a self-limiting reaction, ALD allows for deposition of metal-oxide thin films on extremely complex architectures.[55–58] In general, vapor deposition techniques have been

successfully used for incorporating metal-oxide thin films in a wide variety of devices. While these techniques generally produce high-quality films, there is a need for methods that are less costly, less equipment-intensive, more amenable to compositional tuning and compatible towards integration with other components.

Solution-phase deposition provides a simpler way to deposit relatively large area metal oxide films that are dense, uniform and nearly atomically flat. Equipment and precursors needed for solution deposition are relatively modest and inexpensive. Two common methods for solution-phase deposition are described below.

Solution-Phase Metal-Oxide Thin Film Precursors

Solution-phase deposition of thin films generally relies upon the application (via spray deposition or spin-coating) of a precursor solution to a substrate with subsequent heating to transform the precursor to a metal oxide. Perhaps the most common method for solution-phase deposition is sol-gel synthesis. This synthetic route commonly relies on precursor solutions containing metal alkoxide complexes dissolved in an organic solvent. An alternative method, which is the basis for the work presented in this thesis, involves the use of aqueous solutions of simple inorganic metal salts or clusters. Although both types of precursor solutions have been used to prepare high quality metal-oxide thin films, they differ substantially in reactivity, toxicity and in the chemistry of film formation.

In the traditional sol-gel route, metal alkoxide precursors are employed, which are highly reactive towards water. Controlled addition of water, acid or base to metal alkoxides dissolved in organic solvents causes hydrolysis and condensation of metals to

colloidal ‘sols’.[59–62] Alternatively, sol-gel precursors sometimes contain stable metal salts (e.g. acetates) dissolved in organic solvents, often methoxyethanol.[59,63,64] Additional chelating agents are added to aid in establishing a homogeneous precursor solution.[59,65,66] Although some pre-condensation of metal centers is achieved in these methods, the use of organic ligands, chelating agents and organic solvents can be difficult to effectively remove to form fully dense metal oxide films upon heating. Any trapped organic material manifests as residual carbon contaminants within the resulting thin films.[59,60,62]

Precursors consisting of simple metal salts with inorganic counterions dissolved in water can also be manipulated to form oligomeric structures or discrete clusters in solution. For a variety of metal nitrates (Al^{3+}, Ga^{3+}, In^{3+}, Sc^{3+}, Y^{3+} and many of the lanthanides), increasing pH towards solubility limit induces oligomerization and cluster formation (Figure 1.1).[22,67–76] The pH can be raised by directly adding base, but methods that effectively remove counterions, or reduce the counterion-to-metal ratio, have also been developed.[67,68,70–72,76,77] For example, group 13 clusters can be prepared by raising the pH via reduction of hydrogen ions, either chemically (e.g. Zn metal) or electrochemically.[68,77] The nitrate:metal ratio can also be reduced by directly dissolving an oxide component into a nitric acid precursor solution (see Chapter II). Such methods allow for simultaneous precondensation and reduction of nitrate:metal ratio, leading to a facile conversion to the metal oxide. In principle, aqueous solution deposition has several advantages over sol-gel synthesis. It requires less expensive precursors and eliminates the need for toxic organic solvents and organic ligands/stabilizers. Because the organic components used in sol-gel synthesis need to be thermally removed, this method often

produces porous films with carbon contamination. Aqueous deposition therefore generally produces denser, less porous films. For these reasons, water is generally an excellent solvent for deposition of metal-oxide thin films.

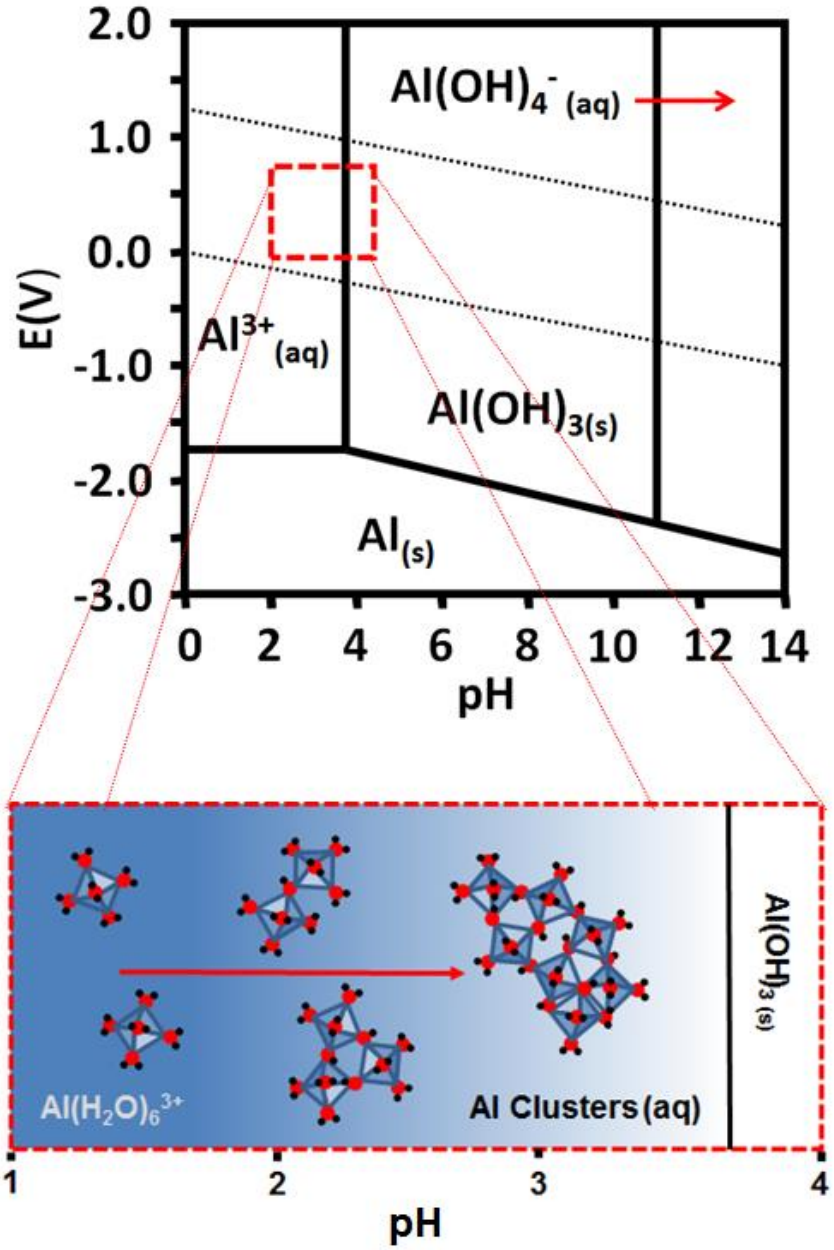

Figure 1.1. Aluminum Pourbaix diagram illustrating the effects of pH on Al speciation

Aside from its role as a non-toxic, abundant and benign solvent, water plays an important role in the precursor solution and in the many reactions that occur as it converts to a metal oxide film. Perhaps most importantly, water acts as a ligand for the metal cations in the precursor solutions. In the case of aqueous metal nitrate precursor solutions, water and nitrates compete for direct binding in the 'inner sphere' of the metal centers. It has been shown that inner sphere coordination directly influences the decomposition temperature of the salt (higher hydration in the inner sphere leads to lower decomposition temperature).[78,79] As shown in Chapter V, the concentration of the solution directly influences the degree of inner-sphere hydration, with consequences on decomposition temperature and pathway. Ultimately, water elimination is crucial in forming the desired fully dense metal oxide. Water molecules are eliminated when hydroxyl bridges in metal complexes or clusters react to form oxo-bridged oligomeric solution species.[80–85] The presence of atmospheric water can affect the equilibrium for the latter process. Additionally, water forms an azeotrope with nitric acid, and boiling of this species can aid elimination of nitrate counterions. Humidity in the annealing atmosphere appears to enhance azeotrope formation and elimination from the films. Effects of humidity during annealing are presented in Chapter IV. Surprisingly, humidity also has a profound effect upon film thickness in the initial stages of films formation via spin-deposition (Chapter III). A significant portion of this dissertation is focused on the role of water at different points in the film formation process

Film Formation: From Solution-Phase Precursors to Metal-Oxide Thin Films

Although metal-oxide thin films can be deposited from solution-phase precursors using a variety of methods, this thesis focuses exclusively on spin-deposited metal-oxide thin films. Accordingly, the processes described below pertain specifically to those involved in the conversion of aqueous precursor solutions to thin film metal oxides via spin-deposition and subsequent heating under various conditions.

Spin deposition consists of two partially overlapping processes. The first process involves depositing filtered precursor solution onto a cleaned substrate and spinning rapidly to produce a thin film. The second (overlapping) process involves evaporation of solvent which results in increased concentration and viscosity. Many parameters, such as spin speed, precursor concentration and humidity can have an effect on the spin-coating process and the thickness of the resulting film, which can generally be described as a viscous precursor 'gel' (Figure 1.2).

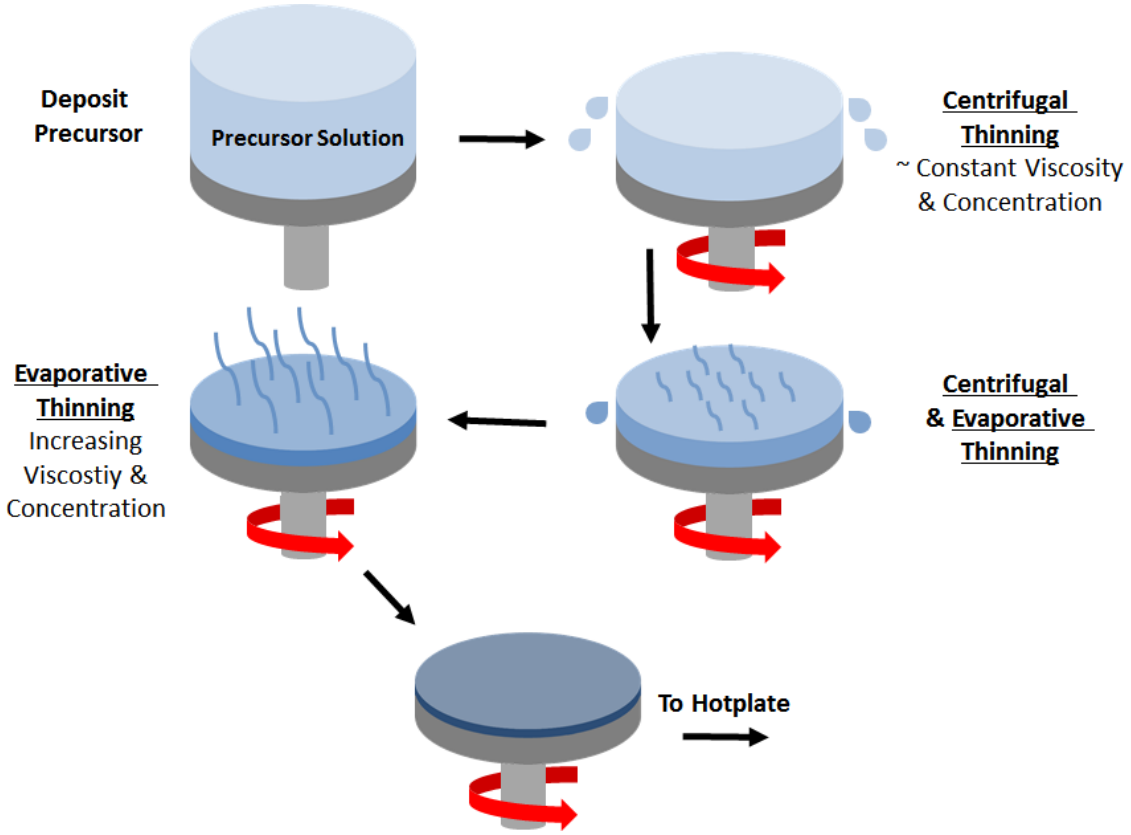

Figure 1.2. Illustration of the processes that occur during spin deposition.

The spin-deposited precursor gel is typically converted to a metal-oxide thin film by heating.[22,59,61,63,64,70,75,80–84,86] There are several overlapping and interdependent chemical and physical processes that occur during thermal conversion of precursors. The chemical processes include: evaporation of solvent H_2O; elimination of counterions through evaporation of the nitric acid-water azeotrope and through thermal decomposition; loss of bound water; formation of metal hydroxides; and condensation of metal hydroxides to metal oxides. Physical processes include: decreasing thickness, densification and stiffening (Figure 1.3). It follows from the interdependence of these

processes that time-temperature profiles during conversion can have an impact on how these processes overlap and the characteristics of the resulting metal-oxide thin films. Determining the temperatures at which these processes occur and how they overlap is a recurring theme in this dissertation (particularly in chapters IV and V).

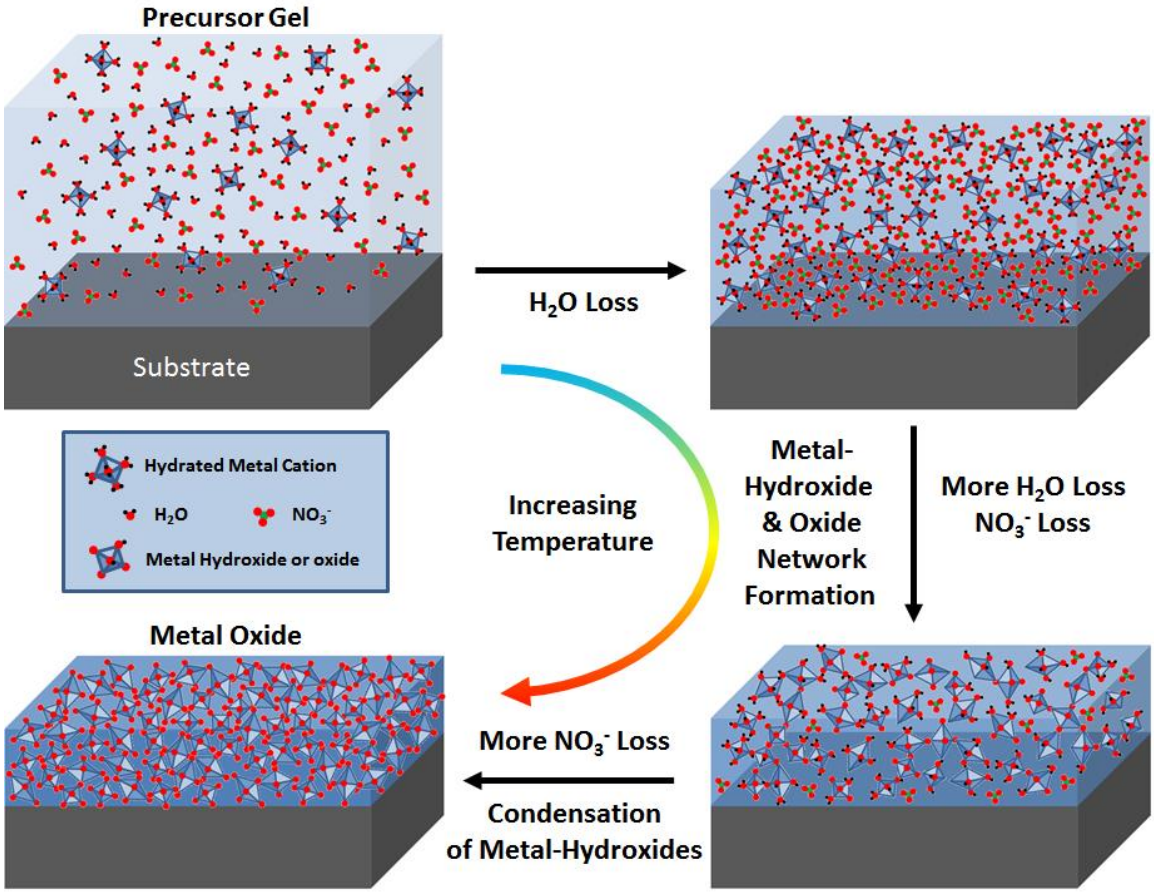

Figure 1.3. Illustration of the overlapping and interdependent processes that occur during thermal treatment of a thin-film of viscous precursor gel.

During both the spin-deposition and film-formation processes water is either evaporated or released as a byproduct of chemical reactions. The amount of atmospheric

water in equilibrium with the film during these steps will influence the processes and their interplay. During spin-deposition, evaporation of H_2O from precursors can be controlled by manipulating the relative humidity. Evaporation rates can have profound effects on film thickness, as discussed in Chapter III. Evaporation serves both to increase the concentration, and to cool the film via evaporative cooling (this latter effect may be the more important factor for viscosity, and consequently for film thickness). Following deposition, the thin films of precursor gels are heated, and the resulting solvent evaporation and subsequent metal hydroxide condensation leads to oxide formation. High partial pressures of H_2O during annealing should allow hydroxides to persist to higher temperatures, which in turn could affect the pathways of metal-oxide formation and the characteristics of the resulting metal-oxide thin film. These effects are explored in Chapter IV.

Techniques Employed to Investigate Precursor to Metal-Oxide Film Evolution

The ability to rationally design precursors and annealing sequences to produce high-quality metal-oxide thin films depends on establishing correlations between precursor chemistry, annealing protocol and thin-film characteristics. This section provides a description of the techniques used for characterizing precursors and films in order to investigate these correlations.

Precursor speciation can be examined using a combination of Raman spectroscopy, Fourier-transform infrared spectroscopy (FTIR), nuclear magnetic resonance spectroscopy (NMR), dynamic light scattering (DLS), pH measurements and thermogravimetric analysis (TGA). In this thesis, precursor solutions containing metal

nitrate salts and oligomeric metal cluster species are the primary focus. In most cases it is desirable to decrease the counterion:metal ratio which generally leads to a greater degree of oligomerization (precondensation). Raman spectroscopy can be used to detect changes in the -OH and NO_3^- species that occur with changing pH and oligomerization.[68,70,75,76] In cases of nuclei with appropriate nuclear spin, NMR can be used to examine the coordination environments of the metal.[68,76,87–89] Finally, DLS yields information pertaining to the size distribution of species in solution.[87,90–92] TGA of 'bulk' dried precursor powder (derived from rotary evaporation of the solution) can give an indication of thermal decomposition behavior of the precursor gel, but this may differ from the thermal decomposition of the film because of differences in the gel formed by rotary evaporation vs spin-processing and the very different length scales involved.[82,83,93–99]

As an illustration of the utility the aforementioned techniques, it has been shown using DLS, Raman and NMR that aluminum nitrate precursor speciation can be changed by reducing the NO_3^-:Al^{3+} ratio (e.g. by addition of La_2O_3), which simultaneously increases pH and promotes formation of Al-hydroxo clusters from isolated hydrated Al^{3+} complexes (see Chapter II). A cartoon illustrating possible aluminum and lanthanum speciation and the information gleaned from these techniques is shown in Figure 1.4.

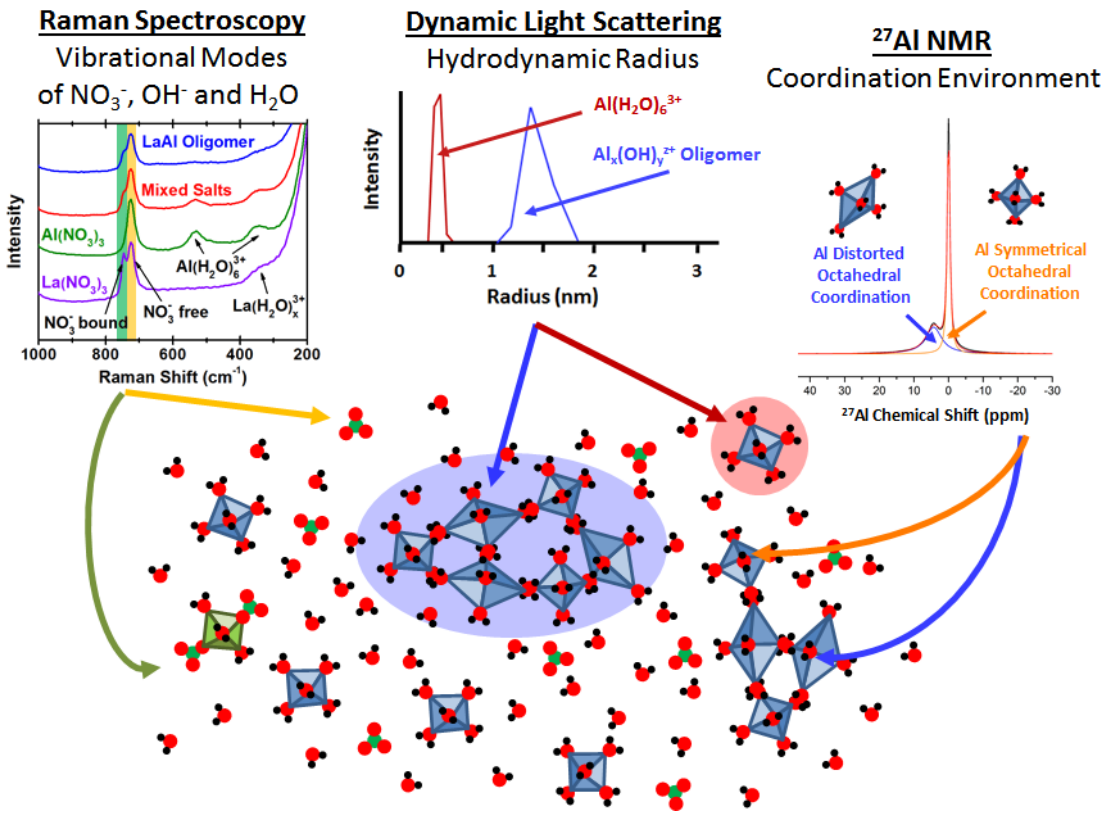

Figure 1.4. Depiction of a precursor solution illustrating the utility of Raman spectroscopy, dynamic light scattering and ^{27}Al NMR to determine solution speciation.

After precursor solutions are deposited onto substrates, the chemical and physical characteristics can be studied using a variety of techniques as the films progress from gels to metal oxides. The chemical composition of thin films can be examined using X-ray photoelectron spectroscopy (XPS), electron-probe microanalysis (EPMA), temperature programmed desorption (TPD), and fourier-transform infrared spectroscopy (FTIR). XPS yields elemental composition data and is sensitive to slight changes in oxidation states.[35,78,97,100,101] XPS can also be used to measure the composition of a film as a function of depth. EPMA yields elemental composition data as well, but to a higher degree of precision than XPS.[102] TPD provides higher sensitivity to molecular species

containing elements that EPMA and XPS have difficulty detecting, such as N and O, and gives insight into the decomposition pathways of reactive species retained within thin films.[81,103–106] Fourier-transform infrared spectroscopy (FTIR) is useful for detecting NO_3^-, H_2O and OH retained within films.[22,80,97,107] However, for very thin films signal-to-noise ratios are too low to draw meaningful conclusions from FTIR data, so techniques such as TPD are more informative.

The physical characteristics of thin films (thickness, density roughness) can be determined using techniques such as X-ray reflectivity (XRR), ellipsometry, atomic force microscopy (AFM) and various electron-microscope techniques (Figure 1.5). XRR is a non-destructive technique that allows measurement of film thickness,[108–110] density, and roughness. Ellipsometry can be used to determine thickness and optical properties of films.. AFM can be used to measure roughness of the film surface independent of film-substrate roughness (unlike XRR).[80,111,112] Finally, electron-microscopy techniques such as scanning electron microscopy (SEM) can give valuable information pertaining to the morphology and density profiles of thin films.[15,80,81,84,113–117] However, electron microscopy techniques can be destructive, since they expose films to high energy electron beams which may alter the samples.[113–115,117] This can be especially problematic for films that have been annealed at low temperatures.

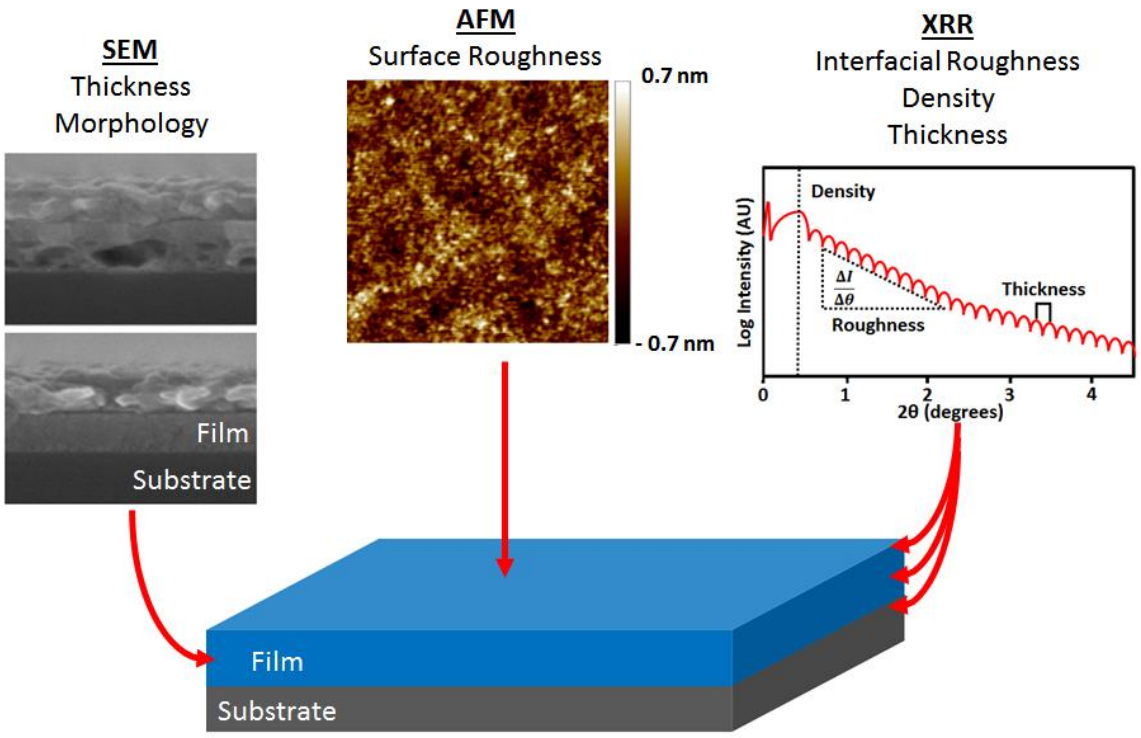

Figure 1.5. Depiction of a metal-oxide thin film illustrating the utility of SEM, AFM and XRR in examining its physical characteristics.

To build a comprehensive picture of the processes involved in film formation, it is important to use a host of characterization techniques and to monitor films at various points along the processing pathway, correlating composition, structure and morphology with processing conditions. All of the techniques described above can be used 'ex-situ' at various points in the film evolution.

Although correlations between precursor chemistry, processing conditions and thin-film characteristics can be drawn by ex-situ characterization, a more thorough understanding of the film-formation process can be obtained if films can be tracked in-situ as they convert from precursors to metal oxides. In-situ experiments on thin films are

effective for several reasons. Rapid thickness, density or roughness changes that occur during annealing may not be evident from examination of 'snapshots' at intermediate stages or of the fully-processed films. Furthermore, precursor films that have only been partially converted to metal oxides are sensitive to water-absorption (after relatively low temperature anneals), so the characteristics of these films may change before they can be measured ex-situ. In-situ techniques that allow monitoring film properties while heating avoid these problems. Chapter V investigates changes in the thermal evolution of precursors as a function of initial concentration using in-situ XRR experiments in combination with TPD experiments to investigate mass loss and densification as a function of temperature.

Electrical Properties of Metal-Oxide Thin Films

Thin-film metal oxides are used in a wide variety of electronic devices, as stated earlier. The electrical properties of the films are critical to their use in devices. Conversely, devices made employing these films enable the determination of key electronic properties, and allow correlations between precursor, processing, and device-performance to be established. The majority of the metal-oxides thin films studied in this dissertation are high-bandgap insulators that are potentially useful as gate-dielectrics in thin-film transistors (TFTs). Consequently, electrical characterization is focused on how well the films block the flow of current, screen an electric field, and perform when incorporated as gate-dielectrics in TFTs. One way to measure the insulating and screening properties of a thin-film dielectric is to incorporate it into a MOS (metal-oxide-semiconductor) capacitor (Figure 1.6a). To make the MOS capacitor, the metal oxide

film is deposited onto a conductive Si substrate and, after processing, aluminum top contacts are deposited to form an array of parallel plate capacitors. Leakage-current density is determined by measuring current as a function of electric field. Low leakage-current densities are desired for gate dielectrics. Capacitance (related to polarizability) is measured by applying a small, sinusoidally varying electric field across the MOS capacitor and measuring the magnitude of the current and its phase with respect to the varying electric field. If the thickness and area of the capacitor are known, an intrinsic property relating to the polarizability of the metal-oxide, the dielectric constant (K), can be determined. Generally, a higher K is desired for gate-dielectrics. Although leakage current may be low and K high, the only way to determine if a material is a suitable gate dielectric is by directly examining its function in a thin film transistor (TFT) (Figure 1.6b). A TFT is composed of a gate metal (p^+-Si), a gate dielectric (in this case a solution-deposited metal oxide thin film), and a semiconductor (such as indium gallium zinc oxide, IGZO) contacted by metallic (in this case Al) source and drain contacts. A TFT acts as a switch in which the current flowing from source to drain can be controlled by varying the voltage applied to the gate. Increasing K of the dielectric reduces the magnitude of the voltage needed to switch the flow of current. Reducing this voltage reduces the power consumption of the device. In principle, it would seem that a high-K should always be used in TFTs, but the interface between the gate dielectric and the semiconductor channel (where most of the current flows) dominates the performance of the TFT. The electrical properties and TFT performance of aqueous-solution deposited $LaAlO_3$ thin films are briefly discussed in Chapter II.

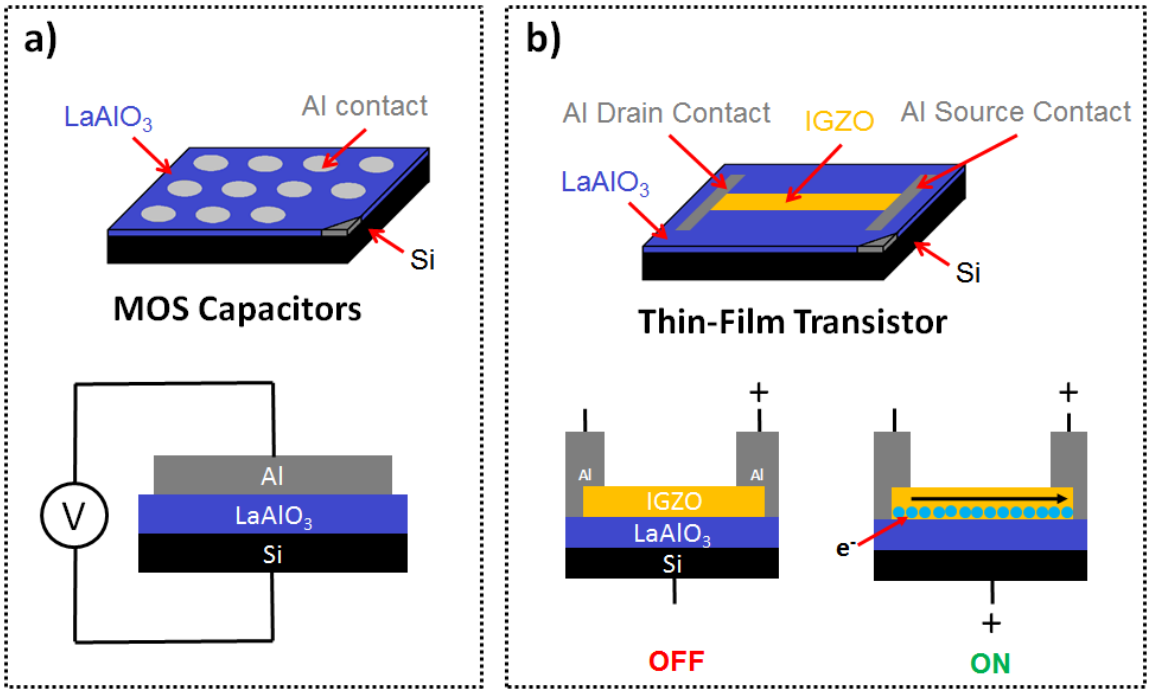

Figure 1.6. a) A diagram of a Si/$LaAlO_3$/Al MOS capacitor and b) a diagram and operation of a TFT with a Si gate, $LaAlO_3$ gate dielectric, IGZO semiconductor channel and Al source/drain contacts

The following chapters detail work on the precursor chemistry, film formation processes and applications of metal-oxide thin films deposited via spin-deposition from aqueous solutions. Using $LaAlO_3$ as a target material, Chapter II provides a general overview of precursor chemistry, physical and chemical evolution of thin films, and incorporation and characterization of a $LaAlO_3$ thin films into electronic devices. Many of the characterization techniques in Chapter II are used throughout this dissertation. A closer look at film-formation processes is provided Chapters III and IV with a particular emphasis on the impacts of H_2O(g) during spin-deposition of precursors and annealing of spin-deposited precursors, respectively. In Chapter V, the effects of precursor concentration on the film-formation process are observed in-situ using X-ray reflectivity. Furthermore, the speciation of the precursors is shown to be concentration-dependent and

affect the film formation process. Together these chapters provide new insights into the importance of $H_2O(g)$ and precursor concentration during the formation of thin film metal oxides from thin films of spin-deposited precursors.

This dissertation contains previously published and unpublished coauthored material. Chapter II was previously published with Kevin Archila, John F. Wager, and Catherine J. Page. Contributions to Chapter III were made by Gavin Mitchson, Catherine J. Page, and David C. Johnson. Contributions to Chapter IV were made by Keenan N. Woods, Deok-Hie Park, Catherine J. Page, and Douglas A. Keszler. Contributions to Chapter V were made by Keenan N. Woods, Deok-Hie Park, Catherine J. Page, and Douglas A. Keszler.

Bridge

The following body of work presents research on metal oxide thin films spin-deposited from aqueous solutions containing only inorganic species. Using this method in place of more complex vapor- and solution-phase deposition methods allows for relatively simple and environmentally benign metal oxide thin film deposition.

Although there are various techniques for depositing solution-phase precursors on a substrate, the work in this dissertation is focused exclusively on spin-deposition of aqueous precursors. Spin-deposition has been used in combination with many different types of precursors to produce a wide range of thin film materials with varying degrees of success. However, many of the finer details associated with spin-deposition of thin film materials have not been thoroughly explored.

This work focuses on elucidation of many of these details as they relate to spin-deposition of metal oxide thin films from all-inorganic and aqueous precursors. Chapter I examines the precursor solution chemistry, general film formation processes and electrical properties of aqueous-deposited $LaAlO_3$ thin films. The work in Chapter III, explores the impact of relative humidity during the spin-deposition process, and pertinent generally to spin-coating from aqueous solutions. Chapters IV and V focus on the effects of humidity during thermal processing and the effects of precursor concentration on oxide film formation, respectively, and should be broadly applicable to solution-phase deposition techniques. This work not only contributes new insights into the processes involved in the formation of metal-oxide thin films deposited from aqueous precursors, but many of the results should also be relevant for understanding the formation of metal oxide thin films deposited using alternative techniques and precursor chemistries.

CHAPTER II

LANTHANUM ALUMINUM OXIDE GATE-DIELECTRICS DEPOSITED FROM AQUEOUS SOLUTION

This chapter was previously published as Plassmeyer, P. N.; Archila, K.; Wager, J. F.; Page, C. J. Lanthanum Aluminum Oxide Thin-Film Dielectrics from Aqueous Solution" in Applied Materials and Interfaces, 2015, 7, 1678-1684. P.N.P. wrote the publication, performed lab-work and analysis, and wrote the publication. K.A. Fabricated and analyzed thin-film transistors. J.F.W. provided editorial assistance. C.J.P. provided editorial assistance and served as the principle investigator.

Introduction

Rare earth aluminum oxides are of interest as scintillators and laser host materials,[1-4] as dielectric resonators,[5] as active components in nonvolatile memory elements,[6-9] and as high-dielectric gate oxides for thin film transistors.[10, 11] For the latter applications, thin films are required. Where the rare earth element is lanthanum, crystalline and amorphous $LaAlO_3$ thin films have been widely studied as gate dielectrics in transistors,[12-14] as template layers for heteroepitaxial growth of high-T_c superconductors,[15, 16] and for the intriguing electronic phenomena that arise at $LaAlO_3/SrTiO_3$ interfaces.[17]

A variety of techniques have been developed for the deposition of metal-oxide thin films.[18] Vapor deposition techniques such as atomic layer deposition (ALD), metal–organic chemical vapor depositions (MOCVD) and pulsed laser deposition (PLD) can yield thin films with excellent electronic and morphological properties, but stringent

processing conditions and costly precursor materials are often required to obtain the desired film properties.[19-21] Much of the research directed toward thin-film $LaAlO_3$ has focused on deposition using such techniques.[22-30]

For applications tolerating higher defect levels and rougher topologies, solution deposition techniques, such as sol–gel, have been employed to make metal-oxide thin films.[15, 16] However, the expulsion of bulky organic ligands during annealing tends to reduce the density and smoothness of films prepared in this way.[31] Deposition of $LaAlO_3$ has also been attempted using methanol solutions of nitrate salts.[32] Epitaxial growth of crystalline $LaAlO_3$ on $SrTiO_3$ substrates was achieved by this method, but the resultant films had large voids and irregular morphologies that would be problematic for electrical characterization or use in electronic devices.

In contrast to this previous report of crystalline $LaAlO_3$ films from methanol-based nitrate solutions, we report here the preparation of high-quality, ultrasmooth *amorphous* $LaAlO_3$ films prepared from *aqueous* nitrate-containing solutions. Importantly, using this solution-based route, we are able to produce amorphous thin films that approach the quality normally associated with vapor deposition techniques. Our solution-phase approach to these materials employs inexpensive inorganic salts with small, easily decomposed counterions. By controlling the concentration, pH, and degree of condensation of solution-phase precursors, spun films can be heated quickly to promote prompt condensation to an oxide network.

The term ‘Prompt Inorganic Condensation’ (PIC) has been recently coined to describe this general approach, which has been used to produce a variety of metal oxide, metal oxide/phosphate, and metal oxide/sulfate films, including insulating films of Al_2O_3–

$_{3x}(PO_4)_{2x}$, HfO_2, $ZrO_{2-x}(SO_4)_x$, and $HfO_{2-x}(SO_4)_x$ and semiconducting ZnO and SnO_2.[33-38] Thicknesses of single layer films are typically in the 30–50 nm range for solutions that are 1 M in metal ion concentration, and overall film thickness can be adjusted by controlling solution concentration and the number of layers deposited. In the case of aluminum oxide and aluminum oxide phosphate, $Al_2O_{3-3x}(PO_4)_{2x}$, films produced using PIC have demonstrated relatively high dielectric breakdown voltages and low leakage currents.[33,39] When used as the insulating layer in thin-film transistors, high quality devices exhibiting small turn-on voltages with minimal hysteresis and high channel carrier mobility have been demonstrated.

For optimized condensation of metal-oxo networks using PIC, it is desirable to have "precondensed" solution-phase oxo- or hydroxo-bridged cluster species in the precursor solutions. In addition to being partially condensed, these species also have reduced positive charges and fewer counterions, which leads to increased atom-economy and less disruptive expulsion of ligands during film formation. Speciation of aluminum in aqueous solution is relatively well understood and can be controlled via concentration and solution pH. At low pH (≤1.5), isolated $Al(H_2O)_6^{3+}$ species dominate, but as pH is increased to ~3.2 aluminum oxo-hydroxide clusters form.[40] The aqueous behavior of lanthanum is not unlike that of aluminum, although lanthanum is soluble to higher pH (~7). No oxo- or hydroxyl-bridged lanthanum clusters have been isolated and characterized to date, although hexanuclear clusters with the general formula $[Ln_6O(OH)_8(NO_3)_6(H_2O)_{14}]^{2+}$ are known for other lanthanide ions.[41] It is possible that increasing the pH toward the solubility limit and/or removing counterions from a $La^{3+}_{(aq)}$ solution could produce similar oligomeric hydroxyl-bridged lanthanum species.

In this contribution, we report the PIC synthesis of high quality, amorphous $LaAlO_3$ thin films achieved by controlling precursor solution pH and reducing nitrate counterion concentration relative to solutions of metal nitrate salts. Dissolving La_2O_3 in $Al(NO_3)_{3(aq)}$ increases pH to levels where partial condensation of aluminum species is likely to occur (~3.2) while reducing the nitrate anion to metal cation ratio. Moreover, the addition of highly polarizable lanthanum (La_2O_3has a dielectric constant K = 27) increases the dielectric constant of the resulting thin films and suppresses crystallization. While we have focused exclusively on a 1:1 lanthanum aluminum oxide in this work, the synthetic route is broadly applicable to other stoichiometries and rare earth aluminum oxides.

Experimental Section

Solution Preparation

Typical $LaAlO_3$ thin-film precursor solutions were prepared by dissolving $Al(NO_3)_3 \cdot 9H_2O$ (18.757 g, 0.050 mol) in 80 mL of 18.2 MΩ·cm H_2O and adding ~15.8 M $HNO_{3\,(aq)}$ (3.17 mL, 0.050 mol HNO_3). These solutions were heated to 70 °C and La_2O_3 (8.145 g, 0.025 mol) was added over 10 min while stirring. The solutions were then heated at 70 °C and stirred for an additional 3 h to ensure complete dissolution. Excessively high heating temperatures and/or times resulted in precipitation or gelation. After dissolution of La_2O_3, the solutions were diluted to 100 mL using 18.2 MΩ·cm H_2O. The resulting solutions were 0.5 M $Al(NO_3)_{3\,(aq)}$, 0.5 M $La^{3+}{}_{(aq)}$, 0.5 M $HNO_3$with pH near 3.4.

Solution Characterization

Hydrodynamic radii of solution species were determined using a Möbius dynamic light scattering (DLS) model WMOB-03 using an acquisition time of 20 s. Correlation decays were modeled using a cumulant fit. Solution Raman spectra were collected using a Wytec 300S Raman spectrometer with laser power of 45 mW and excitation wavelength of 532 nm. Thermogravimetric analyses were performed using a TA Instruments Q500 using a temperature ramp rate of 10 °C min^{-1} and ambient air.

Thin-Film Preparation

Moderate resistivity (~45Ωcm) p-type and low resistivity (~0.001 Ω·cm) n^+- or p^+-type Si were used as substrates for thin film deposition. Prior to deposition substrates were cleaned by sonication in a 5% Contrad 70 solution at 45 °C for 1 h. After thorough rinsing with 18.2 MΩ·cm H_2O, this procedure yielded a highly hydrophilic surface. Thin films were prepared by depositing precursor solutions onto the native oxide of Si substrates through 0.45 μm PTFE filters followed by rotation at 3000 rpm for 30 s. The wet films were then immediately soft-annealed at 100 °C on a hot-plate followed by a 12.5 °C min^{-1} ramp to a final target temperature between 200 and 700 °C. Solutions with 1 M total metal concentrations yielded films with a thickness of approximately 50 nm after a 300 °C anneal. Films used for electrical measurements (and thin-film transistors) were prepared by sequential deposition of three layers of slightly lower concentration

(chosen to give a final total thickness of 100 nm), annealed to 300 °C between depositions, and then at the final annealing temperature for 1 h.

Thin-Film Characterization

Film thicknesses were determined by X-ray reflectivity (XRR) measurements on a Bruker D8 Discover diffractometer with a Cu Kα radiation source (λ_{avg} = 1.5418 Å). Analysis of reflectivity data was accomplished using Bede REFS software. Grazing-incidence X-ray diffraction experiments to determine film crystallinity (or lack thereof) were also performed on the Bruker D8 Discover diffractometer. Transmission IR measurements were performed on a Nicolet 6700 Fourier transform infrared (FTIR) spectrometer using a spectrum collected from a bare silicon substrate (45 Ω·cm) as the background. Electron probe microanalysis (EPMA) was performed using a Cameca SX-50. The resultant raw X-ray intensities were corrected as outlined by Donovan and Tingle.[42] Electron micrographs were obtained using a Zeiss Ultra-55 FESEM with a 20 μm aperture and 5 kV accelerating voltage.

Metal–Insulator–Semiconductor Device Fabrication

Metal–insulator–semiconductor (MIS) capacitors were constructed for impedance and current–voltage measurements by depositing 100 nm thick aluminum top contacts through a shadow mask onto annealed $LaAlO_3$ dielectric films deposited on Si substrates. This resulted in an array of MIS capacitors, each with an area of 0.011 cm^2. Potentials were always applied to the aluminum top contacts. Leakage current and dielectric

strength measurements were performed on a Keithley 2400 source meter using a 50 mV step size and 50 ms delay. Impedance, phase-angle and capacitance–voltage measurements were conducted using a Hewlett-Packard 4284a impedance analyzer at 1 kHz with 50 mV oscillation amplitude.

Thin-Film Transistor Device Fabrication

Fabrication of thin-film transistors was performed on ~100 nm thick $LaAlO_3$ thin films deposited on highly doped Si substrates annealed between 500 and 700 °C in air for 1 h. After annealing in air, a subset of samples was annealed in $5\%H_2/95\%N_2$ (forming gas) at 300 °C. Amorphous $InGaZnO_4$ (a-IGZO) semiconductor channels with dimensions W/L = 1000 μm/150 μm and thickness of 35 nm were sputter-deposited at a power of 75 W, gas flow of Ar/O_2 = 9/1 sccm, pressure of 5 mTorr and postdeposition anneal at 150 °C. Thermally evaporated Al was used for source/drain contacts. Transfer curves were measured on an Agilent 4155C semiconductor parameter analyzer.

Results and Discussion

Solution Characterization

Use of La_2O_3 instead of $La(NO_3)_3$ as a source of lanthanum allows for the preparation of a precursor solution with a ratio of 4 NO_3^-:1 La^{3+}:1 Al^{3+} (i.e., a nitrate/metal ratio of 2:1) and a pH = 3.4, in contrast to a simple mixture of aluminum and lanthanum nitrate salts, for which the pH is significantly lower (1.6) and the nitrate/metal ratio is 3:1. Due to the low NO_3^-/M^{3+} ratio of our precursor solutions, monomeric or oligomeric metal-oxo or -

hydroxyl species must exist in solution to achieve charge balance. DLS measurements indicate that there is an increase in the hydrodynamic radii of species in these solutions relative to those containing a mixture of nitrate salts, suggesting these species are oligomeric (Figure 1). It is thus likely that the hydroxide (or oxide) ligands serve as bridges between metal centers to give oligomeric species. We have attempted to isolate and identify these species without success. However, to distinguish the speciation in these solutions relative to those in solutions of nitrate salts, we will denote them as aqueous "LaAl oligomer " species throughout the remainder of the text.

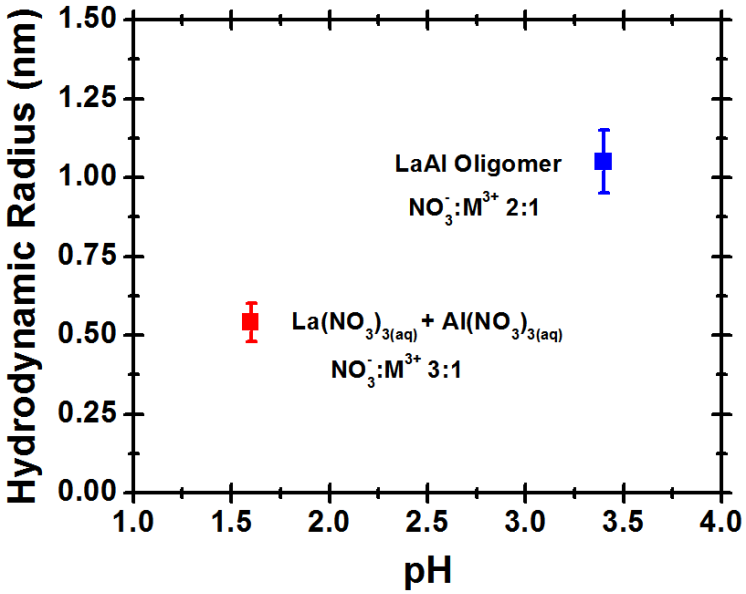

Figure 2.1. Dependence of hydrodynamic radius on solution pH and NO_3^-/M^{3+}.

The formation of oligomeric metal-hydroxyl/oxo species requires alterations to the inner hydration sphere of solvated metal cations as H_2O is replaced by OH^- or O^{2-}. In Figure 2 the Raman spectra of $Al(NO_3)_{3(aq)}$, $La(NO_3)_{3(aq)}$, $1La(NO_3)_3/1Al(NO_3)_{3(aq)}$, and

"LaAl oligomer species" are compared to determine changes induced by increasing pH and reducing NO_3^-concentration. The reduced intensity of the $Al(OH_2)_6^{3+}$ modes at 530 and 340 cm^{-1} in "LaAl oligomer species" indicates that OH^- or O^{2-} may be substituting for H_2O in the inner sphere of Al^{3+},[43] although a weak shoulder attributable to the hydration sphere of La^{3+} still remains at ~350 cm^{-1}. The modes at 725 and 745 cm^{-1} arise from free NO_3^- and inner sphere NO_3^-bound to La^{3+}, respectively.[44-46] An overall decrease in the intensity of the free NO_3^- peak was observed in the "LaAl oligomer" solution as expected. The bound NO_3^- peak associated with La^{3+} remains essentially unchanged in the "LaAl oligomer" solution relative to that of lanthanum nitrate, which indicates that if lanthanum is incorporated into an oligomeric species it retains its coordinated nitrate ligand(s).

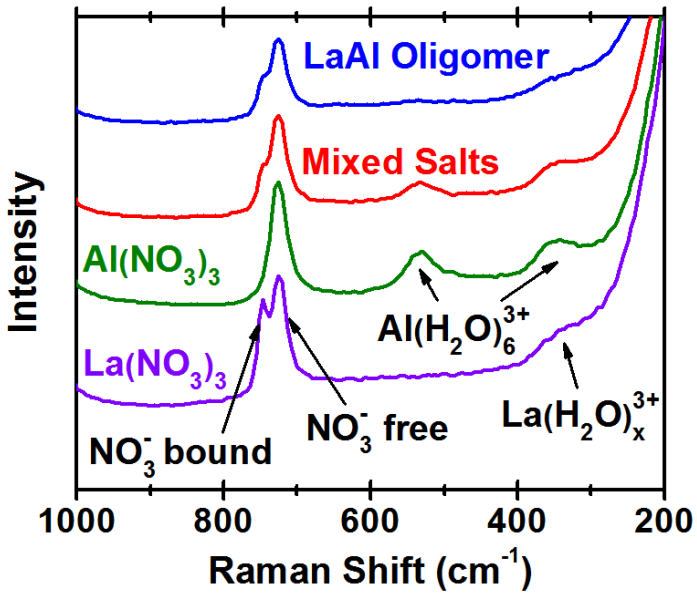

Figure 2.2. Raman spectra of $La(NO_3)_{3(aq)}$, $Al(NO_3)_{3(aq)}$, 1 $La(NO_3)_{3(aq)}$:1 $Al(NO_3)_{3(aq)}$ and "LaAl" oligomer".

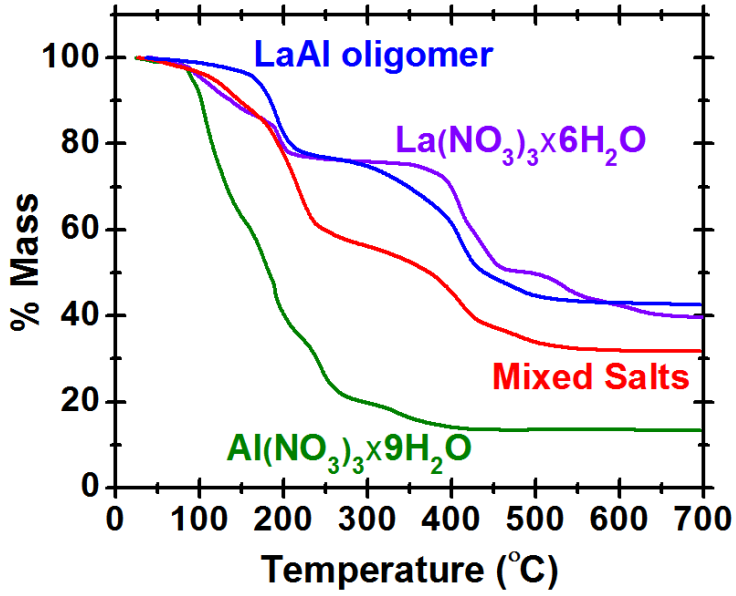

Figure 2.3. TGA curves of $La(NO_3)_3 \cdot 6H_2O$, $Al(NO_3)_3 \cdot 9H_2O$, and powders obtained by drying solutions of a mixture of the nitrate salts and of 1 La^{3+}: 1 Al^{3+}: 2 NO_3^- (denoted as "LaAl oligomer") in air.

Upon deposition and subsequent annealing, condensation reactions occur between the remaining hydroxyl ligands while H_2O and NO_x gases are expelled. TGA experiments were performed on bulk powders of $La(NO_3)_3 \cdot 6H_2O$ and $Al(NO_3)_3 \cdot 9H_2O$, and dried powders obtained from solutions of "LaAl oligomer species" (Figure 3), to gain insight into the oxide formation process during annealing. For bulk $La(NO_3)_3 \cdot 6H_2O$, temperatures above 600 °C are required to remove a significant portion of water, hydroxides, and nitrate groups to yield La_2O_3. In contrast, most dehydration and counterion expulsion occurs by 300 °C for $Al(NO_3)_3 \cdot 9H_2O$. These results are not particularly surprising as it is known that the decomposition temperature of a given metal nitrate decreases as the metal ion charge density increases.[47] The high charge density of Al^{3+} draws electron density from the nitrate, effectively weakening the N–O bonds and making bond breakage associated with decomposition of the nitrate more facile. The

large La^{3+} (~5 times the ionic volume of Al^{3+}) is less effective polarizing these bonds. Furthermore, NO_3^- coordinates in La^{3+} in a bidentate fashion, resulting in less N–O bond polarization.[46] TGA experiments on dried powders obtained from solutions containing "LaAl oligomer species" show that mass loss is essentially complete by 500 °C. This indicates that the presence of aluminum acts to decrease nitrate removal/decomposition temperature of the mixture relative to that required for $La(NO_3)_3 \cdot 6H_2O$. It should be noted these dried powders may not be truly representative of our rapidly dried films because sequential precipitation of salts may have occurred with the slower drying employed, but these results are consistent with the temperatures needed to expel nitrate from the films, as shown by IR and electrical data (see below).

Thin Film Physical and Chemical Characterization

Residual H_2O and NO_x species have a significant impact on the properties of the thin films. To track the chemical processes during annealing, ex-situ infrared spectra of thin films were taken immediately after annealing at various temperatures (Figure 4). By monitoring the broad O–H stretching mode centered near 3500 cm^{-1} and the H–O–H bending mode at 1650 cm^{-1}, it can be seen that a significant portion of the water is lost between 200 and 300 °C. Disappearance of the H–O–H bending mode in this temperature range suggests low levels of H_2O, and the remaining OH absorption is predominately due to residual metal hydroxides. However, we note that films annealed below 250 °C are hygroscopic and the bands at 3500 and 1650 cm^{-1} grow if the films are exposed to ambient atmosphere. The OH absorption at 3500 cm^{-1} remains until annealing temperatures >400 °C, indicating that condensation is not complete until approximately

500 °C. The absorptions at 1280 and 1460 cm^{-1} correspond to residual nitrate trapped within the films.[44, 45] Nitrate content also decreases throughout the annealing process, but it is still detectable even after annealing at 500 °C. The weak absorptions at 1040, 810, and 740 cm^{-1} present after annealing at only 200 °C are indicative of hydrated metal-nitrate species.[44, 45] As annealing temperatures are increased, these absorptions are eliminated and a broad feature at 740 cm^{-1} appears. This absorption is related to the formation of metal–oxygen–metal bonds.[48]

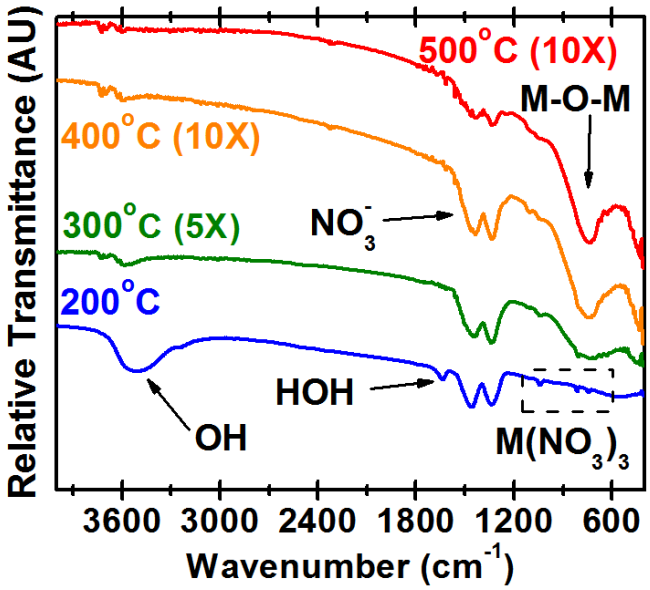

Figure 2.4. Fourier transform infrared (FTIR) spectra of thin films annealed between 200 and 500 °C in air.

XRR was employed to determine the thickness, roughness, and density of the thin films (Figure 5a). The hygroscopic instability of thin films annealed at temperatures <250 °C led to significant variations in the XRR, so these are not reported here. As annealing temperatures are increased from 300 to 600 °C, film thicknesses decrease by ≈35%, consistent with counterion expulsion and condensation. This is accompanied by a density increase from 61% to 72% of the single-crystal $LaAlO_3$ density of 6.51 $g \cdot cm^{-3}$. These relative densities are similar to those attained by condensing Al_2O_3 thin films from similar conditions.[39] Cross-sectional and surface SEM micrographs reveal films with a high degree of uniformity and minimal surface and interfacial roughnesses (Figure 5b). Thin films crystallize between 800 and 900 °C to the rhombohedral perovskite phase (JCPDS File Card No. 31-22) (Figure 5c).

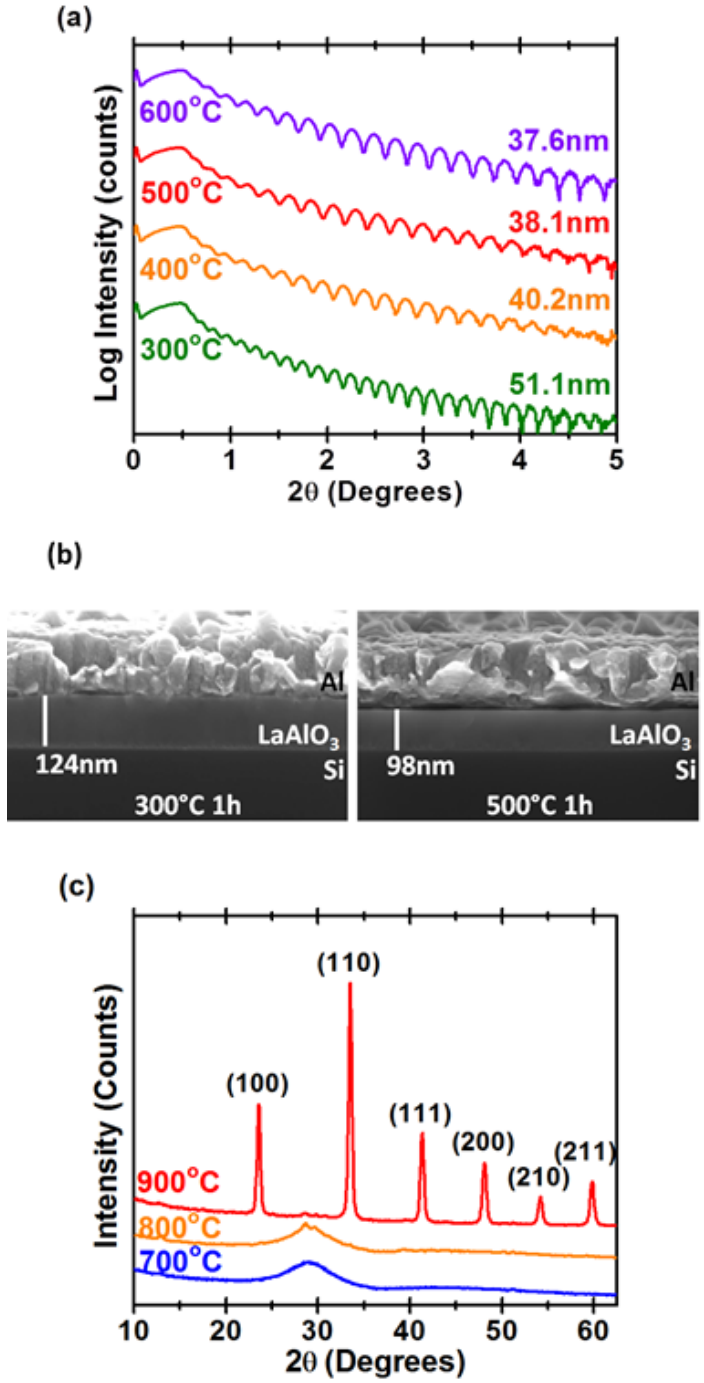

Figure 2.5. (a) XRR patterns of $LaAlO_3$ thin films annealed between 300 and 600 °C, (b) SEM micorgraphs of $LaAlO_3$ thin films annealed at 300 and 500 °C, (c) X-ray diffraction of $LaAlO_3$ thin films annealed at 700, 800 and 900 °C. The 900 °C pattern is indexed as the rhombohedral perovskite $LaAlO_3$ phase.

Thin Film Electrical Characterization

Dielectric breakdown and leakage current characteristics were examined by performing current–voltage measurements on MIS capacitors consisting of thin $LaAlO_3$ films sandwiched between highly doped n-type Si substrates and aluminum top contacts (Figure 6). Leakage currents are high for films annealed at temperatures ≤400 °C, likely related to defects associated with incomplete condensation. Catastrophic breakdown generally occurs at electric fields >3.5 $MV \cdot cm^{-1}$. Leakage current profiles decrease in slope with increasing annealing temperature, suggesting a reduction in electronic defects. This reduction is most likely associated with removal of counterions and residual hydration and is consistent with the TGA and IR data.

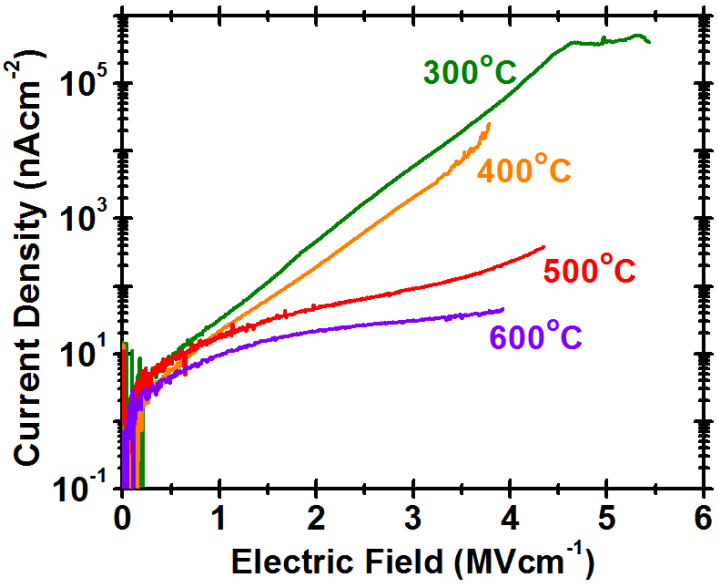

Figure 2.6. Leakage current densities as a function of electric field for $LaAlO_3$ thin films annealed at 300. 400, 500 and 600 °.

Dielectric constants and loss tangents of the films are shown in Figure 7a. The dielectric constant decreases as annealing temperatures are increased from 300 to 450 °C and then increases slightly for samples annealed above 450 °C. The loss tangent, which is related to current passage, decreases with increasing annealing temperatures up to 500 °C and then levels off. We attribute the trends between 300 and 450 °C to removal of water, hydroxides, and nitrates, reducing the amount of mobile charged species in the films. The presence of mobile charged species also contributes to the overall polarizability (and thereby the dielectric constant) of the material. Above 450 °C, most of the mobile ions have been removed (hence the relatively constant loss tangent), so the dielectric constant increase for films annealed above 450 °C can be attributed to densification of the remaining metal-oxide framework.

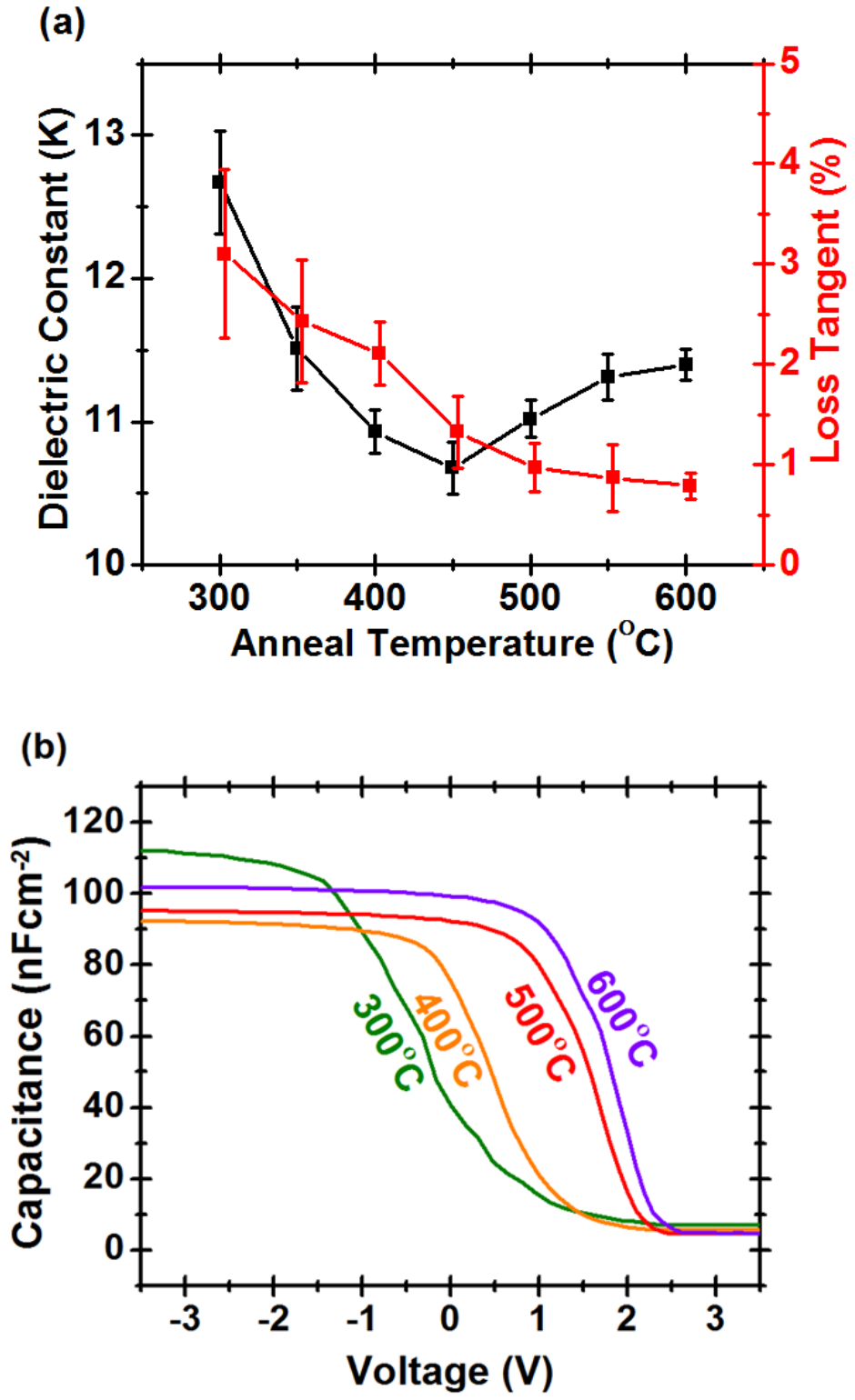

Figure 2.7. Dielectric constant (a) and Capacitance-voltage curves (b) of $LaAlO_3$ thin films annealed between 300 and 600 °C.

Capacitance–voltage measurements reveal that higher annealing temperatures result in an increased flatband potential (Figure 7b). Generally, a positive (negative) shift in the flatband voltage indicates the presence of a negative (positive) fixed charge in the oxide near the semiconductor interface.[49] When in contact with SiO_2, most metal oxides, including La_2O_3, have positive fixed charge at this interface, which results in a negative flatband shift. However, positive shifts in flatband voltages in photovoltaics are well documented for recombination-passivating Al_2O_3/SiO_2 interfaces. At these interfaces, tetrahedrally coordinated Al centers possess a partial negative charge, pushing electrons away from the interface and shifting the flatband potentials toward positive values.[50, 51] Assuming that the observed flatband shifts originate from fixed charges near this interface, the fixed charge density, Q_f, can be expressed as $Q_f = -C_I \Delta V_{fb}$ (1) where C_I is the insulator capacitance density and ΔV_{fb} is the difference between the observed and expected flatband voltages. The calculated interface charge densities at the $LaAlO_3/SiO_2$ interface range from $+1.45 \times 10^{11}$ cm^{-2} for films annealed at 300 °C to -1.75×10^{12} cm^{-2} for films annealed at 600 °C. The values calculated for films annealed at 600 °C match well with values from Al_2O_3 films deposited on the oxide of p-Si described in the literature.[50, 51] We postulate that Al may preferentially bind to the native SiO_2 layer and create a similar interfacial charge in $LaAlO_3$ films deposited via PIC.

Thin-Film Transistor Characterization

To investigate the performance of these amorphous $LaAlO_3$ films in thin-film transistors, devices were fabricated by sputter depositing a-IGZO channels, with $L = 150$ μm and $W = 1000$ μm, and Al source/drain contacts on solution-processed $LaAlO_3$ deposited

on p^+-Si (annealed at 600 °C in air). Although the characteristics of the capacitance–voltage data shown in Figure 7b suggest the presence of *some* inhomogeneous charge distribution and charge trapping defects at the $LaAlO_3/SiO_2$ interface, these thin-film transistors indicate there is a *large* concentration of empty electronic traps at the a-IGZO/$LaAlO_3$ interface, indicated by high turn-on voltages (≥24 V), moderate drain-current hysteresis and relatively low average mobilities of ∼4.5 $cm^2 \cdot V^{-1} \cdot s^{-1}$(Figure 8). Similar results have been found for IGZO transistors that incorporate a $LaAlO_3$dielectric in direct contact with the IGZO channel.[52] Typically, the performance of such transistors has been improved by incorporating a passivating dielectric layer between the IGZO channel and the $LaAlO_3$ dielectric.[12, 14, 52] In this work, we employed an alternative "surface passivation" achieved by a second annealing at 300 °C in 5%H_2/95%N_2 (forming gas) after initial preparation of the $LaAlO_3$ thin film but prior to a-IGZO deposition. Surface passivation drastically lowered the turn-on voltage to ∼6 V, minimized drain-current hysteresis, and increased average mobility to ∼11.1 $cm^2 \cdot V^{-1} \cdot s^{-1}$ (Figure 8). According to the discrete donor trap model the turn-on voltage, V_{ON}, is given by $V_{ON} = \frac{-q}{C_I}(n_{co} - p_{to})$ (2) where q is the electronic charge, C_I is the insulator capacitance density, n_{co} is the free electron sheet density, and p_{to} is the empty trap sheet density.[53] From this relationship, a turn-on voltage of 26 V corresponds to an empty trap sheet density of 1.7×10^{13} cm^{-2}, whereas a turn-on voltage of 6 V corresponds to a trap sheet density of 3.8×10^{12} cm^{-2}. Thus, the surface passivation anneal significantly reduces the empty trap sheet density. Although the detailed nature of the chemical origin of this dramatic reduction in the empty trap density is unknown at present, it (i) is clearly associated with the insulator, rather than the semiconductor, since the semiconductor is

deposited subsequent to annealing, and (ii) is likely due to the removal of moisture and/or impurities in the $LaAlO_3$ film since the surface passivation anneal is performed in a reducing ambient.

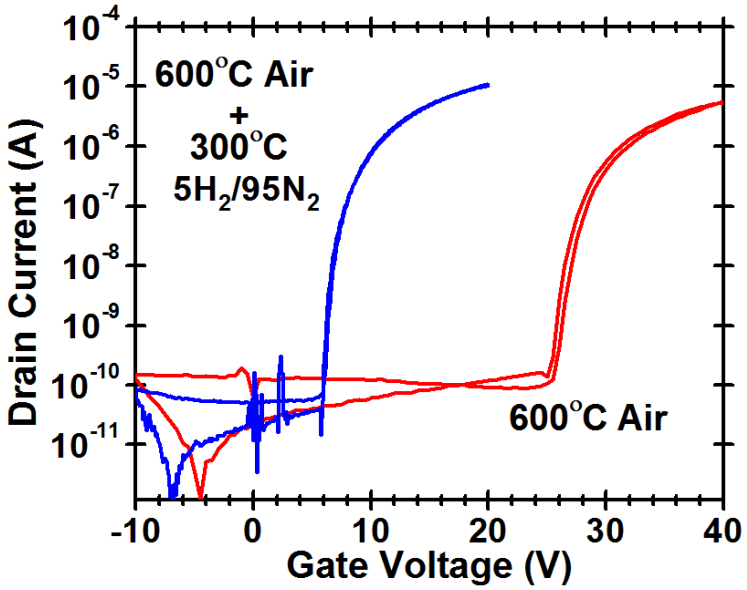

Figure 2.8. Transfer curves for bottom-gate TFTs with $LaAlO_3$ gate and sputtered IGZO channels. $LaAlO_3$ gates were annealed at 600 °C in air or at 600 °C in air followed by 300 °C in $5\%H_2/95\%N_2$.

Conclusions

The formation and properties of $LaAlO_3$ thin films deposited on Si using a 'prompt inorganic condensation' (PIC) process have been examined. In contrast to using a precursor solution of aluminum and lanthanum nitrates, dissolution of $La_2O_{3(s)}$ into $Al(NO_3)_{3(aq)}$ results in an increased solution pH, a lower nitrate/metal ratio and the formation of oligomeric hydroxyl- or oxo-metal species, which are postulated to aid in the condensation of the metal-oxide network upon annealing. Thermogravimetric analysis (TGA) and IR data suggest essentially complete condensation, dehydration, and

counterion expulsion by 500 °C. X-ray reflectivity (XRR) and scanning electron microscopy (SEM) indicate very uniform films with low surface and interfacial roughness. Temperatures above 400 °C are required to achieve low leakage currents and expel the remaining mobile species, which likely contribute to the higher dielectric constants at lower annealing temperatures. Capacitance–voltage measurements indicate the presence of trapped negative charge near the $LaAlO_3/SiO_2$ interface, most notably at higher annealing temperatures. The trapped charge in the $LaAlO_3$ thin film could be useful for surface-recombination passivation in p-type emitter solar cells.

TFTs with sputtered a-IGZO channels were fabricated with PIC-deposited $LaAlO_3$ gate dielectrics. For $LaAlO_3$ gates annealed in air at 600 °C, large turn-on voltages, large drain-current hystereses, and relatively small average mobilities were observed. A low temperature post anneal step of the $LaAlO_3$ gate in reducing atmosphere decreased turn-on voltages and drain-current hystereses while increasing average mobility. This interesting result indicates a promising future direction for improving the electrical properties of these films to make them attractive candidates as dielectrics in thin-film transistors.

Bridge

Although the work in Chapter II focused on demonstrating successful synthesis of high quality $LaAlO_3$ thin films from aqueous precursors and their incorporation into functioning thin-film transistors, many important aspects of precursor chemistry and film-formation processes were touched upon. In particular, this work described how precursors can be manipulated in solution to initiate the formation of a metal-oxide framework, and how the general chemical and physical processes that occur during annealing can be monitored.

Chapter III focuses on the effects relative humidity during spin-deposition of precursors. The processes occurring during spin deposition are generally not well-understood, and the importance of parameters such as humidity are not well-documented or appreciated, especially for films deposited from aqueous solutions. In Chapter III we demonstrate that relative humidity during the spin-deposition process has a dramatic impact on film thickness, and also more subtly affects the cross-sectional distribution of elements in the film. In general, this work shows that humidity plays an important role in controlling the evaporation rate of solvent H_2O, which influences the viscosity by increasing concentration and lowering temperature. We also show that this effect is general for a number of aqueous metal precursor solutions, and that the film thicknesses resulting from solutions of the same metal ion concentration are essentially the same for a given humidity when other spin processing parameters are held constant.

CHAPTER III

THE IMPACT OF RELATIVE HUMIDITY DURING SPIN-DEPOSITION OF METAL OXIDE THIN FILMS FROM AQUEOUS SOLUTION

HAADF-STEM images and sample preparations for HAADF-STEM were performed by Gavin A. Mitchson. Editorial assistance was provided by Caterine J. Page and David C. Johnson.

Introduction

The proliferation of mass-produced display media, such as smart phones and tablets, has accelerated research into new processes for deposition of thin-film components. Most thin-film components are currently deposited via vapor-phased deposition (VPD), which produce high-quality films, but require expensive equipment and precursors, and are not atom-efficient. Furthermore, VPD is not amenable to producing materials with variable composition or more than one metal component.[1,2] Solution deposition of metal-oxide thin films has been shown to be an attractive alternative to traditional vapor-phased techniques. For example, high performance amorphous $In_xZn_yO_z$ transistors have been fabricated by annealing sol-gel precursors[3] and $La_2Hf_2O_7$ thin films deposited from organic solution show excellent performance as gate dielectrics in thin film transistors (TFTs).[4] Examples of film formation using aqueous precursor solutions are also known, employing either water-soluble complexes with organic ligands [5] or all-inorganic clusters or salts. The latter systems can lead to high-quality films without the use of toxic or expensive precursors and the generation of volatile organic byproducts.[6–13]

Due to its ubiquitous nature, water has the potential to play important roles in many of the film formation processes that occur as precursors are converted to metal oxides. Many examples of the importance of water in film formation exist. For example, water plays an integral role in sol-gel processes, water vapor can dramatically increase thermal oxide growth rates on Si,[14,15] and water vapor decreases the temperatures at which $Zn(CH_3COO)_2$ and $Zn(acac)_2$ thermally decompose.[16–18] Once fabricated, some thin-metal oxides absorb atmospheric H_2O resulting in altered physical and chemical properties, often adversely affecting electrical performance.[19,20] These examples highlight the importance of measuring and/or controlling atmospheric H_2O during the various steps of thin-film processing and measurement. While the importance of water in the context of chemical processes during *synthesis* has been previously reported, the effect of water vapor during *spin-processing* of aqueous solutions is virtually unreported. To our knowledge, there has been only one report focusing on the effect of humidity in the spin-coating chamber on the thickness of films made via spin-processing of aqueous solutions. This report demonstrated an inverse relationship between thickness and humidity for films of bone gelatin.[21]

Herein we report the impact of relative humidity during the spin-coating process on thickness of amorphous $HfO_{1.3}$ $(SO_4)_{0.7}$ (HafSOx) amorphous films deposited from all-inorganic aqueous precursors. In the humidity range studied, lower humidity yielded films of more than twice the thickness of those deposited with higher humidity using the identical precursor solution. The thickness difference persists as films are annealed. We use HAADF-STEM to examine the heavy atom density profiles of HafSOx films deposited under low and high humidities; while the overall heavy atom densities are

similar, the density profiles show subtle differences. Furthermore, we show that these results are general for metal oxide films deposited from aqueous solution. Film thicknesses of amorphous Al_2O_3 and $La_2Zr_2O_7$ deposited from aqueous precursors are also highly dependent on the relative humidity during spin coating and the thickness trends for all systems studied are similar to those derived empirically for the previously reported aqueous bone-gelatin thin films.

Experimental Section

Precursor Preparation

A modified method of the version used by Fairley et. al. was used for the preparation of 1.0 M HafSOx precursors.[22] 1.0 M H_2SO_4(aq) (VWR) and 30 wt % H_2O_2(aq) (EMD Millipore). $HfOCl_2 \cdot 8H_2O$ (Alfa, 98+ %, Zr < 1.5 %) in 18.2 MΩ·cm H_2O were used to prepare a solution with a Hf^{4+}:SO_4^{2-}:H_2O_2 ratio of 1.0 : 0.7 : 3.0. The solution was diluted to a combined [Hf^{4+}/$SO4^{2-}$] of 1.0 M.

Al_2O_3 precursors were prepared by using an electrochemical method described elsewhere.[23] Briefly, a reductive current was passed through a ~ 1.2 M $Al(NO_3)_3$(aq) (99.9% Alfa) solution until a pH of ~ 3 was achieved. Exact concentration was determined by slowly heating a 5 ml portion of the reduced solutions to 800 °C and obtaining the mass of the remaining Al_2O_3. The reduced Al_2O_3 precursor solution was diluted to 1.0 M [Al^{3+}] for deposition.

$La_2Zr_2O_7$ precursors were prepared by dissolving $La(NO_3)_3 \cdot 6H_2O$ (99.9 % Fisher) and $ZrO(NO_3)_2 \cdot 8H_2O$ (99.9 % Sigma) in H_2O to achieve a 1:1 La:Zr ratio and a total metal concentration of 1.0 M.

Thin-Film Deposition

N-type, P-doped silicon substrates (0.008-0.02 Ω·cm) were cut to approximately 1" x 1", sonicated for 10 min in a 5% in Decon Labs Contrad 70 solution and plasma cleaned for 5 min in a Plasma Etch, Inc. PE-50 Benchtop Plasma Cleaner using 30 % O_2/70 % N_2 and maximum power. Thin-films were prepared by depositing 7-8 drops of precursor through a 0.2 μm PTFE syringe filter onto a freshly cleaned silicon substrate. Precursors were allowed to rest on the substrate for 5-6 s before spin-coating at 3000 RPM for 30 s. For low relative humidities, the relative humidity during the spin-coating process was controlled by gently blowing air through the spin-coater chamber while taking care not to alter the air-flow around the sample during spinning. High relative humidities were achieved by filling the spin-coater trough with warm water. Relative humidity and temperatures in the spin coater were measured using a RH511 multimeter (Omega) immediately prior to solution deposition using conditions identical to those used for subsequent deposition. After spinning, films were transferred to a hot plate set to 50 °C then ramped at a rate of 12.5 °C·min^{-1} to 300 °C for 1 hr. Films for in-situ XRR measurements were immediately transferred to a hot-plate set to 50 °C and transferred to a preheated, temperature programmable XRR stage set to 50 °C. In-situ XRR measurements were recorded from 0 - 6 2theta with 0.016 ° increments and 1 sec/step then immediately ramped to the next temperature.

Results and Discussion

The impact of relative humidity on the resulting thickness of spin-cast films can be easily seen by eye, as shown in Figure. 1 for two films prepared using 1.0 M aqueous HafSOx precursors deposited under two different relative humidities (~ 22 % or ~ 75 %) while keeping temperature, spin-speed, acceleration time and solution composition constant.

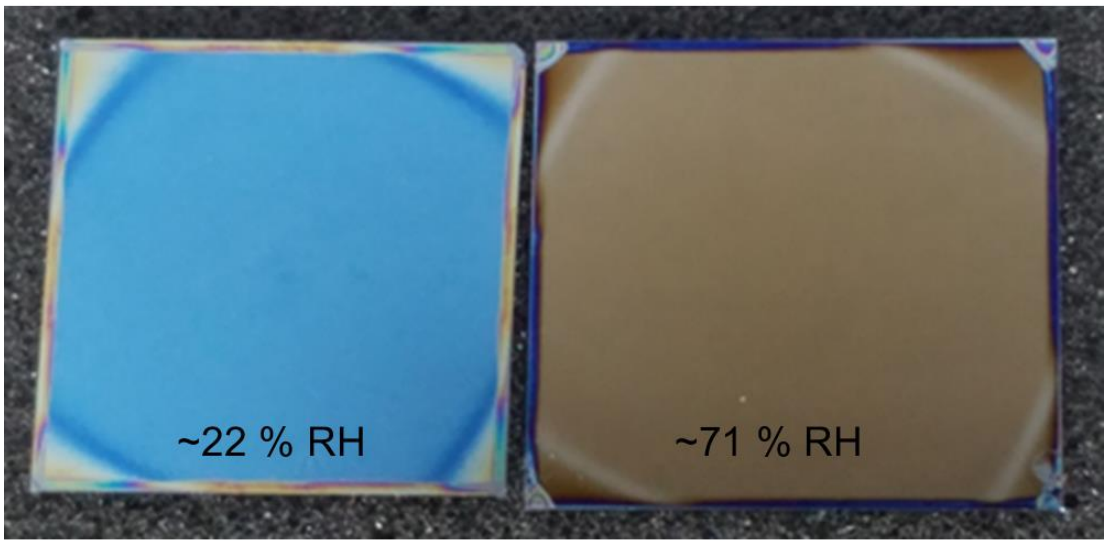

Figure 3.1. Pictures of as-deposited HafSOx thin films deposited at ~ 22 and ~ 71 % RH. The films thicknesses (by XRR) are 78 and 42 nm, respectively.

To investigate whether effects of relative humidity during deposition persist with annealing, thickness measurements were obtained at selected temperatures via X-ray reflectivity (XRR) as the HafSOx films were heated in-situ. While the films deposited at 22 and 75 % RH have very different initial thicknesses, similar trends are observed upon heating. For both films, the critical angle (corresponding to the angle of maximum intensity) shifts towards higher angle (Figure 2), indicating increasing density with

heating. Simultaneously, the Kiessig fringe spacing increases, indicating a decrease in thickness with heating.

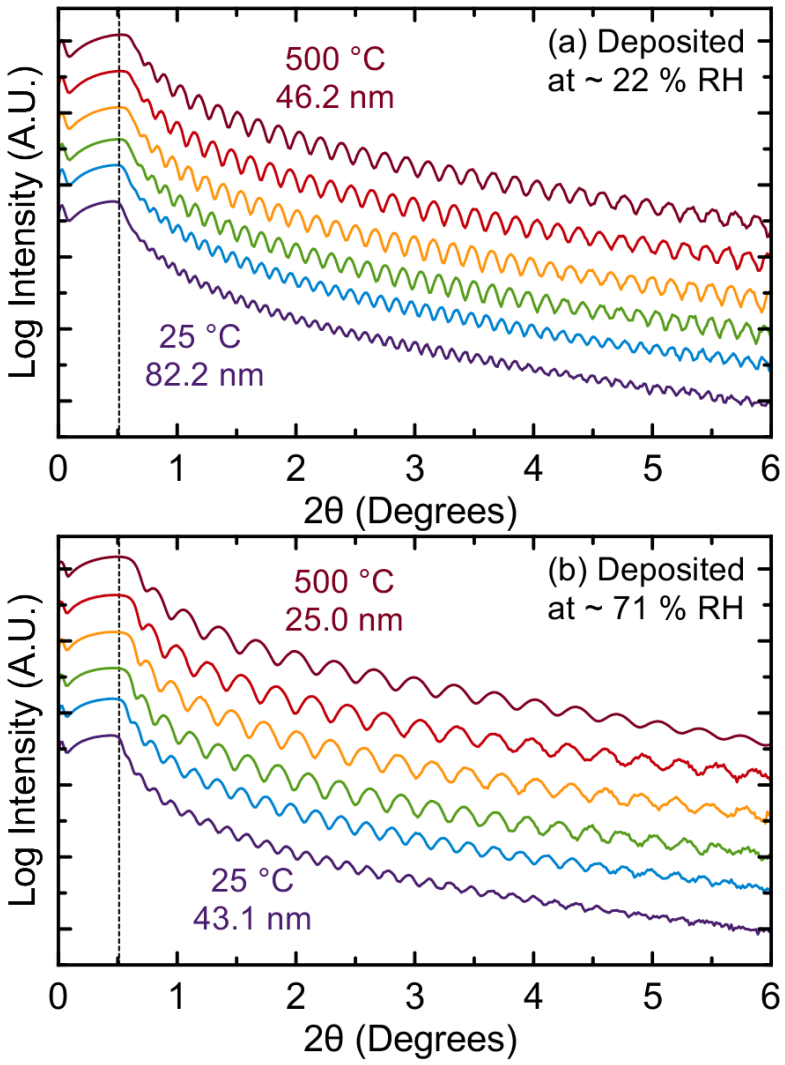

Figure 3.2. XRR of HafSOx films deposited at ~ 22 % (a) and ~ 75 % (b) RH as a function of processing temperature (RT, 100 °C, 200 °C, 300 °C, 400 °C and 500 °C).

As processing temperatures increase, both films become thinner, but the ratio of their thicknesses remains essentially constant (Figure 3). This implies that humidity primarily influences the quantity of material deposited on the substrate. Furthermore, in the ranges

studied here, deposition RH and consequent thickness do not alter the temperatures at which the films densify.

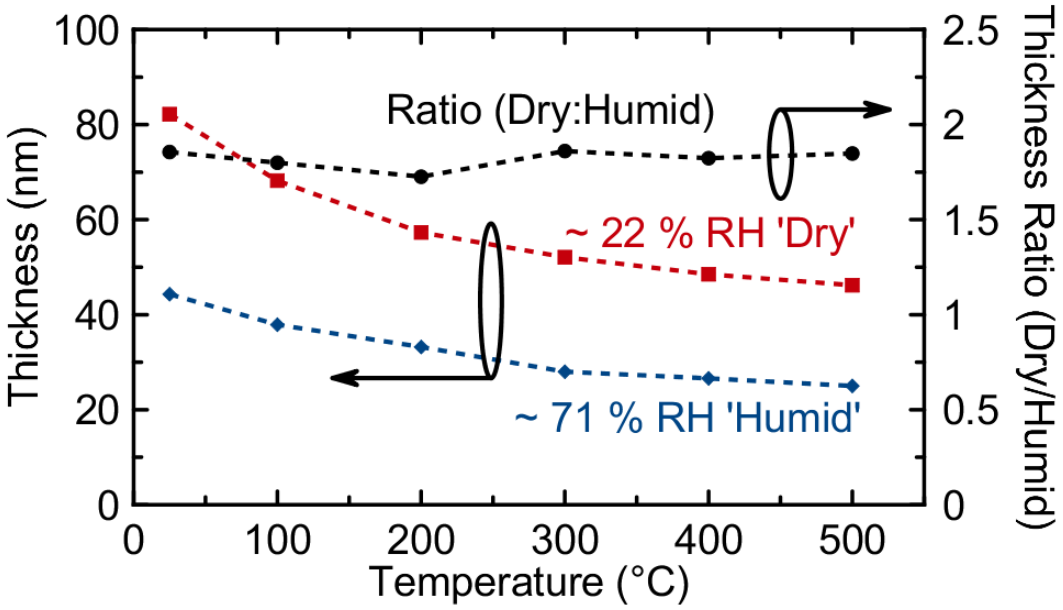

Figure 3.3. Thickness comparison of HafSOx films deposited at ~ 22 and ~ 75 % RH.

A recent report on aqueous-deposited HafSOx films demonstrates that spin-processing produces films with inhomogeneous chemical and density profiles, accentuated with a denser, hafnium-rich surface layer.[22] This previous study did not measure or control humidity. To determine whether humidity would affect the density profile of these films, we examined films spin-processed under different humidities using HAADF-STEM (Figure 4a, b). The HAADF-STEM images reveal that films deposited at either humidity exhibit a gradual decrease in heavy atom density (corresponding to brightness in the images) from the bottom to the top of the films. Furthermore, films deposited under both conditions have thin and relatively high-density layers at their surfaces. However, a steeper density profile and more pronounced ‘crust’ is observed in the film deposited at

higher relative humidity, which can be more easily seen in the integrated intensity profiles from the HAADF-STEM images (Figure 4c).

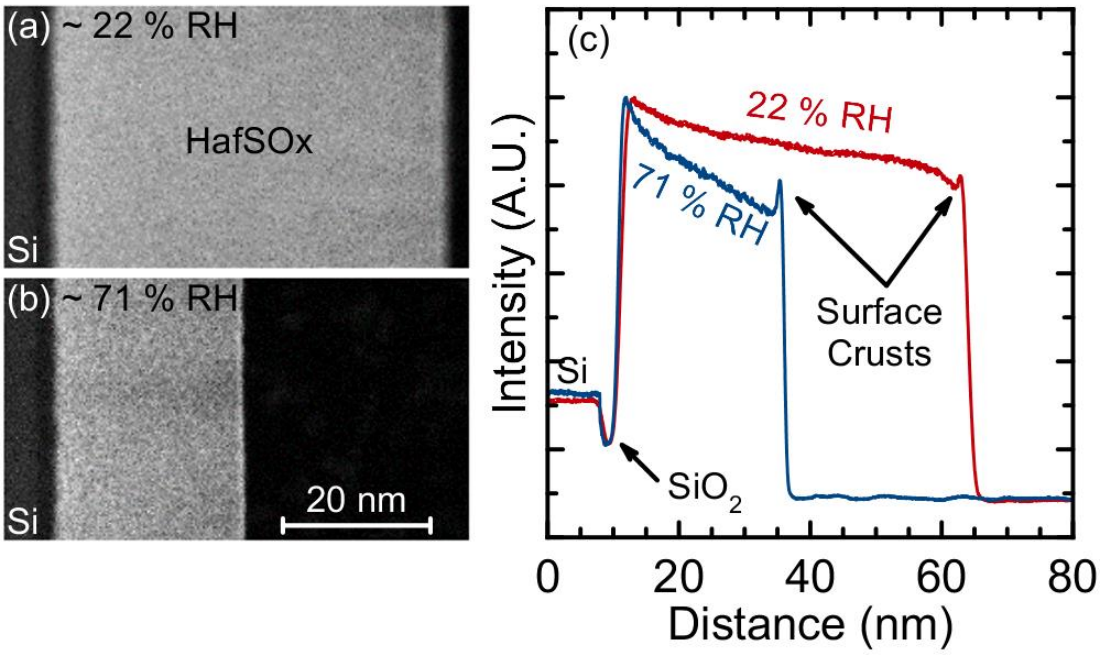

Figure 3.4. HAADF-STEM images of HafSOx films deposited at 22 % RH (a) and 71 % RH (b). Heavy-atom density profiles derived from HAADF-STEM images (c).

The spin-coating process can be described by two partially overlapping processes. The first process, spin-off, involves physical 'thinning' of the solution adhered to the substrate as centrifugal force removes excess solution from the rapidly spinning substrate.[23,24] The second process is evaporation, in which the precursor is concentrated, in many cases to a viscous gel state. [23] The amount of precursor solution (or gel) retained on the substrate is determined by the viscosity of the solution and surface-solution interactions. In the second process, evaporation serves to both concentrate and to cool the precursor film, both of which will result in an increase in the viscosity, yielding a thicker film. Because evaporation rates are proportional to (100-RH%),[24] at low RH, the evaporation rate is

high, resulting in higher concentrations and lower temperatures. At high RH, evaporation rates are slower, so the concentrations remain lower and the temperatures higher than at low RH. The resulting differences in viscosity cause the observed differences in film thickness.

To investigate the generality of relative humidity affecting thickness, experiments were also performed on two other aqueous-deposited metal oxide systems ($La_2Zr_2O_7$, Al_2O_3). Films were prepared by spinning 1.0 M solutions of aqueous precursors for these systems (as well as HafSOx) at four different relative humidities between 20 and 95 %, followed by annealing at 300 °C (Figure 5). The 300 °C processing temperature was chosen because LZO and Al2O3 films are difficult to study as-deposited (water absorption and dewetting are issues). Because the HafSOx study indicated the thickness of thermally processed films track those of as-deposited films, comparing films heated to the same temperature should allow a valid comparison. By heating to 300°C, most of the nitrate counterions are removed (in contrast to the sulfate counterions which persist).[25]

The films deposited from these three aqueous precursor solutions display very similar thicknesses and similar dependence on the relative humidity during spin depositions (Figure 5). Because all precursor solutions were 1.0 M in total metals (or in metal and sulfate ions in the case of HafSOx), this suggests that, to a first approximation, the total concentration of metal cations determines the resulting film thickness for a given humidity and thermal treatment.

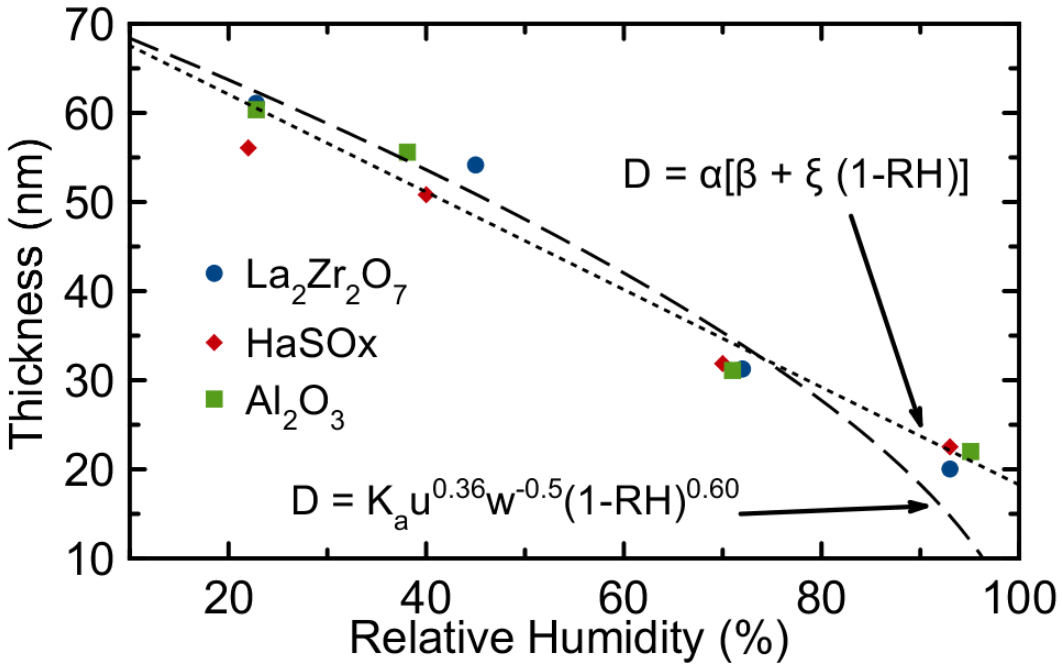

Figure 3.5. Thickness vs Spin RH for Al_2O_3, HafSOx, and $La_2Zr_2O_7$ derived from aqueous precursors. Empirically-derived trend of thickness vs RH represented by dashed line. Solid line is a linear fit to the data.

In the previous study on bone gelatin, the authors derived an empirical relationship between humidity and film thickness (shown as dashed line in Fig. 5):,

$$D = K_a \mu^{0.36} \omega^{-0.5} (1\text{-}RH)^{0.6} \qquad (1)$$

where D is thickness in nm, K_a is the concentration, ω is the angular velocity during deposition and RH is the fractional relative humidity. The numerical values for the exponents were adjustable parameters used to fit the effect of humidity on thickness of polymeric 'bone-gelatin' films.[21] Equation (1) has the unphysical result that film thickness is zero at 100% humidity and there is no physical meaning to the empirical relationship or the value of the fitted parameters.

We have fitted our results to a linear relationship (shown as solid line in Fig. 5):

$$D = \alpha[\beta + \xi (1\text{-}RH)] \qquad (2)$$

Where α is proportional to the concentration of the initial solution and inversely proportional to the square root of the spin speed. The strength of the substrate-solution interaction (wetting) and the surface tension of the solution probably also affect the value of α, although the dependence of the thickness on these parameters has not been well documented in the literature. β is the viscosity of the initial solution at ambient temperature. The temperature of the solution on the substrate during spin coating will be the ambient temperature at 100% relative humidity since the evaporation rate is zero. ξ is a term that describes the change in the viscosity of the solution as a function of (1-RH), which is proportional to the evaporation rate.[25] Evaporative cooling during spin-deposition can account for a factor of two change in the viscosity, as the viscosity of pure water changes by a factor of ~2 in the temperature range of 5 to 25 °C.[26] Concentration increases due to evaporation will increase the viscosity further. Qualitatively, at low deposition RH, cooling and concentration of the solution from rapid evaporation rates increases the viscosity of the remaining solution on the substrate significantly leading to thicker films. Conversely, deposition at high RH (corresponding to low evaporation rates, and thus lower viscosity) will yield thinner films. Equation (2) is an oversimplification, since the magnitude of the temperature change with evaporation rate will depend on the thermal conductivity of the various components (solution, the substrate and the spin coater chuck, their thicknesses and the thermal impedance of the interfaces between them), and the temperature dependence of the viscosity of H_2O is not linear.[26] Within the uncertainty of our data, however this expression fits the thickness trend seen in Fig. 5 better than the previous empirical relationship, and provides some insights to parameters

that impact ξ. The dramatic changes in thickness as a function of humidity highlight that this must be controlled during processing to obtain reproducible thicknesses.

Conclusions

In this study, the effect of relative humidity during spin-deposition of all-inorganic aqueous precursors showed that increasing relative humidity resulted in thinner films (all other conditions kept constant). The thicknesses of films derived from the three different 1.0 M aqueous metal oxide precursors were very similar for a given set of processing conditions. This indicates that the properties of the water solution (e.g. viscosity and evaporation rate) likely govern the processes occurring during spin coating from aqueous precursors that determine film thickness.

This is the first report focused on the impacts of relative humidity during spin deposition of aqueous-derived metal-oxide thin films. The observed thickness change with relative humidity can be fit to an equation linear in (1-RH), highlighting the importance of evaporation rate in controlling the thickness of spin-cast films. Although this report focuses on the importance of relative humidity during the spin deposition, the rate of water loss upon annealing also likely plays an important role in the chemical reactions that occur during film densification, and humidity may be important in these processes as well.

Bridge

Chapter III focused of the presence of $H_2O(g)$ during spin-deposition of metal-oxide from aqueous precursors. Under high-humidity deposition conditions restricted evaporation, limiting the viscosity increase that would result from increased concentration or evaporative cooling. The lower viscosity under humid conditions results in thinner films. The differing evolution of viscosity for precursor films spinning under low and high relative humidities also correlates to differences in the density profiles of the resulting thin films, as demonstrated with HafSOx.

Water is also involved in the chemical processes that occur as thin films of precursors are thermally converted to thin film metal oxides. Water is released during solvent evaporation, may aid in the release of counterions, and is a by-product of metal hydroxide condensation to the metal oxide. Maintaining a high partial-pressure of $H_2O(g)$ should, in principle, shift the equilibrium of each of these processes. Chapter IV investigates the effects of $H_2O(g)$ during the thermal conversion of precursor thin films to metal oxide thin films and shows that H_2O plays a role that is much more complex than simply as a convenient solvent.

CHAPTER IV

THE EFFECTS OF ANNEALING ATMOSPHERE HUMIDITY ON METAL OXIDE THIN FILM FORMATION FROM AQUEOUS SOLUTION

Significant portions of lab-work, data collection, data analysis, and writing were performed by Keenan N. Woods. Deok-Hie Park performed TPD experiments and analysis. Editorial assistance was provided by Catherine J. Page and Douglas A. Keszler.

Introduction

Amorphous metal oxide thin films are central to a wide range of technological applications, and mass production of thin film-based electronic materials has fueled interest in developing low-cost deposition methods. Vacuum-based deposition techniques produce high quality (dense, homogenous, atomically smooth) films,[1–4] but require expensive equipment, complex precursors, and large energy inputs. In contrast, solution-deposition techniques are relatively simple and offer scalable, inexpensive routes to thin-film materials.[5–8]

Sol-gel synthesis, and similar routes utilizing organic stabilizers and solvents, have dominated thin-film solution-deposition.[7–15] These deposition routes can lead to porosity, roughness, cracking, and residual carbon contamination in thin films, but proper adjustment of the precursor chemistry and processing conditions allow for the production of high-quality thin films.[16] However, sol-gel chemistry often relies on toxic solvents and

expensive precursors.[17,18] Aqueous, all-inorganic deposition methods avoid the need for organic additives and solvents, while also producing high-quality films.

The simplest aqueous deposition routes utilize metal nitrate and chloride salts dissolved in water.[19–27] An alternate aqueous paradigm is the "Prompt Inorganic Condensation" (PIC) method, which employs inorganic metal clusters as a pre-condensed oxide species to promote facile condensation to the final metal oxides of interest.[28–36] In comparison to simple salt solutions, the number of counterions in solution for PIC routes is reduced, which aids in the condensation and densification of the metal oxide network and enables the formation of smooth, dense films at relatively low processing temperatures.

In all of these solution deposition techniques, water is a key component in the film formation process. This is true especially for sol-gel routes involving metal alkoxides, which must be hydrolyzed to metal hydroxides for subsequent condensation to form the metal oxide network. It should therefore not be surprising that annealing sol-gel derived films in the presence of water vapor aids in complete hydrolysis and formation of the oxide.[8,37,38] Indeed, a similar effect is observed for bulk powders derived from acetylacetonate and organometallic precursors.[39–41] However, in the case of aqueous-derived metal oxides, it might be expected that the presence of water vapor in the annealing atmosphere would impede oxide formation because aqueous precursors are already hydrolyzed and condensation to the oxide requires removal of water. Additionally, the presence of water vapor should limit evaporation of the aqueous solvent.

We report the surprising result that increasing the humidity in the annealing atmosphere dramatically lowers the temperature of water and nitrate removal for aqueous-deposited thin films. This appears to be a general effect and we show that ZnO, Al_2O_3, and lanthanum zirconium oxide (LZO) films are more fully condensed when annealed under "humid" annealing atmospheres compared to films annealed under ambient "dry" conditions. In the case of chloride-containing LZO films, void formation is observed after thermal processing in a dry atmosphere. Remarkably, annealing in a humid atmosphere prevents void formation and residual counterion content is significantly reduce. We show that void formation is also suppressed by adjusting precursor concentration and annealing ramp rate for dry-annealed films. The results from this study on film morphology and chemistry provides general insight into film formation processes for metal oxide thin films from aqueous precursors.

Experimental Methods

Precursor and Solution Synthesis

1.8 M ZnO and 1.8 M Al precursor solutions were prepared from $Zn(NO_3)_2 \cdot 6H_2O$ (Sigma-Aldrich, ≥ 99.0%) and $Al(NO_3)_3 \cdot 9H_2O$ (Alfa Aesar, 98.0-102.0%), respectively, in 18.2 MΩ cm Millipore H_2O. Lanthanum zirconium oxide (LZO) thin films were deposited from a 0.5, 1.0, 1.5, or 1.8 M (total metal, 1:1 La:Zr) solutions synthesized from dissolving $La(NO_3)_3 \cdot 6H_2O$ (Alfa Aesar, 99.9%) and $ZrOCl_2 \cdot 8H_2O$ (Sigma-Aldrich, 99%) in 18.2 MΩ cm Millipore H_2O. All solutions were filtered through 0.45 μm PTFE syringe filters.

Thin Film Synthesis

Si substrates (2 cm^2) were sonicated in 5% Decon Labs Contrad-70 solution for 5 min, thoroughly rinsed with 18.2 MΩ cm Millipore H_2O, and spin-dried using a spin-coater. Substrates were then exposed to a 1 min O_2/N_2 plasma etch using a Plasma Etch, Inc. PE-50 Benchtop Plasma Cleaner set to maximum power. Substrates were then rinsed with 18.2 MΩ cm Millipore H_2O and spin-dried before film deposition. This treatment ensured a highly hydrophilic substrate surface for good solution wetting.[42] Samples prepared for Fourier transform infrared (FTIR) spectroscopy and thermal programmed desorption (TPD) analysis were deposited on lightly-doped double-side polished p-type Si substrates. Samples for TPD analysis were deposited on 1 in^2 substrates and physically cleaved into 1 mm^2 samples.

ZnO, Al_2O_3, and LZO precursor solutions were filtered through a 0.2 μm PTFE syringe filter onto prepared Si substrates and spin-cast at 3000 RPM for 30 s. Samples were then immediately transferred to a pre-heated heating stage at 125 °C and annealed under either a "dry" or "humid" annealing atmosphere. "Dry"-annealed samples were annealed on a custom-built hotplate under ambient laboratory atmosphere (~45% RH at RT). "Humid"-annealed samples were annealed in a tube furnace equipped with a removable heating stage and a water vaporizer. Both hotplate and heating stage were equipped with a PID controller to offer careful control of annealing temperature and ramp rate. All samples were annealed using a ramp rate of 25 °C min^{-1}, unless otherwise noted. Samples were annealed at their final annealing temperature for 1 h.

Thin Film Characterization

Water and residual counterion content was probed via FTIR and TPD analysis. FTIR spectra were collected using a Thermo Fisher Nicolet 6700 spectrometer, using the spectrum collected from a bare, Si substrate heated to match the thermal processing of each sample for background subtraction. TPD analysis was conducted using Temperature programmed desorption mass spectrometry (TPD-MS) study under ultrahigh vacuum (UHV) was performed using the TPD Workstation (Hiden Analytical) with a quadrupole mass analyzer (3F PIC, Hiden Analytical). The base pressure was $< 5 \times 10^{-9}$ Torr. The thin film samples on doubly polished Si substrates, which were cleaved to 1 x 1 cm^2, were heated from room temperature to 900 °C at the heating rate of 30 °C/min. Electron impact (EI) mass spectra were acquired with a 70 eV ionization energy and 20 μA emission current. Selected mass-to-charge (m/z) ratios (m/z 18, 30, and 32 for H_2O, NO, and O_2, respectively) for each sample were monitored in multiple ion detection (MID) mode with a dwell time of 200 ms and a settle time of 50 ms.

X-ray reflectivity (XRR) was conducted using a Rigaku SmartLab diffractometer (Cu Kα radiation, 40 kV and 44 mA). Cross-sectional scanning electron microscopy (SEM) using a FEI Helios Dual Beam FIB was performed on samples coated with thermally evaporated Al to prevent charging during imaging (5.0 keV accelerating voltage, 86 pA current).[43]

Results and Discussion

The effect on the chemical evolution of films derived from ZnO, AlOx and LZO aqueous precursors was probed using FTIR (Figure 1). In comparison with films annealed under ambient "dry" laboratory humidity, films annealed under "humid" conditions had reduced water and/or nitrate content (indicated by the shoulder at 1650 cm^{-1} and the peak at 3500 cm^{-1} for water and by peaks at 1280 cm^{-1} and 1460 cm^{-1} for nitrate).[44–47] This effect was most pronounced in the case of films deposited from $Zn(NO_3)_2$ precursors (Figure 1a), with all water and nitrate removed by 150 °C under humid annealing conditions (Figure 1a), but was less pronounced in the case of films derived from $Al(NO_3)_3$ precursors (Figure 1b). LZO films demonstrated a moderate decrease in nitrate content, although water content appeared to remain approximately the same regardless of annealing atmosphere (Figure 1c). Overall, the data indicate that films annealed under humid conditions generally have expelled more counterions and condensation byproducts at lower temperatures comparatively. Indeed, peaks indicative of hydrated metal salts for the LZO films (1000 cm^{-1} and ~800 cm^{-1})[47,48] are significantly diminished for films annealed under humid conditions. Furthermore, films annealed under a humid atmosphere at low temperatures are significantly more stable with respect to water reabsorption than films annealed under dry atmosphere at the same temperature (Figure 2). This suggests that oxide formation is more complete, at least at the surface of the film for the humid-annealed film.

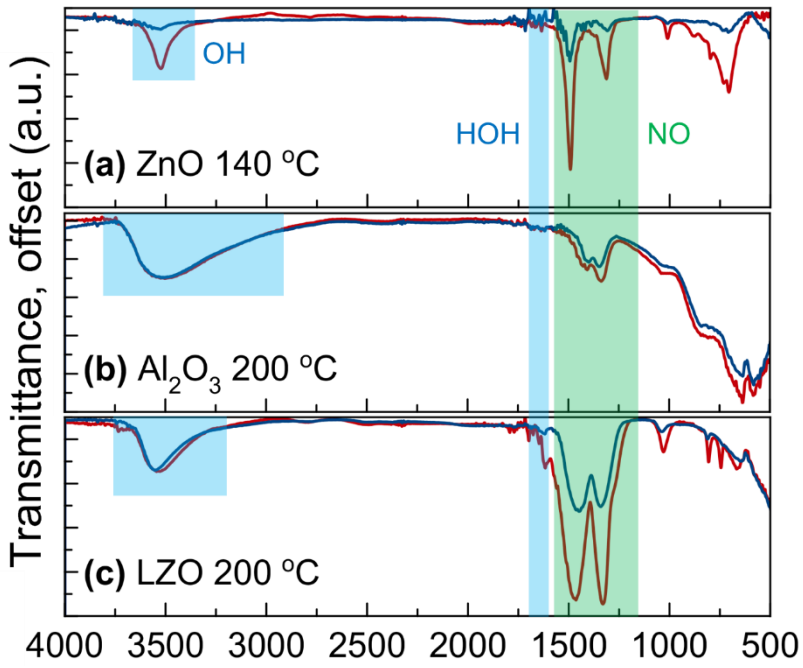

Figure 4.1. FTIR spectra of (a) ZnO, (b) Al_2O_3, and (c) LZO films deposited from aqueous precursors and annealed under dry- (red) or humid (blue) conditions.

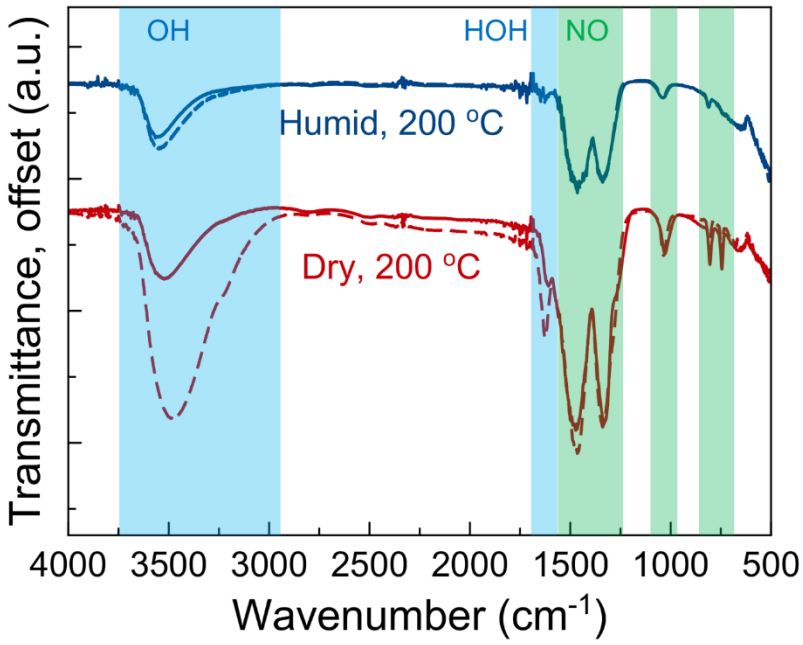

Figure 4.2. FTIR spectra of LZO films taken immediately after annealing under humid (blue) and dry (red) atmospheres and spectra taken after 1 h in ambient lab air (~45% RH, dashed lines).

The morphology of $La_2Zr_2O_7$ (LZO) thin films was examined by cross-sectional SEM (Figure 3). The SEM images of dry-annealed films (Figure 3a) reveal a porous region in the lower region of the film capped by a continuous, dense surface layer. A thin, continuous layer of material can also be seen at the LZO/Si interface, indicating that the film porosity in not caused by dewetting of the precursor solution. Interestingly, the surface morphology of the dry-annealed film is not compromised by this porosity and film roughness is < 1 nm by XRR. Remarkably, films annealed under humid conditions were observed to be uniform and homogenous with no signs of porosity (Figure 3b).

TPD measurements of films annealed at 200 °C under dry and humid atmospheres corroborate the FTIR data and offer additional insight into the underlying chemistry of oxide formation (Figure 4). The humid-annealed film loses much less water on heating (Figure 4a), suggesting that the water content in this film is much lower. It should be noted that both films measured were exposed to ambient atmosphere prior to the TPD measurements, and so larger quantity of water in the dry-annealed film may be due in part to water reabsorption (Figure 2). The NO and O_2 traces (Figure 4b and Figure 4c, respectively) are attributed to residual NO_3^- released from the film.[49,50] The two distinct mass loss events in the NO trace for the dry annealed film, indicated by the broad and sharp peaks, is consistent with the release of unbound and bound NO_3^- species, respectively. The NO and O_2 traces for the humid annealed films are dominated by the sharp feature at higher temperatures, indicating that most of the NO_3^- has been removed during the 200 °C anneal and only strongly bound NO_3^- remains. Moreover, dry-annealed films contain detectable levels of Cl, while humid-annealed films do not (Figure 4d). We postulate that trapped HCl gas generated by decomposition of chloride-containing $ZrOCl_2$

precursor may be responsible for film porosity (Figure 3a). Indeed, films deposited from all-nitrate containing solutions in ambient atmosphere do not show porosity and are currently under investigation as dielectric components for TFT devices. Although the void formation appears to be specific to films made using the chloride-containing precursor under dry conditions, they provide a useful probe for investigating the competing effects of film condensation and counterion thermal decomposition and diffusion.

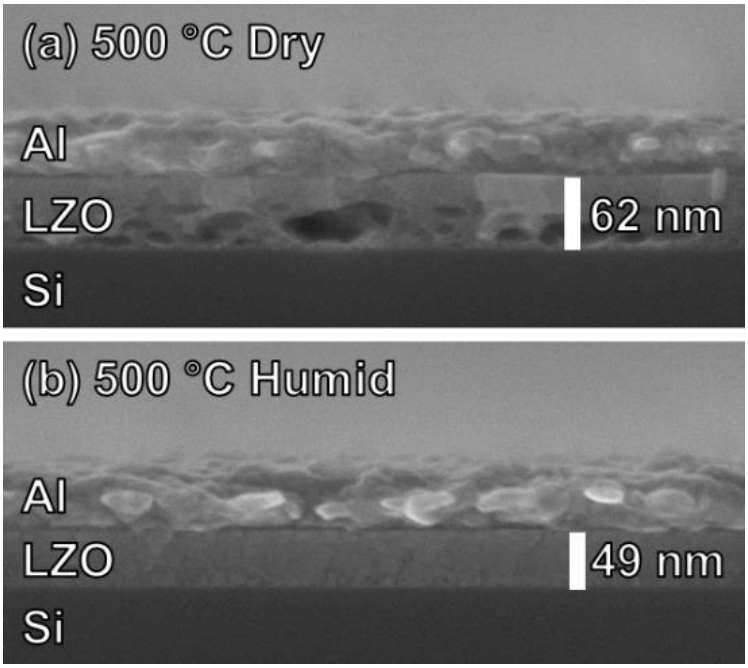

Figure 4.3. SEM images of LZO films from a 1.5 M solution annealed at 500 °C under (a) an ambient "dry" atmosphere and (b) humid conditions.

In general, the thermal conversion of metal salts to metal oxide films requires the decomposition and expulsion of water and counterion species. In order to be removed from the film, these byproducts must diffuse to the film surface. Based on the SEM

image of dry-annealed LZO films in Figure 3a, it appears there may be a limit to the distance that gaseous species can diffuse to escape through the film surface. This distance appears to be on the order of 20 nm, since the top portion of the film is dense and pore-free. To test this hypothesis, we examined films of different thicknesses (deposited from different precursor solution concentrations[51]). SEM images of these films (Figure 5) show that the porosity is effectively eliminated in the thinnest film. Interestingly, the dense, pore-free surface region in all of the thicker films is approximately the same thickness (~ 20 nm).

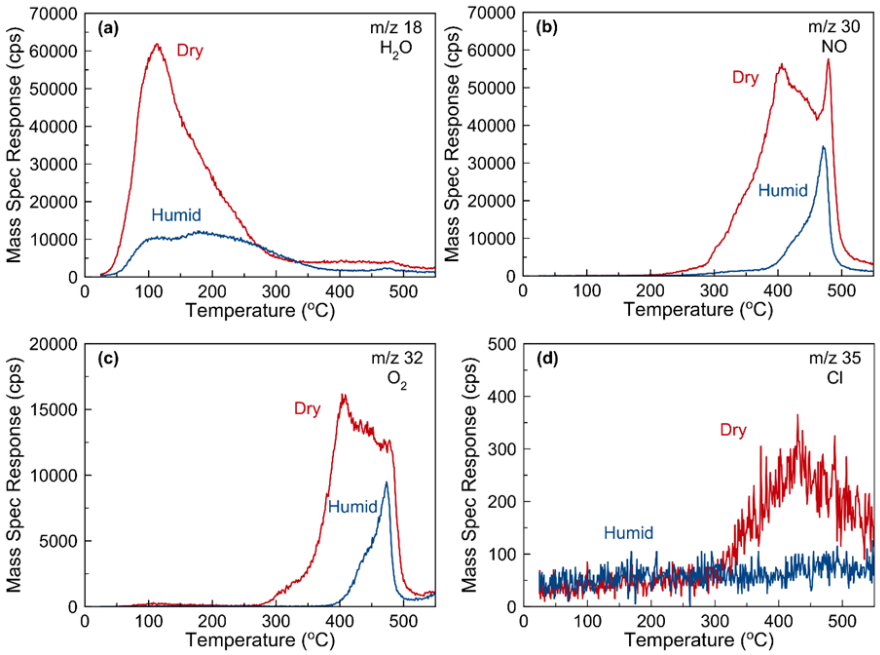

Figure 4.4. TPD of dry- (red) and humid-annealed (blue) LZO films deposited from a 1.5 M solution: (a) m/z 18, (b) m/z 30, (c) m/z 32, and (d) m/z 35.

It is possible that a dense surface layer forms early in the film formation process, which inhibits diffusion and removal of gaseous byproducts from the interior of the film. Therefore, film morphology will be dependent on the rate of formation of this surface layer relative to the rates of the thermal decomposition of counterions and diffusion of their byproducts. We investigated the dependence of film morphology on annealing ramp rate, which should affect both film condensation and byproduct diffusion. SEM images of films annealed to 500 °C at three different ramp rates show that a reduced ramp rate results in reduced film porosity (Figure 6). The thickness of the dense, pore-free capping layer appears to increase as the ramp rate decreases, indicating that gaseous byproducts can escape more readily and from deeper within the film. A small degree of porosity can still be observed in the film annealed using the slowest ramp rate, indicating that some byproducts are trapped even with the slower rate.

As described above, we postulate that the final structure of the LZO thin films can be explained by considering the simultaneously occurring processes of film densification and byproduct generation, diffusion, and expulsion (Scheme 1). At high ramp rates, the byproduct-diffusion rates are outpaced by the film densification rate. In this scenario, the diffusion lengths are less than the film thickness, and counterion decomposition byproducts can escape only from the surface region. The trapped byproducts enter the gas phase and result in pore formation. Reducing the ramp rate results in a balance between diffusion and densification, and byproducts can leave the film before significant densification of the metal-oxide network occurs.

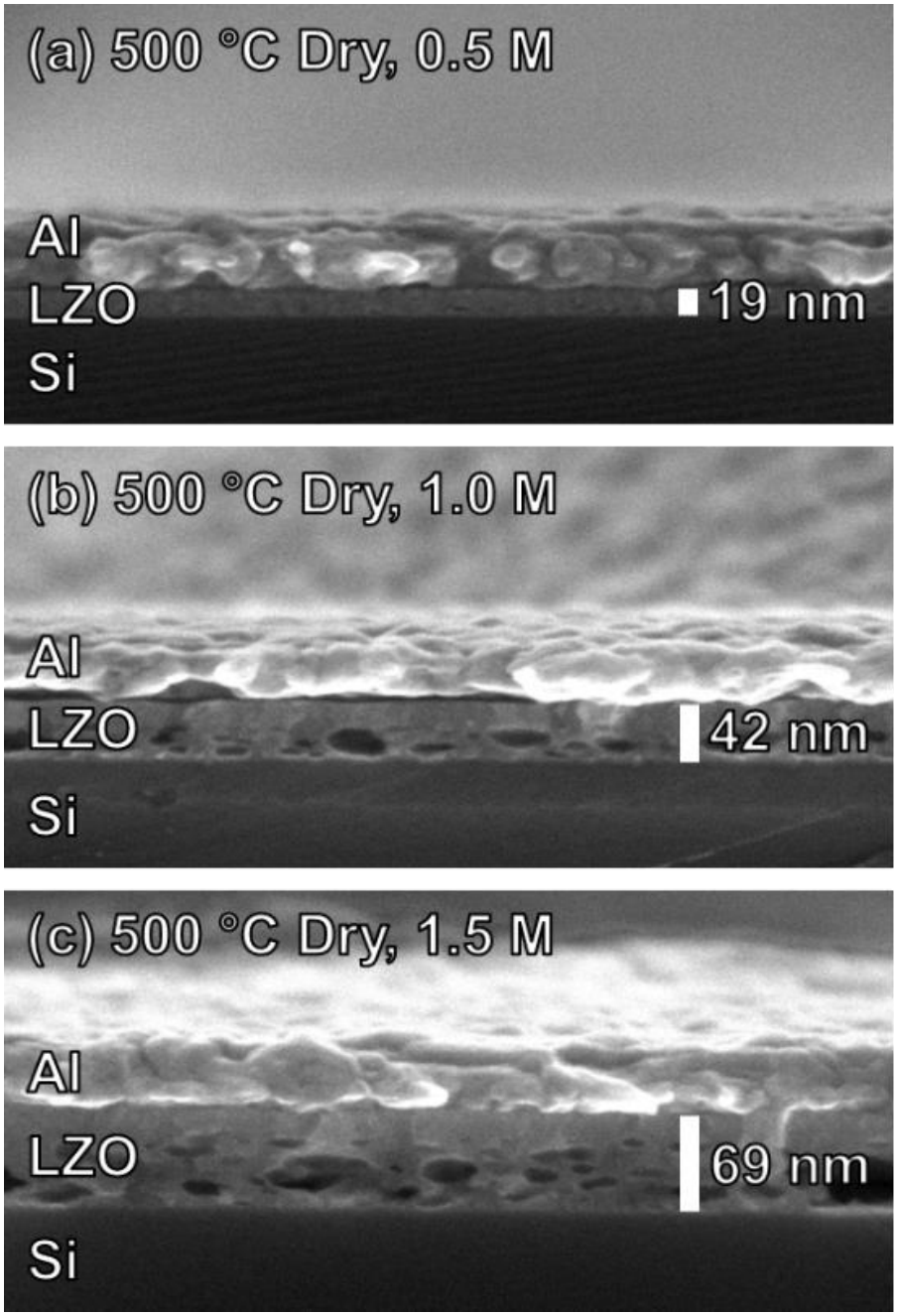

Figure 4.5. SEM images of LZO films deposited from (a) 0.5, (b) 1.0, and (c) 1.5 M solutions annealed at 500 °C under dry conditions.

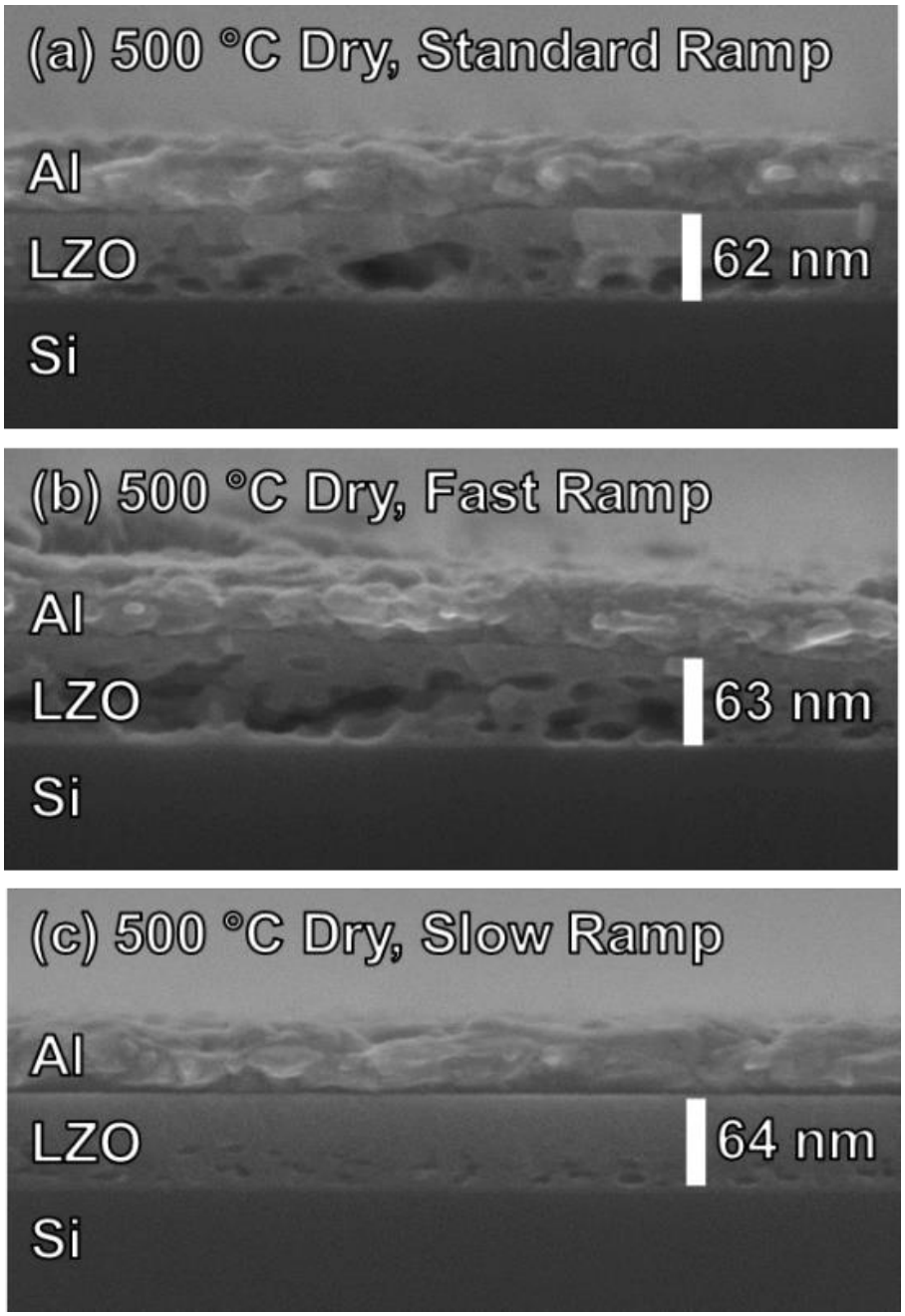

Figure 4.6. SEM images of LZO films annealed at 500 °C under dry conditions using (a) standard (25 °C min^{-1}), (b) fast (125 °C min^{-1}), and (c) slow ramps (0.25 °C min^{-1}).

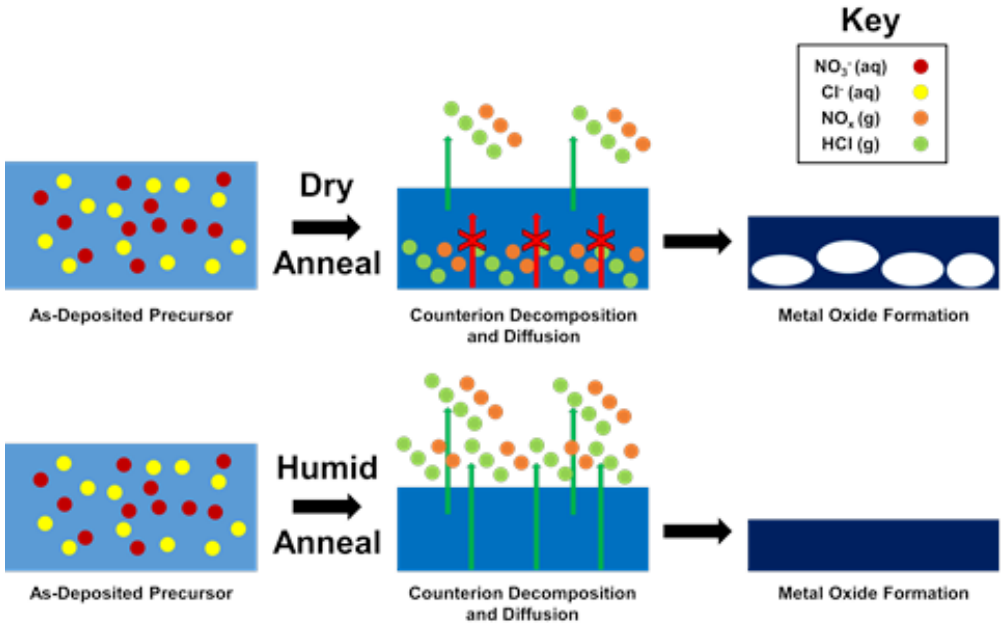

Scheme 4.1. A cartoon representation of the formation of LZO films under dry and humid conditions illustrating the competing processes of film densification and byproduct generation, diffusion, and expulsion.

Introduction of H_2O to the annealing atmosphere prevents pore formation at all ramp rates and thicknesses investigated. The FTIR and TPD data suggest that the rates of the chemical processes leading to byproduct release are increased with the addition of H_2O to the annealing atmosphere. We propose that the high H_2O partial pressures during annealing causes a retention of a more hydrated inner-sphere of Zr and La cations up to higher annealing temperatures, preventing nitrate and chloride binding in the inner coordination sphere of the metal cations and facilitating loss of counterions. This hypothesis is supported by previous studies, which show that decomposition temperatures of metal nitrate salts are lowered with increased levels of inner-sphere hydration.[26]

Counterion removal may also be assisted under humid annealing conditions by vaporization of nitric acid/water and HCl/water azeotropes (68% HNO_3/32% H_2O and 20% HCl/80% H_2O, which boil at 120 °C and 110 °C, respectively). Because evaporation of water from the surface is rapid under dry conditions, maintaining a vapor pressure of water above the surface may enable azeotrope formation to provide an alternative low-temperature pathway for counterion removal (in addition to thermal decomposition). This is consistent with the TPD data, which shows reduced NO content and no chloride in the humid annealed LZO films.

Additionally, humid annealing conditions may enhance diffusion of decomposition byproducts by suppressing the condensation reaction to form metal oxides, illustrated by *Eq. 1*.

Eq. 1. $\text{M-OH} + \text{HO-M} \leftrightarrow \text{M-O-M} + H_2O$

In principle, condensation byproducts should be able to diffuse to the surface more readily in a hydroxylated, less condensed network, resulting in more facile counterion removal.

Conclusions

We report a surprising and dramatic effect of annealing atmosphere humidity on metal oxide thin film formation from aqueous precursor solutions. Residual water and nitrate counterion content is lower in a variety of metal oxide films annealed under humid conditions compared to films annealed under ambient annealing atmospheres. While this

result appears to be general, we show that in the case of LZO films, humid annealing results in increased film stability relative to reabsorption of water. Additionally, humid annealing eliminates pore formation observed in dry-annealed chloride-containing LZO films, attributed to trapped gaseous byproducts. We postulate that the presence of water in the annealing atmosphere increases the degree of hydration of the metal cations (preventing nitrate binding), facilitates removal of nitrate and chloride through the water/acid azeotropes of these species, and slows the condensation of a dense metal oxide network to allow better diffusion and expulsion of byproduct species. These studies show that humidity during annealing affects the temperatures and chemical pathways for decomposition of spin-cast gels from aqueous solutions, and suggest a promising avenue for producing a variety of high-quality, dense metal oxide films at low processing temperatures.

Bridge

Chapters III and IV demonstrated that the presence of $H_2O(g)$ during deposition and heating of aqueous precursors can have significant impacts on both the chemical and physical characteristics of the resulting metal-oxide thin films. Chapter IV also highlighted the importance of diffusion of byproducts through the forming metal-oxide thin film and their release (or trapping) during thin-film formation. We demonstrated that the maintained presence of significant $H_2O(g)$ during annealing at high temperatures facilitates counterion loss and prevents pore formation in $La_2Zr_2O_7$ films. Under dry annealing conditions, nonporous films can be deposited, but only if they are deposited with slow ramp rates or from low concentration precursors (corresponding to thinner films). This finding suggests that either byproducts can diffuse rapidly enough from the upper several nanometers of a film to prevent pore formation or that dilution of the precursors results in an alternate and less destructive conversion to the resulting metal oxide. Chapter V investigates the impact that precursor concentration has on the evolution of precursor thin films as they are thermally processed. The findings in Chapter V suggest byproducts can escape from thinner films (deposited from more dilute precursors) at lower temperatures. We also show that dilution impacts the precursor solution speciation, influencing the degree of nitrate binding in the inner coordination of metal ion precursors, which has previously been shown to affect the thermal degradation of metal salts. Results from our studies are intriguing, and suggest that thinner films deposited from low concentration solutions densify at lower temperatures both because byproduct diffusion pathways are shorter and possibly also because precursor speciation influences the decomposition pathways.

CHAPTER V

THE EFFECTS OF CONCENTRATION ON THE CHEMICAL EVOLUTION OF AQUEOUS DEPOSITED LANTHANUM ZIRCONIUM OXIDE THIN FILMS

Keenan N. Woods collected and analyzed TGA data. Deok-Hie Park performed TPD experiments and analysis. Editorial assistance was provided by Catherine J. Page and Douglas A. Keszler.

Introduction

The advent of smart phones, tablets, touch screens and other display technologies has fueled intense interest in new processes for the deposition of metal oxide thin films and the fabrication of TFTs. Currently, most of the metal oxides for these devices are deposited using vacuum-based techniques which, although they produce excellent materials, are energy intensive, costly, and waste a large fraction of the deposition material. Deposition from solution addresses many of the issues associated with vacuum-based deposition, and in many cases produces thin films with properties comparable to those deposited using vacuum techniques.[1-5]

Solution deposition methods can be categorized according to precursors chemistry and by the method employed for film deposition. Precursor chemistry ranges from use of reactive metal alkoxides dissolved in organic solvents to less reactive metal salts dissolved in organic solvents or or water. Sol-gel precursor solutions containing metal alkoxides, tend to be unstable with respect to hydrolysis and condensation, and decomposition to metal oxides generally occurs at reduced processing temperatures.[6-9]

However, trapped byproducts of the hydrolysis and condensation processes, and the significant volume losses incurred by ligand expulsion can have adverse effects on the resulting thin-film morphology and electrical properties.[10, 11] Less reactive precursors dissolved in organic solvents and/or using organic stabilizers have also been employed with varying degrees of success.[12-14] In these cases, the precursors are usually dissolved in toxic and relatively expensive solvents such as 2-methoxyethanol. Recent efforts by our group and others have demonstrated that much simpler non-reactive precursors derived from aqueous metal-nitrate solutions can be used to prepare films that are remarkably smooth and dense using similarly low processing temperatures, with properties that match or surpass those of films deposited from organic-containing precursor solutions.[15-17]

The deposition method is also quite important. Methods such as spray pyrolysis can produce conformal films with satisfactory electrical performance at relatively low deposition temperatures. With this technique, the facile loss of counterions and solvent that occurs as the precursors rapidly decompose on the substrate enables low-temperature processing, but often produces relatively rough films. By contrast, spin-coating cannot be used to conformally coat non-planar subtrates, but routinely produces significantly smoother films.[18, 19] The thicknesses of films derived from spin-coating can vary widely depending on spin-speed, solvent-evaporation rate and concentration (amongst others). The resulting precursor thickness could have important consequences for the subsequent chemical and physical evolution of the thin film as it is processed post-deposition.

The effects of precursor solution concentration on the resulting physical, chemical and electrical properties of spin-deposited metal-oxide thin films are relatively underexplored.

Several reports have shown that precursor concentration scales linearly with the resulting thin-film thicknesses.[20-21] Other reports demonstrate that the film thickness can have subtle impacts on electrical properties of the resulting thin films due to interactions with the atmosphere or the substrate.[22] The works mentioned above focus on the effects of precursor concentration on the thickness and properties of fully-processed thin films. However, these studies do not address or report effects of concentration on the chemical evolution of precursor components during processing.

Herein we investigate the effects of precursor-concentration on the thermal evolution of $La_2Zr_2O_7$ (LZO) thin films deposited from aqueous solutions using in-situ X-ray reflectivity (XRR) and temperature programmed desorption (TPD). XRR is sensitive to sub-Å thickness changes and is well-suited for obtaining thicknesses in the 1 to 100 nm range. By making in-situ thickness measurements as thin films of precursors are slowly heated and converted to thin films of LZO, the temperature ranges at which significant thickness decreases occur were determined. Analysis of unreacted species in LZO films that were preannealed at selected temperatures was then performed using TPD. Taken together, the XRR and TPD data show that certain thickness decreases are associated with chemical processes (such as the loss of NO_3^-) and that the temperature at which these processes occur are dependent on the concentration of the precursor-solution. Furthermore, TPD suggests that the films from dilute solutions actually have a different nitrate decomposition pathway. Interestingly, we observe differences in the metal ion coordination in the dilute and concentrated precursor solutions (via Raman spectroscopy). We speculate that this difference in speciation persists in spin-cast films, giving rise to an alternate nitrate decomposition pathway.

Experimental Section

Precursor Solutions

Lanthanum nitrate hexahydrate ($La(NO_3)_3 \cdot 6H_2O$, 99.9%, Sigma) and Zirconium Oxynitrate hydrate ($ZrO(NO_3)_2 \cdot xH_2O$, 98+% < 1.5% Hf, Sigma) were used as purchased. The extent of hydration was determined by heating pre-weighed aliquots of each compound at 950 °C in air for 8 hr and assuming that the final materials were metal oxides. Precursors were prepared by dissolving finely divided $ZrO(NO_3)_2 \cdot xH_2O$ in 18.2 MΩ·cm H_2O maintained at ~ 85 °C followed by addition of $La(NO_3)_3 \cdot 6H_2O$, cooling and dilution to achieve total metal concentrations of 1.0, 0.6 and 0.2 M and keeping a constant 1:1 La:Zr ratio.

Film Deposition

Si substrates (1" x 1", <100>) were sonicated in 5% aqueous Contrad 70 solution for 10 min, followed thorough rinsing with H_2O and plasma cleaning to leave a clean and hydrophilic layer of native SiO_2. Precursors were deposited onto substrates through 0.2 μm PTFE syringe filters onto Si substrates which were then rotated at accelerated at X $rpm \cdot s^{-1}$ to 3000 rpm for a total spin time of 30 s. Relative humidity in the spin-coater was measured to be between 60 and 70%. Precursor-coated substrates were then placed on a hotplate maintained at ~ 55 °C.

In-situ X-ray Reflectivity Measurements (XRR)

Films were maintained at 50 – 55 °C while transported to a Bruker 8D Discover equipped with a temperature programmable stage held a 50 °C. Freshly deposited precursor thin films are sensitive to H_2O adsorption/desorption from/to the atmosphere, so special care was taken to prevent films from falling outside the 50 to 55 °C temperature range. Thin film annealing was done under a dry N_2 atmosphere at a starting temperature of 50 °C, with incremental temperature increases of 40 °C, up to 450 °C. Temperatures were held at each selected temperature for 125 min. 20 XRR scans from 1-6 2θ were performed consecutively during each temperature hold.

Temperature Programmed Desorption (TPD)

Films were prepared for TPD using conditions and temperature profiles that were identical to those used for in-situ XRR, but were removed from the hotstage at the desired temperature (either 50, 130, 210, or 330 °C). Samples for TPD were cut from the center of samples to ~10 mm x 10 mm squares to avoid any signals from edge effects. Desorption experiments were done using a ramp rate of 30 °C·min^{-1} and positive detector mode on a Hiden TPD.

Precursor Characterization

Raman spectra of precursor solutions were obtained with a Wytec 300S Raman spectrometer (laser power of 45 mW at 532 nm). Thermogravimetric analyses were performed on a TA Instruments Q500 with a temperature ramp of 5 °C·min^{-1} from room temperature to 600 °C in N_2 or a ramp-dwell sequence identical to that used for in-situ XRR experiments.

Results and Discussion

Thermogravimetric analysis (TGA) is commonly used to monitor the thermal decomposition of solution-phase precursors and to assess the processing temperatures required to achieve a fully reacted metal oxide. To understand the concentration-dependent thermal behavior of aqueous $La_2Zr_2O_7$ (LZO) precursors, TGA was performed on equal-volume aliquots of 1.0, 0.6 and 0.2 M precursor solutions, shown below for 1.0 M and 0.2 M in Fig. 1.

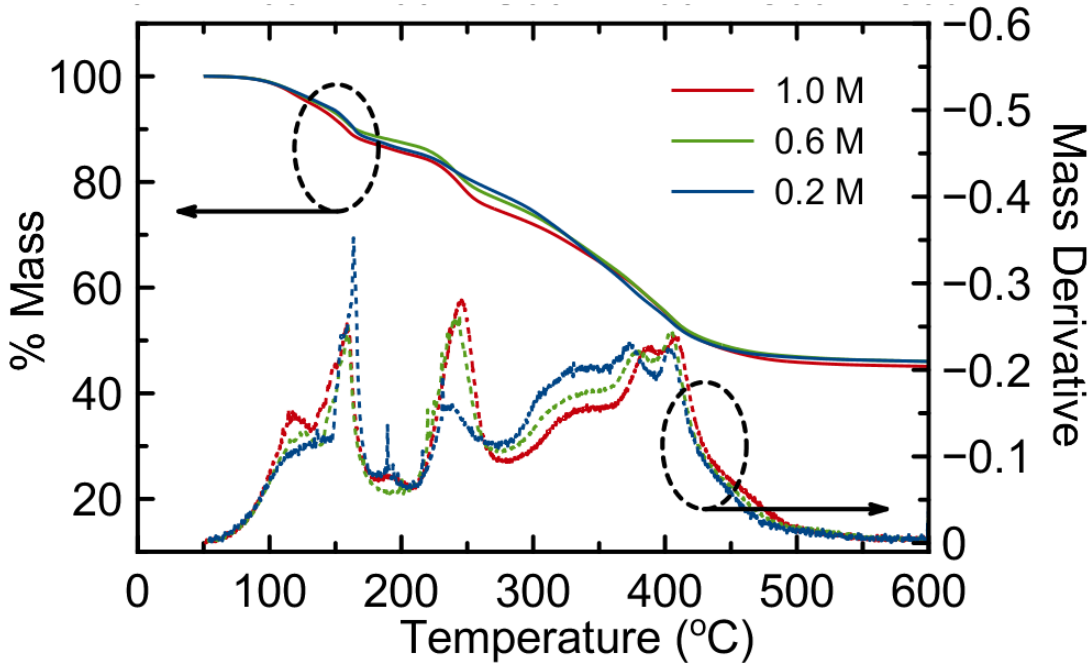

Figure 5.1. TGA and DTGA of dried 1.0, 0.6 and 0.2 M precursors.

Although there are minor differences in the thermal behaviors of precursors from different concentrations, most of the significant mass-loss events are very similar. TGA is a bulk measurement, and, while useful for giving a general roadmap for temperatures at which decomposition of precursor species occurs, it does not necessarily represent the processes by which a gel produced by spin-coating converts to an oxide.

To probe the particular physical aspects of the thermal evolutions of *thin-film* precursors, in-situ temperature dependent X-ray reflectivity (XRR) was employed. In general, XRR allows determination of the thickness, density and interfacial roughnesses of thin-film materials. Measuring film thickness as a function of annealing temperature provides information that is similar to that obtained for the dried precursor solution by TGA, with some important distinctions. While mass loss events in TGA are usually associated with chemical processes (evaporation of solvent, decomposition of counterions, and condensation), thickness decreases with increased temperature observed via XRR are not necessarily accompanied by mass losses. For the present case a step/dwell temperature profile was used, which in addition to allowing determination of thickness changes as a function of temperature, allows an assessment of the timescales over which thickness changes occur. For these experiments, temperatures were held at each temperature for two hours (starting at 50 °C, stepping by 40 °C up to 450 °C). Thickness data as a function of time and dwell temperature for films prepared using 0.2, 0.6 and 1.0 M precursor solutions are shown in Figure 2.

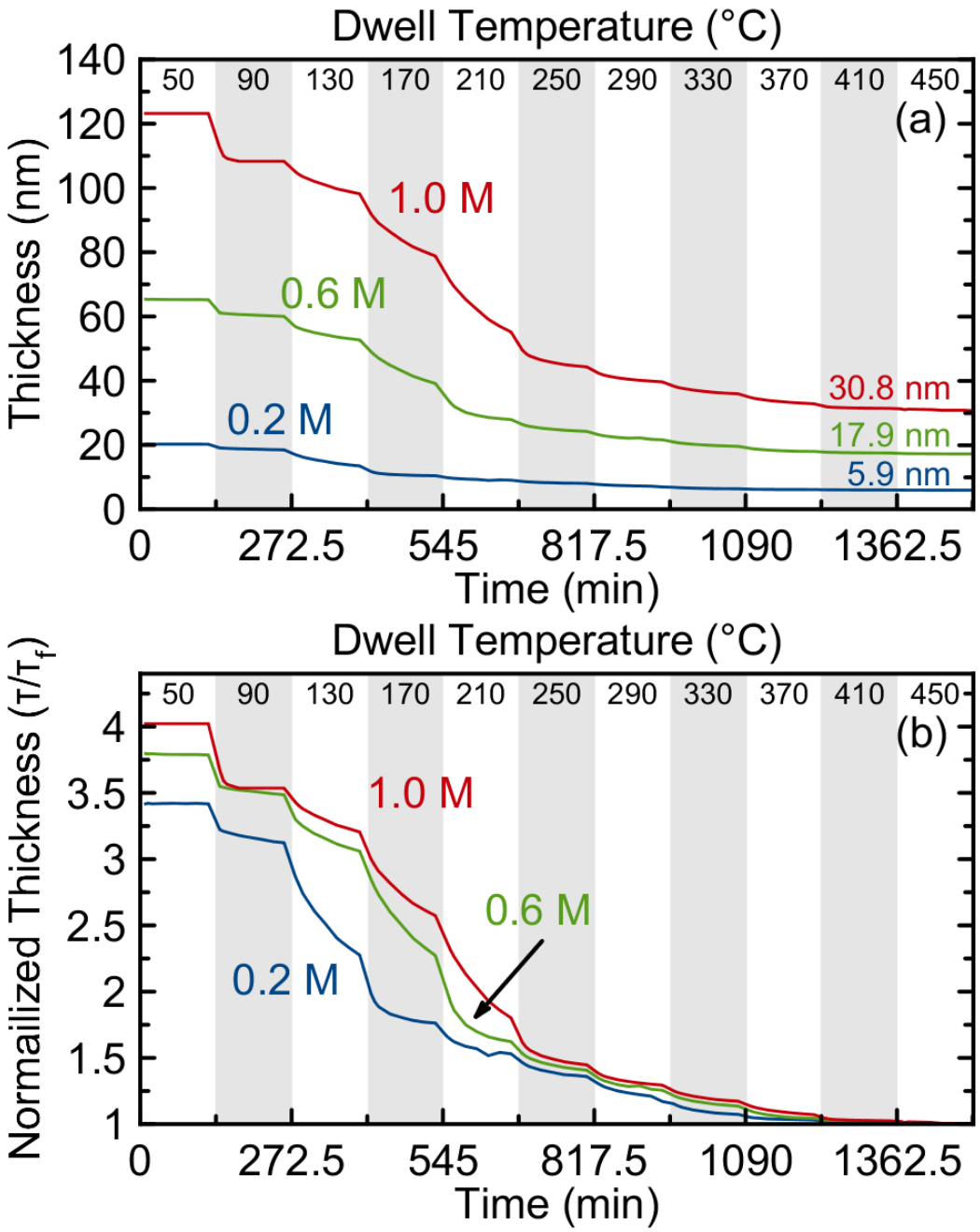

Figure 5.2. Thicknesses (a) and normailized thicknesses (b) of LZO thin films deposited from 1.0, 0.6 and 0.2 M precursors vs time and dwell temperature. Grey and white bars indicate temperature dwells, with the temperature indicated at the top of the bar.

As can be seen in Figure 2(a), the films change little in thickness above ~410 °C. The thickness ratios at 450°C are 1.00 : 0.61 : 0.20, in line with the precursor concentration ratio of 1.0 : 0.6 : 0.2 . This is consistent with the linear relationship between concentration and thickness observed in other thin films deposited using spin-coating.[K] Interestingly, the precursor concentration and initial film thickness (at 50 °C) ratios were 1.00 : 0.54 : 0.16, suggesting that more water is retained in the as-cast film for the more concentrated precursor solutions..

Notably, in the 130 to 250 °C range thicknesses are still decreasing at the end of 2 hr temperature dwells. This has important ramifications for thermally-processed solution-deposited thin films. Typically, solution deposited thin films are rapidly heated to some initial 'softbake' temperature (by placing directly onto a hotplate) ranging from 100 to 300 °C, followed by a ramp to some 'hardbake' temperature. The overlap of various temperature-dependent chemical and physical processes could vary significantly depending on the softbake temperature and the following ramp rate. For kinetic products (such as the amorphous metal-oxide thin films prepared here) changes in the overlap of these processes could significantly impact the properties of the fully processed material. To better compare the changes in thickness occurring with heating, thicknesses normalized to the final thickness for each film (T/T_f) are shown in Figure. 2(b). In contrast to the TGA data, which suggests the different dried precursor solutions have similar mass-loss profiles, the normalized thickness plots show that the films prepared from different concentration precursors have different thickness-loss profiles. The film deposited from 0.2 M solution loses thickness more abruptly and at a lower temperature than either the 0.6 or 1.0 M films. To ensure that the difference observed in these in-situ

XRR experiments (relative to the TGA measurements) is a consequence of the thin film chemistry and geometry rather than the temperature ramp/dwell sequence, a TGA experiment was performed on dried precursor solutions with the same ramp/dwell heating protocol as used in the XRR experiments. These TGA experiments showed little concentration dependence, confirming that the concentration-dependent effects observed in XRR reflect chemical and physical changes associated with thin film evolution. Transmission FTIR is commonly used to assess residual water and nitrates in solution-deposited thin-film materials as a function of processing temperature. However, low signal-to-noise for films deposited from 0.2 and 0.6 M LZO precursors makes meaningful comparisons difficult. As an alternative means for evaluating water and nitrate loss as a function of temperature, we used temperature-programmed desorption (TPD) to evaluate thin films preannealed to selected temperatures (130 °C, 210 °C and 330 °C). Although the high ramp-rates (30 °C·min^{-1}) and hard vacuum required for TPD alters the temperatures at which species desorb, its high sensitivity allows for detection of small amounts of off-gased species, enabling meaningful comparisons to be made between films examined in this study.

In the TPD studies we focus on the detection of H_2O (from solvent loss and condensation), and NO and O2 (from nitrate loss and thermal decomposition),[23] because they are byproducts of the most pertinent reactions occurring as the aqueous nitrate precursors convert to metal oxides. Other M/Z ratios, likely originating from adventitious carbon contamination, are excluded here for clarity. To aid in interpretation of NO desorption, we compare TPD data for the 1.0 M LZO film with TPD data for a film made with a 1.0 M solution containing only the Zr component ($ZrO(NO_3)_2$) (Fig. 3). Based on

the TPD traces for these films, there appear to be three distinct NO desorption features. We ascribe the broad NO desorption feature between 200 and 400 °C primarily to nitrate decomposition associated with $ZrO(NO_3)_2$ (Fig. 3). The second (400 - 450 °C) and third features (450 – 500 °C) are attributed to the decomposition of nitrates associated with La (since these features are absent in the $ZrO(NO_3)_2$ TPD). The simultaneous detection of desorbed O_2 in this temperature range suggests these higher-temperature NO features are related to an alternate NO_3^- decomposition pathway (i.e. thermal decomposition).[24] TPD on films deposited from 1.0 and 0.6 M solutions pre-annealed at 130, 210 and 330 °C show similar profiles for H_2O, NO and O_2 loss. However, the film deposited from 0.2 M solution has strikingly different desorption behavior. For this reason, we restrict our discussion to a comparison of the films deposited from 1.0 and 0.2 M precursors as they provide the most contrast in chemical evolution (Fig. 4).

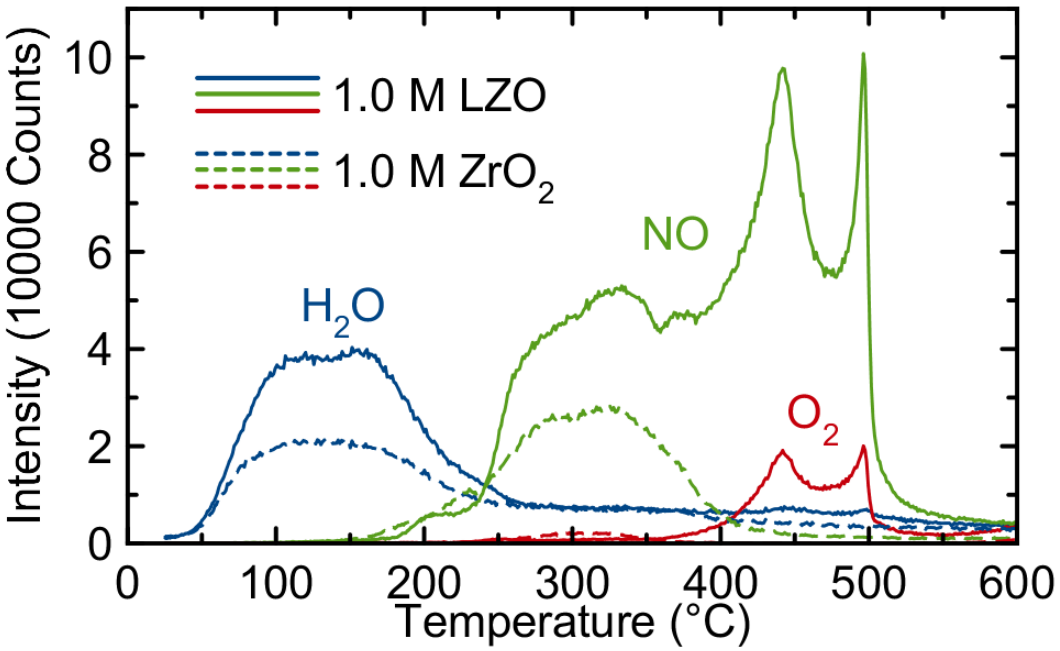

Figure 5.3. TPD of H_2O, NO and O_2 from thin films deposited from 1.0 M LZO precursor and 1.0 ZrO_2 precursor ($ZrO(NO_3)_2$) pre-annealed at 50 °C.

In the TPD scans for films pre-annealed at 130 °C, most of the H_2O is desorbed at temperatures less than 200 °C. For the samples pre-annealed to 210°C and 330 °C, a portion of the H_2O trace is therefore likely a consequence of water absorption by the film between the initial pre-anneal and the TPD experiment.

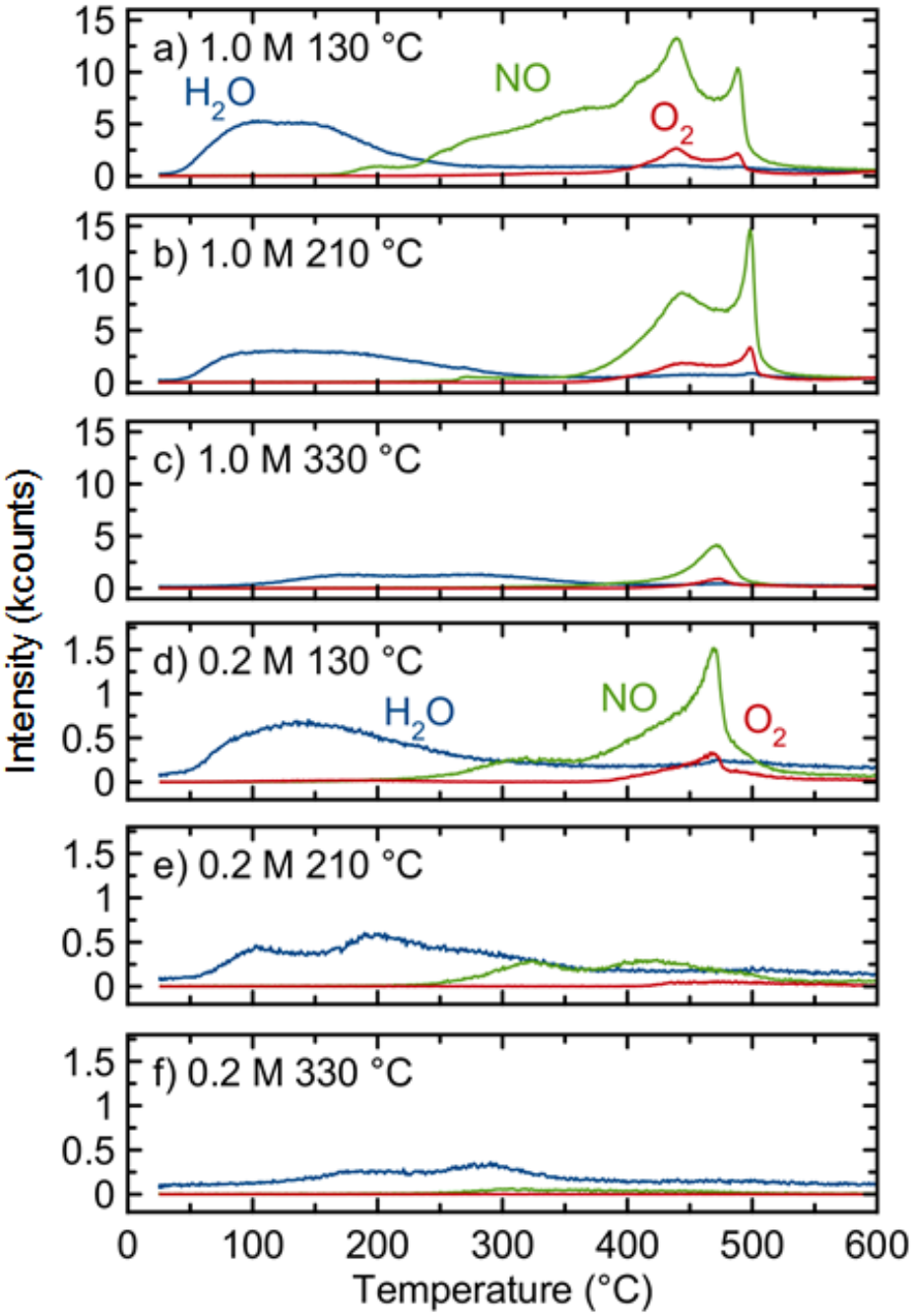

Figure 5.4. TPD of H_2O, NO and O_2 from thin films deposited from 1.0 M and 0.2 M precursors preannealed at 130 (a), 210 (b) and 330 °C (c) and TPD of H_2O, NO and O_2 from thin films deposited from 0.2 M precursors preannealed at 130 (e), 210 (f) and 330 °C (g).

The film deposited from 1.0 M precursor retains all NO features mentioned above after pre-annealing at 130 °C. Significant amounts of NO_3^- from $ZrO(NO_3)_2$ and, to a lesser extent, $La(NO_3)_3$ decompose after a 210 °C pre-anneal, leaving only NO_3^- associated with La after a 330 °C pre-anneal (Figure 4a-c). In contrast, the NO desorption traces from the film deposited from 0.2 M precursor suggests that similar processes have already taken place after pre-annealing at only 130 °C (Figure 4d). Only small amounts of NO remain to be desorbed after 210 and 330 °C pre-anneals (Figure 4e,f).

As a consequence of differences in thickness between 0.2 and 1.0 M films, the diffusion distances for desorption differ significantly. This is manifested in both the in-situ XRR and TPD data. While thinner films deposited from 0.2 M precursors undergo significant thickness decrease and NO_3^- loss at 130 °C, annealing temperatures of 210 °C are needed to achieve similar results in thicker films deposited from 1.0 M precursors.

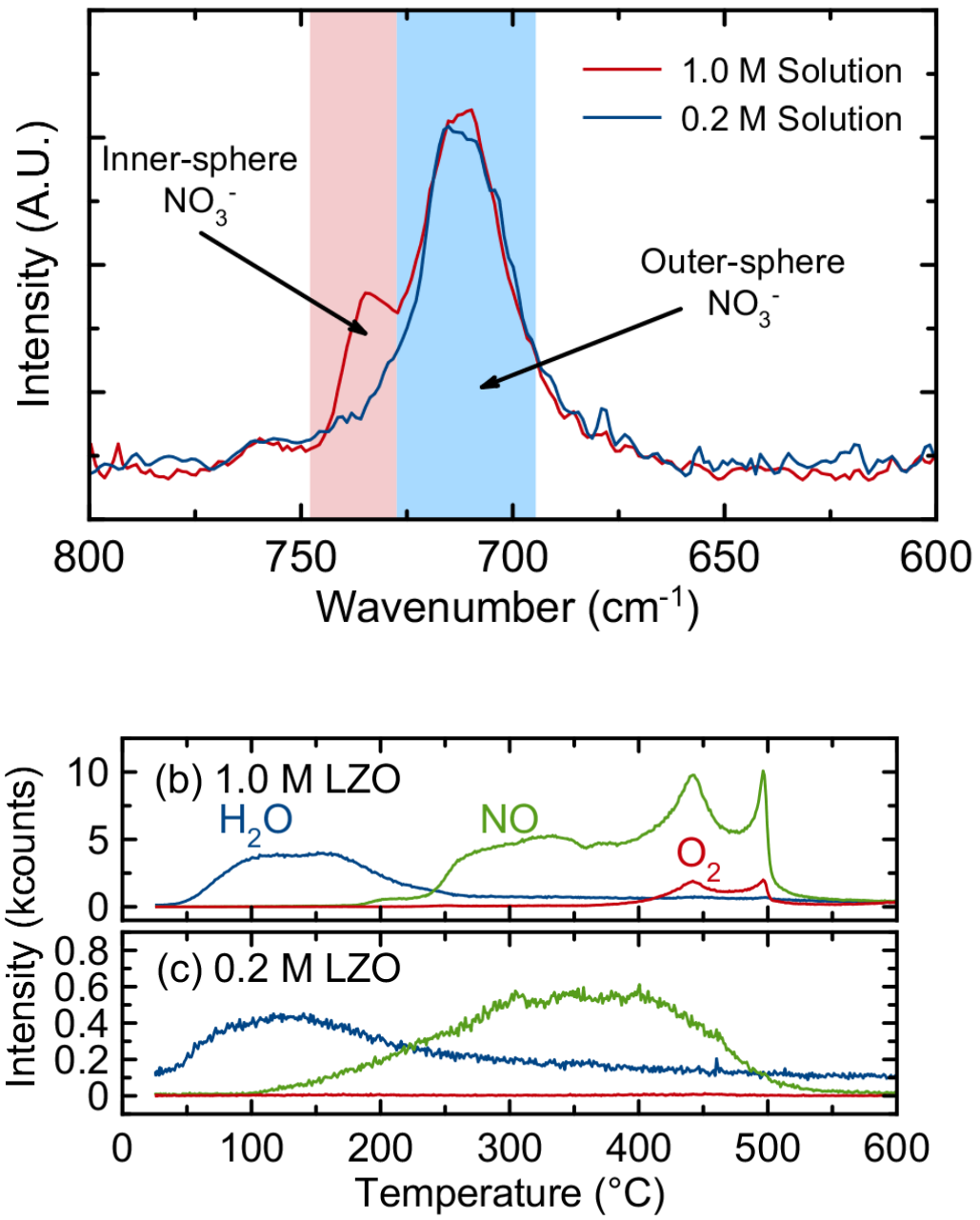

Figure 5.5. Raman spectra of 1.0 and 0.2 M precursors (a). TPD of H_2O, NO, and O_2 from an LZO film deposited from a 0.2 M solution and preannealed at 50 °C.

Although film thickness and byproduct diffusion likely play a significant role, concentration-dependent metal-nitrate interactions in the precursor solutions may also be related to the temperatures at which nitrate is desorbed. Previous studies have correlated

metal salt decomposition temperatures to degree of metal cation inner sphere hydration.[25] Raman spectroscopy has been used to give insight into the ligand binding modes of particular species, including nitrates.[25-28] These previous studies allow us to use Raman spectroscopy to examine the nitrate binding in the LZO precursor solutions (Fig. 5a). The Raman spectrum of a 0.2 M precursor solution shows a single feature at ~ 715 cm^{-1}, corresponding to the symmetric stretching mode of NO_3^-. This mode has been correlated to 'free' nitrates in the outer sphere of hydrated metal cations.[26-28] The Raman spectrum of a 1.0 M precursor solution shows an additional distinct shoulder at 735 cm^{-1} corresponding to a distorted stretching mode, indicating the presence of bound inner-sphere NO_3^-.[26-28] It follows that if nitrate is bound in the inner sphere of one or both metal cations, the degree of hydration of the inner sphere is reduced in the 1.0 M precursor solution. IF these metal cation-hydration effects are maintained in the precursor gel upon spin-casting and rapid heating, decomposition temperatures would be increased for the 1.0 M film relative to the 0.2 M film. While we are unable to directly determine whether the degree of inner sphere hydration is maintained upon spinning, this effect would be consistent with our observations, especially the TPD data. In Figure 5b we show TPD traces for 0.2 M and 1.0 M films pre-annealed at 50 °C. The dramatic differences in these traces (lack of distinct NO features between 400 and 500 °C) and the increased fraction of NO desorbed at lower temperatures may be related to a higher degree of hydration for cations in the 0.2 M precursors, resulting in desorption of the nitrate at lower temperatures. Furthermore, we hypothesize that the mechanism of loss for nitrates bound in the 'outer' sphere is different than that for nitrates directly bound to metal cations (inner sphere). We suggest that the higher temperature desorption which we

attribute to bound nitrate decomposition occurs via thermal decomposition to form both NO and O_2 (as evidenced by the parallel NO and O_2 traces). We propose that the lower temperature outer sphere NO desorption is related to removal via the water-nitric acid azeotrope. While no mass fragments consistent with HNO_3/H_2O species are observed by TPD, it has been previously reported that nitric acid decomposes in the TPD detector to give NO species.

We note that the TPD traces for the 0.2 M samples pre-annealed at 50 °C (Fig. 5b) and 130 °C (Fig. 4d) look significantly different. The high temperature NO/O_2 desorption features in the 400-500 °C range are not seen in the sample pre-annealed to 50 °C, suggesting that the species giving rise to this feature is not present. The appearance of the high temperature NO/O_2 desorption feature in the film pre-annealed at 130 °C may due to the thermal history of this sample, which includes 2 h dwells at 50 °C, 90 °C and 130 °C. We note that $La(NO_3)_3 \cdot 6H_2O$ melts at ~70°C, at which point ion mobility should be enhanced. This thermal treatment may be sufficient to allow nitrate to bind in the inner sphere, giving rise to the observed high temperature NO/O_2 desorption peaks. In the TPD experiment, the rapid temperature ramp does not allow for nitrate rearrangement, so nitrate desorption should reflect the relative amounts of nitrate bound in the outer and inner spheres in the pre-annealed samples.

Conclusions

The thermal evolution of LZO thin films deposited from different concentrations of aqueous nitrate solutions was investigated. Not surprisingly, thermogravometric analysis (TGA) of dried precursors reveals negligible dependence on concentration. In-situ XRR

experiments show that initial precursor concentration and final film thickness scale linearly, but films deposited with low concentration precursors undergo thickness decreases at lower temperatures than films deposited from more concentrated precursors. Temperature-programmed desorption (TPD) of films preannealed to selected temperatures reveal that these thickness decreases are concurrent with loss of NO_3^-. Raman spectra of precursor solutions reveal concentration-dependent differences in the nitrate binding modes. The lowest concentration precursor solution studied (0.2 M) shows only symmetric stretching modes corresponding to 'free' (outer sphere) nitrate, whereas more concentrated solutions also show a shoulder attributed to an unsymmetric mode associated with inner-sphere nitrate binding. We correlate the metal coordination with the nitrate desorption events in order to relate the precursor chemistry with the thermal evolution and film thickness of the films.

The insights provided here allow important conclusions to be drawn. Altering simple parameters, in this case the precursor concentration, can have significant consequences on the thermal evolution of a solution-deposited metal oxide. Such concentration dependent effects are not apparent by measuring thickness, but the precursor-concentration dependent differences in the temperatures at which various chemical and physical processes occur could impact the characteristics of kinetic products, such as amorphous metal-oxide thin films. When making rigorous comparisons between solution deposition techniques of a given material, the effects of precursor concentration should be taken into account.

Summary and Outlook

This research details the many aspects of aqueous-deposited metal-oxide thin films. Chapter II touched on many of the aspects of precursor-solution chemistry, film formation processes, film morphology, and electrical properties of lanthanum aluminum oxide films. Chapter III focused on the effects of humidity during spin-deposition. Water vapor during spin deposition can affect evaporation rates, and hence viscosity, which affect both film thicknesses and density profiles in the final films. In Chapter IV, the effects of humidity were explored further. Humidity during the annealing process enhances counterion removal, and generally lowers the temperatures required to remove counterions. Together, Chapters III and IV show that water is not only a suitable solvent for deposition of metal-oxide thin films, but is a dynamic player at many points in the film formation process. The work in Chapter V demonstrates that the dilution of a precursor solution can have an impact on film densification and loss of counterions caused by a combination of film thickness and precursor-speciation effects. At least some portions of each chapter reflect the multiple roles of water at various points in the film formation process.

The work presented in this dissertation highlights the nuanced processes that occur as precursor solutions are concentrated to thin films and as the resulting thin-film precursors are thermally converted to metal-oxide thin films. The effects detailed in this work also emphasize the importance of variables (such as humidity and solution speciation) that have been neglected or under-appreciated in the formation of films via spin-deposition. However, as shown in this work, these variables impact the thickness, density and chemical composition profiles of films produced via this method, and likely

also significantly impact the properties of the resulting metal oxide thin films. More broadly, these variables also may impact the spin-deposition and chemical processes occurring for other types of precursor solutions (e.g. sol-gel) used to prepare metal oxides. Ultimately, a deeper understanding of the processes that occur as solution-deposited metal-oxide thin films form should allow for deposition of higher-quality materials at lower temperatures, enhancing their utility in low-cost, flexible device applications.

References Cited

Chapter I

(1) Esro, M.; Vourlias, G.; Somerton, C.; Milne, W. I.; Adamopoulos, G. High-Mobility ZnO Thin Film Transistors Based on Solution-Processed Hafnium Oxide Gate Dielectrics. *Adv. Funct. Mater.* **2015**, *25* (1), 134–141.

(2) Nayak, P. K.; Hedhili, M. N.; Cha, D.; Alshareef, H. N. High Performance In_2O_3 Thin Film Transistors Using Chemically Derived Aluminum Oxide Dielectric. *Appl. Phys. Lett.* **2013**, *103* (3), 033518 1-5.

(3) Park, J. H.; Yoo, Y. B.; Lee, K. H.; Jang, W. S.; Oh, J. Y.; Chae, S. S.; Lee, H. W.; Han, S. W.; Baik, H. K. Boron-Doped Peroxo-Zirconium Oxide Dielectric for High-Performance, Low-Temperature, Solution-Processed Indium Oxide Thin-Film Transistor. *ACS Appl. Mater. Interfaces* **2013**, *5* (16), 410–417.

(4) Robertson, J. High Dielectric Constant Gate Oxides for Metal Oxide Si Transistors. *Reports Prog. Phys.* **2005**, *69* (2), 327–396.

(5) Xu, F.; Liu, A.; Liu, G.; Shin, B.; Shan, F. Solution-Processed Yttrium Oxide Dielectric for High-Performance IZO Thin-Film Transistors. *Ceram. Int.* **2015**, *41*, S337–S343.

(6) Jeong, D. S.; Thomas, R.; Katiyar, R. S.; Scott, J. F.; Kohlstedt, H.; Petraru, A.; Hwang, C. S. Emerging Memories: Resistive Switching Mechanisms and Current Status. *Reports Prog. Phys.* **2012**, *75*, 076502 1-31.

(7) Kim, S.; Choi, S.; Lu, W. Comprehensive Physical Model of Dynamic Resistive Switching in an Oxide Memristor. *ACS Nano* **2014**, *8* (3), 2369–2376.

(8) Maikap, S.; Lee, H. Y.; Wang, T.-Y.; Tzeng, P.-J.; Wang, C. C.; Lee, L. S.; Liu, K. C.; Yang, J.-R.; Tsai, M.-J. Charge Trapping Characteristics of Atomic-Layer-Deposited HfO_2 Films with Al_2O_3 as a Blocking Oxide for High-Density Non-Volatile Memory Device Applications. *Semicond. Sci. Technol.* **2007**, *22*, 884–889.

(9) Sawa, A. Resistive Switching in Transition Metal Oxides. *Mater. Today* **2008**, *11* (6), 28–36.

(10) Specht, M.; Reisinger, H.; Hofmann, F.; Schulz, T.; Landgraf, E.; Luyken, R. J.; Rösner, W.; Grieb, M.; Risch, L. Charge Trapping Memory Structures with Al_2O_3 Trapping Dielectric for High-Temperature Applications. *Solid. State. Electron.* **2005**, *49* (5), 716–720.

(11) Strukov, D. B.; Snider, G. S.; Stewart, D. R.; Williams, R. S. The Missing

Memristor Found. *Nature* **2008**, *453*, 80–83.

(12) Tsui, S.; Baikalov, A.; Cmaidalka, J.; Sun, Y. Y.; Wang, Y. Q.; Xue, Y. Y.; Chu, C. W.; Chen, L.; Jacobson, A. J. Field-Induced Resistive Switching in Metal-Oxide Interfaces. *Appl. Phys. Lett.* **2004**, *85* (2), 317–319.

(13) Waser, R.; Aono, M. Nanoionics-Based Resistive Switching Memories. *Nat. Mater.* **2007**, *6* (11), 833–840.

(14) Ahn, B. Du; Jeon, H.; Sheng, J.; Park, J.; Park, J.-S. A Review on the Recent Developments of Solution Processes for Oxide Thin Film Transistors. *Jpn. J. Appl. Phys.* **2014**, *53* (6), 02BA02 1-10.

(15) Kast, M. G.; Enman, L. J.; Gurnon, N. J.; Nadarajah, A.; Boettcher, S. W. Solution-Deposited F : SnO_2 / TiO_2 as a Base Stable Protective Layer and Anti-Reflective Coating for Micro-Textured Buried-Junction H 2 -Evolving Si Photocathodes. *ACS Appl. Mater. Interfaces* **2014**, *6*, 22830–22837.

(16) Nomura, K.; Takagi, A.; Kamiya, T.; Ohta, H.; Hirano, M.; Hosono, H. Amorphous Oxide Semiconductors for High-Performance Flexible Thin-Film Transistors. *Japanese J. Appl. Physics, Part 1 Regul. Pap. Short Notes Rev. Pap.* **2006**, *45* (5 B), 4303–4308.

(17) Omar, A.; Abdullah, H. Electron Transport Analysis in Zinc Oxide-Based Dye-Sensitized Solar Cells: A Review. *Renew. Sustain. Energy Rev.* **2014**, *31*, 149–157.

(18) Thomas, S. R.; Pattanasattayavong, P.; Anthopoulos, T. D. Solution-Processable Metal Oxide Semiconductors for Thin-Film Transistor Applications. *Chem. Soc. Rev.* **2013**, *42* (16), 6910–6923.

(19) Barnes, T. M.; Reese, M. O.; Bergeson, J. D.; Larsen, B. A.; Blackburn, J. L.; Beard, M. C.; Bult, J.; Van De Lagemaat, J. Comparing the Fundamental Physics and Device Performance of Transparent, Conductive Nanostructured Networks with Conventional Transparent Conducting Oxides. *Adv. Energy Mater.* **2012**, *2* (3), 353–360.

(20) Chen, Z.; Li, W.; Li, R.; Zhang, Y.; Xu, G.; Cheng, H. Fabrication of Highly Transparent and Conductive Indium-Tin Oxide Thin Films with a High Figure of Merit via Solution Processing. *Langmuir* **2013**, *29*, 13836–13842.

(21) Lany, S.; Zunger, A. Dopability, Intrinsic Conductivity, and Nonstoichiometry of Transparent Conducting Oxides. *Phys. Rev. Lett.* **2007**, *98* (4), 045501 1-4.

(22) Nadarajah, A.; Carnes, M. E.; Kast, M. G.; Johnson, D. W.; Boettcher, S. W. Aqueous Solution Processing of F-Doped SnO_2 Transparent Conducting Oxide Films Using a Reactive tin(II) Hydroxide Nitrate Nanoscale Cluster. *Chem. Mater.* **2013**, *25* (20), 4080–4087.

(23) Araki, T.; Hirabayashi, I. $YBa_2Cu_3O_{7-X}$ -Coated Superconductors — Metalorganic Deposition Using Trifluoroacetates. *Supercond. Sci. Technol.* **2003**, *16*, R71–R94.

(24) Ammundsen, B.; Paulsen, J. Novel Lithium-Ion Cathode Materials Based on Layered Manganese Oxides. *Adv. Mater.* **2001**, *13* (12–13), 943–956.

(25) Johnson, C. S.; Li, N.; Vaughey, J. T.; Hackney, S. A.; Thackeray, M. M. Lithium-Manganese Oxide Electrodes with Layered-Spinel Composite Structures XLi_2MnO_3 $(1 - X)Li_{(1+y)}Mn_2$-YO_4 $(0 < X < 1, 0 < Y < 0.33)$ for Lithium Batteries. *Electrochem. commun.* **2005**, *7* (5), 528–536.

(26) Ohta, S.; Komagata, S.; Seki, J.; Saeki, T.; Morishita, S.; Asaoka, T. All-Solid-State Lithium Ion Battery Using Garnet-Type Oxide and Li_3BO_3 Solid Electrolytes Fabricated by Screen-Printing. *J. Power Sources* **2013**, *238*, 53–56.

(27) Whittingham, M. S. Lithium Batteries and Cathode Materials. *Chem. Rev.* **2004**, *104* (10), 4271–4301.

(28) Matsui, M.; Takahashi, K.; Sakamoto, K.; Hirano, A.; Takeda, Y.; Yamamoto, O.; Imanishi, N. Phase Stability of a Garnet-Type Lithium Ion Conductor $Li_7La_3Zr_2O_{12}$. *Dalt. Trans.* **2014**, *43* (3), 1019–1024.

(29) Thangadurai, V.; Narayanan, S.; Pinzaru, D. Garnet-Type Solid-State Fast Li Ion Conductors for Li Batteries: Critical Review. *Chem. Soc. Rev.* **2014**, *43* (13), 4714–4727.

(30) Brett, D. J. L.; Atkinson, A.; Brandon, N. P.; Skinner, S. J. Intermediate Temperature Solid Oxide Fuel Cells. *Chem. Soc. Rev.* **2008**, *37* (8), 1568–1578.

(31) Richter, J.; Holtappels, P.; Graule, T.; Nakamura, T.; Gauckler, L. J. Materials Design for Perovskite SOFC Cathodes. *Monatshefte fur Chemie* **2009**, *140* (9), 985–999.

(32) Shim, J. H.; Chao, C. C.; Huango, H.; Prinz, F. B. Atomic Layer Deposition of Yttria-Stabilized Zirconia for Solid Oxide Fuel Cells. *Chem. Mater.* **2007**, *19* (7), 3850–3854.

(33) Avendaño, E.; Berggren, L.; Niklasson, G. A.; Granqvist, C. G.; Azens, A. Electrochromic Materials and Devices: Brief Survey and New Data on Optical Absorption in Tungsten Oxide and Nickel Oxide Films. *Thin Solid Films* **2006**, *496* (1), 30–36.

(34) Manning, T. D.; Parkin, I. P.; Pemble, M. E.; Sheel, D.; Vernardou, D. Intelligent Window Coatings: Atmospheric Pressure Chemical Vapor Deposition of

Tungsten-Doped Vanadium Dioxide. *Chem. Mater.* **2004**, *16* (4), 744–749.

(35) Niklasson, G. A.; Granqvist, C. G. Electrochromics for Smart Windows: Thin Films of Tungsten Oxide and Nickel Oxide, and Devices Based on These. *J. Mater. Chem.* **2007**, *17* (2), 127–156.

(36) Ahn, C. H.; Rabe, K. M.; Triscone, J.-M. J.-M. Ferroelectricity at the Nanoscale: Local Polarization in Oxide Thin Films and Heterostructures. *Science (80-.).* **2004**, *303* (5657), 488–491.

(37) Morón, C.; Cabrera, C.; Morón, A.; García, A.; González, M. Magnetic Sensors Based on Amorphous Ferromagnetic Materials: A Review. *Sensors* **2015**, *15* (11), 28340–28366.

(38) Allibe, J.; Fusil, S.; Bouzehouane, K.; Daumont, C.; Sando, D.; Jacquet, E.; Deranlot, C.; Bibes, M.; Barthélémy, A. Room Temperature Electrical Manipulation of Giant Magnetoresistance in Spin Valves Exchange-Biased with BiFeO3. *Nano Lett.* **2012**, *12*, 1141–1145.

(39) Sugahara, S.; Tanaka, M. A Spin Metal-Oxide-Semiconductor Field-Effect Transistor Using Half-Metallic-Ferromagnet Contacts for the Source and Drain. *Appl. Phys. Lett.* **2004**, *84* (13), 2307–2309.

(40) Prestgard, M. C.; Siegel, G. P.; Tiwari, A. Oxides for Spintronics: A Review of Engineered Materials for Spin Injection. *Adv. Mater. Lett.* **2014**, *5* (5), 242–247.

(41) Bratkovsky, a M. Spintronic Effects in Metallic, Semiconductor, Metal–oxide and Metal–semiconductor Heterostructures. *Reports Prog. Phys.* **2008**, *71* (2), 026502 1-31.

(42) Sproul, W. D. Physical Vapor Deposition Tool Coatings. *Surf. Coatings Technol.* **1996**, *81* (1), 1–7.

(43) Mattox, D. M. Physical Vapor Deposition (PVD) Processes. *Met. Finish.* **1995**, *93*, 394–408.

(44) Lorenz, M.; Ramachandra Rao, M. S. 25 Years of Pulsed Laser Deposition. *J. Phys. D. Appl. Phys.* **2014**, *47* (3), 030301 1-3.

(45) Kelly, P. . J.; Arnell, R. . D. Magnetron Sputtering: A Review of Recent Developments and Applications. *Vacuum* **2000**, *56* (3), 159–172.

(46) Fang, X.; Mak, C. L.; Zhang, S.; Wang, Z.; Yuan, W.; Ye, H. Pulsed Laser Deposited Indium Tin Oxides as Alternatives to Noble Metals in the near-Infrared Region. *J. Phys. Condens. Matter* **2016**, *28* (22), 224009 1-10.

(47) Christen, H. M.; Eres, G. Recent Advances in Pulsed-Laser Deposition of Complex Oxides. *J. Phys. Condens. Mat.* **2008**, *20* (26), 264005 1-16.

(48) Bräuer, G.; Szyszka, B.; Vergöhl, M.; Bandorf, R. Magnetron Sputtering - Milestones of 30 Years. *Vacuum* **2010**, *84* (12), 1354–1359.

(49) Yang, J. L.; An, S. J.; Park, W. I.; Yi, G.-C.; Choi, W. Photocatalysis Using ZnO Thin Films and Nanoneedles Grown by Metal-Organic Chemical Vapor Deposition. *Adv. Mater.* **2004**, *16* (18), 1661–1664.

(50) Soyez, G.; Eastman, J. a; Thompson, L. J.; Bai, G. R.; Baldo, P. M.; McCormick, a W.; DiMelfi, R. J.; Elmustafa, a a; Tambwe, M. F.; Stone, D. S. Grain-Size-Dependent Thermal Conductivity of Nanocrystalline Yttria-Stabilized Zirconia Films Grown by Metal-Organic Chemical Vapor Deposition. *Appl. Phys. Lett.* **2000**, *77* (8), 1155–1157.

(51) Smith, R. C.; Hoilien, N.; Taylor, C. J.; Ma, T. Z.; Campbell, S. A.; Roberts, J. T.; Copel, M.; Buchanan, D. A.; Gribelyuk, M.; Gladfelter, W. L. Low Temperature Chemical Vapor Deposition of ZrO_2 on Si(100) Using Anhydrous zirconium(IV) Nitrate. *J. Electrochem. Soc.* **2000**, *147* (9), 3472–3476.

(52) Gordon, R. G.; Becker, J.; Hausmann, D.; Suh, S. Vapor Deposition of Metal Oxides and Silicates: Possible Gate Insulators for Future Microelectronics. *Chem. Mater.* **2001**, *13* (8), 2463–2464.

(53) Mathur, S.; Sivakov, V.; Shen, H.; Barth, S.; Cavelius, C.; Nilsson, A.; Kuhn, P. Nanostructured Films of Iron, Tin and Titanium Oxides by Chemical Vapor Deposition. *Thin Solid Films* **2006**, *502* (1–2), 88–93.

(54) Alf, M. E.; Asatekin, A.; Barr, M. C.; Baxamusa, S. H.; Chelawat, H.; Ozaydin-Ince, G.; Petruczok, C. D.; Sreenivasan, R.; Tenhaeff, W. E.; Trujillo, N. J.; Vaddiraju, S.; Xu, J.; Gleason, K. K. Chemical Vapor Deposition of Conformal, Functional, and Responsive Polymer Films. *Adv. Mater.* **2010**, *22* (18), 1993–2027.

(55) Ritala, M.; Kukli, K.; Rahtu, A.; Raisanen, P. I.; Leskela, M.; Sajavaara, T.; Keinonen, J.; Schulz, M.; Packan, P. A.; Muller, D. A.; Hubbard, K. J.; Schlom, D. G.; Wilk, G. D.; Wallace, R. M.; McKee, R. A.; Walker, F. J.; Chisholm, M. F.; Niinistö, L.; Ritala, M.; Leskelä, M.; Ritala, M.; Klaus, J. W.; Sneh, O.; George, S. M.; Klaus, J. W.; Sneh, O.; Ott, A. W.; George, S. M.; Ritala, M.; Corriou, R.; Leclercq, D.; Lefèrve, P.; Mutin, P. H.; Vioux, A.; Vioux, A.; Trentler, T. J.; Denler, T. E.; Bertone, J. F.; Agrawal, A.; Colvin, V. L.; Bourget, L.; Corriou, R. J. P.; Leclercq, D.; Mutin, P. H.; Vioux, A. Atomic Layer Deposition of Oxide Thin Films with Metal Alkoxides as Oxygen Sources. *Science* **2000**, *288* (5464), 319–321.

(56) Leskelä, M.; Ritala, M. Atomic Layer Deposition (ALD): From Precursors to Thin Film Structures. *Thin Solid Films* **2002**, *409* (1), 138–146.

(57) Groner, M. D.; Fabreguette, F. H.; Elam, J. W.; George, S. M. Low-Temperature Al2O3 Atomic Layer Deposition. *Chem. Mater.* **2004**, *16* (4), 639–645.

(58) George, S. M. Atomic Layer Deposition: An Overview. *Chem. Rev.* **2010**, *110* (1), 111–131.

(59) Zheludkevich, M. L.; Salvado, I. M.; Ferreira, M. G. S. Sol–gel Coatings for Corrosion Protection of Metals. *J. Mater. Chem.* **2005**, *15* (48), 5099–5111.

(60) Tokudome, Y.; Fujita, K.; Nakanishi, K.; Miura, K.; Hirao, K. Synthesis of Monolithic Al 2 O 3 with Well-Defined Macropores and Mesostructured Skeletons via the Sol-Gel Process Accompanied by Phase Separation. *Chem. Mater.* **2007**, *19* (8), 3393–3398.

(61) Banger, K. K.; Yamashita, Y.; Mori, K.; Peterson, R. L.; Leedham, T.; Rickard, J.; Sirringhaus, H. Low-Temperature, High-Performance Solution-Processed Metal Oxide Thin-Film Transistors Formed by a "sol–gel on Chip" Process. *Nat. Mater.* **2011**, *10* (1), 45–50.

(62) Bahlawane, N.; Watanabe, T. New Sol–Gel Route for the Preparation of Pure α-Alumina at 950°C. *J. Am. Ceram. Soc.* **2000**, *83* (9), 2324–2326.

(63) Alam, M. J.; Cameron, D. C. Preparation and Properties of Transparent Conductive Aluminum-Doped Zinc Oxide Thin Films by Sol–gel Process. *J. Vac. Sci. Technol. A Vacuum, Surfaces, Film.* **2001**, *19* (4), 1642.

(64) Alam, M. J.; Cameron, D. C. Optical and Electrical Properties of Transparent Conductive ITO Thin Films Deposited by Sol-Gel Process. *Thin Solid Films* **2000**, *377–378*, 455–459.

(65) Seo, S.-J.; Choi, C. G.; Hwang, Y. H.; Bae, B.-S. High Performance Solution-Processed Amorphous Zinc Tin Oxide Thin Film Transistor. *J. Phys. D. Appl. Phys.* **2008**, *42* (3), 035106 1-5.

(66) Jeong, S.; Moon, J. Low-Temperature, Solution-Processed Metal Oxide Thin Film Transistors. *J. Mater. Chem.* **2012**, *22* (4), 1243–1250.

(67) Zhang, D.; Ma, B.; Jin, T.; Gao, S.; Yan, C.; Mak, T. C. W. Oxo-Centered Regular Octahedral Lanthanide Clusters. *New J. Chem.* **2000**, *24* (4), 61–62.

(68) Wang, W.; Wentz, K. M.; Hayes, S. E.; Johnson, D. W.; Keszler, D. A. Synthesis of the Hydroxide Cluster $[Al_{13}(\mu_3\text{-}OH)_6(\mu\text{-}OH)_{18}(H_2O)_{24}]^{15+}$ from an Aqueous Solution. *Inorg. Chem.* **2011**, *50* (3), 4683–4685.

(69) Wang, W.; Liu, W.; Chang, I.-Y.; Wills, L. A.; Zakharov, L. N.; Boettcher, S. W.; Cheong, P. H.-Y.; Fang, C.; Keszler, D. A. Electrolytic Synthesis of Aqueous Aluminum Nanoclusters and in Situ Characterization by Femtosecond Raman Spectroscopy and Computations. *Proc. Natl. Acad. Sci.* **2013**, *110* (46), 18397–18401.

(70) Wang, W.; Chang, I.-Y.; Zakharov, L. N.; Cheong, P. H.-Y.; Keszler, D. A. $[Sc_2(\mu\text{-}OH)_2(H_2O)_6(NO_3)_2](NO_3)_2$: Aqueous Synthesis and Characterization. *Inorg. Chem.* **2013**, *52* (4), 1807–1811.

(71) Wang, R.; Carducci, M. D.; Zheng, Z. Direct Hydrolytic Route to Molecular Oxo-Hydroxo Lanthanide Clusters. *Inorg. Chem.* **2000**, *39* (9), 1836–1837.

(72) Ruther, R. E.; Baker, B. M.; Son, J. H.; Casey, W. H.; Nyman, M. Hafnium Sulfate Prenucleation Clusters and the Hf_{18} Polyoxometalate Red Herring. *Inorg. Chem.* **2014**, *53* (8), 4234–4242.

(73) Mensinger, Z. L.; Wang, W.; Keszler, D. a.; Johnson, D. W. Oligomeric Group 13 Hydroxide Compounds—a Rare but Varied Class of Molecules. *Chem. Soc. Rev.* **2012**, *41* (3), 1019–1030.

(74) Mensinger, Z. L.; Gatlin, J. T.; Meyers, S. T.; Zakharov, L. N.; Keszler, D. A.; Johnson, D. W. Synthesis of Heterometallic Group 13 Nanoclusters and Inks for Oxide Thin-Film Transistors. *Angew. Chemie - Int. Ed.* **2008**, *47* (49), 9484–9486.

(75) Kamunde-Devonish, M. K.; Jackson, M. N.; Mensinger, Z. L.; Zakharov, L. N.; Johnson, D. W. Transmetalation of Aqueous Inorganic Clusters: A Useful Route to the Synthesis of Heterometallic Aluminum and Indium Hydroxo-Aquo Clusters. *Inorg. Chem.* **2014**, *53* (14), 7101–7105.

(76) Jackson, M. N. J.; Kamunde-Devonish, M. K.; Hammann, B. A.; Wills, L. A.; Fullmer, L. B.; Hayes, S. E.; Cheong, P. H. Y.; Casey, W. H.; Nyman, M.; Johnson, D. W. An Overview of Selected Current Approaches to the Characterization of Aqueous Inorganic Clusters. *Dalt. Trans.* **2015**, *44* (39), 16982–17006.

(77) Wang, W.; Liu, W.; Chang, I.-Y.; Wills, L. a; Zakharov, L. N.; Boettcher, S. W.; Cheong, P. H.-Y.; Fang, C.; Keszler, D. a. Electrolytic Synthesis of Aqueous Aluminum Nanoclusters and in Situ Characterization by Femtosecond Raman Spectroscopy and Computations. *Proc. Natl. Acad. Sci. U. S. A.* **2013**, *110* (46), 18397–18401.

(78) Rim, Y. S.; Chen, H.; Song, T. Bin; Bae, S. H.; Yang, Y. Hexaaqua Metal Complexes for Low-Temperature Formation of Fully Metal Oxide Thin-Film Transistors. *Chem. Mater.* **2015**, *27* (16), 5808–5812.

(79) Hwan Hwang, Y.; Seo, J.-S.; Moon Yun, J.; Park, H.; Yang, S.; Ko Park, S.-H.; Bae, B.-S. An "aqueous Route" for the Fabrication of Low-Temperature-Processable Oxide Flexible Transparent Thin-Film Transistors on Plastic Substrates. *NPG Asia Mater.* **2013**, *5* (4), e45.

(80) Meyers, S. T.; Anderson, J. T.; Hong, D.; Hung, C. M.; Wager, J. F.; Keszler, D. A. Solution-Processed Aluminum Oxide Phosphate Thin-Film Dielectrics. *Chem. Mater.* **2007**, *19* (16), 4023–4029.

(81) Mansergh, R. H.; Fullmer, L. B.; Park, D. H.; Nyman, M.; Keszler, D. A. Reaction Pathway: Aqueous Hexatantalate Clusters to High-Density Tantalum Oxide Nanofilms. *Chem. Mater.* **2016**, *28* (5), 1553–1558.

(82) Liu, G.; Liu, A.; Zhu, H.; Shin, B.; Fortunato, E.; Martins, R.; Wang, Y.; Shan, F. Lowerature, Nontoxic Water-Induced Metal-Oxide Thin Films and Their Application in Thin-Film Transistors. *Adv. Funct. Mater.* **2015**, *25* (17), 2564–2572.

(83) Liu, A.; Liu, G.; Zhu, H.; Meng, Y.; Song, H.; Shin, B.; Fortunato, E.; Martins, R.; Shan, F. A Water-Induced High-K Yttrium Oxide Dielectric for Fully-Solution-Processed Oxide Thin-Film Transistors. *Curr. Appl. Phys.* **2014**, *15*, S75–S81.

(84) Jiang, K.; Anderson, J. T.; Hoshino, K.; Li, D.; Wager, J. F.; Keszler, D. A. Low-Energy Path to Dense HfO2 Thin Films with Aqueous Precursor. *Chem. Mater.* **2011**, *23* (4), 945–952.

(85) Chang, J.; Chang, K. L.; Chi, C.; Zhang, J.; Wu, J. Water Induced Zinc Oxide Thin Film Formation and Its Transistor Performance. *J. Mater. Chem. C* **2014**, *2*, 5397.

(86) Chang, J.; Chang, K. L.; Chi, C.; Zhang, J.; Wu, J. Water Induced Zinc Oxide Thin Film Formation and Its Transistor Performance. *J. Mater. Chem. C* **2014**, *2*, 5397–5403.

(87) Shafran, K. L.; Perry, C. C. A Systematic Investigation of Aluminium Ion Speciation at High Temperature. Part 1. Solution Studies. *Dalton Trans.* **2005**, No. 12, 2098–2105.

(88) Hammann, B.; Ma, Z. L.; Wentz, K. M.; Kamunde-Devonish, M. K.; Johnson, D.; Hayes, S. E. Structural Study by Solid-State 71Ga NMR of Thin Film Transistor Precursors. *Dalt. Trans.* **2015**, *44*, Ahead of Print.

(89) Hammann, B. A.; Marsh, D. A.; Ma, Z. L.; Wood, S. R.; Eric West, M.; Johnson, D. W.; Hayes, S. E. Synthetic Routes to a Nanoscale Inorganic Cluster $[Ga_{13}(\mu_3\text{-}OH)_6(\mu_2\text{-}OH)_{18}(H_2O)](NO_3)_{15}$ Evaluated by Solid-State ^{71}Ga NMR. *J. Solid State Chem.* **2016**, *242*, 193–198.

(90) Wu, X.; Wang, D.; Ge, X.; Tang, H. Coagulation of Silica Microspheres with Hydrolyzed Al(III)-Significance of Al_{13} and Al_{13} Aggregates. *Colloids Surfaces A Physicochem. Eng. Asp.* **2008**, *330* (1), 72–79.

(91) Georgalis, Y.; Kierzek, A. M.; Saenger, W. Cluster Formation in Aqueous Electrolyte Solutions Observed by Dynamic Light Scattering. *J. Phys. Chem. B* **2000**, *104* (15), 3405–3406.

(92) Cherr, G.; Cardinale, B. J.; Miller, R.; Ji, Z. Stability and Aggregation of Metal Oxide Nanoparticles in Natural Aqueous Matrices. **2010**, *44* (6), 0–5.

(93) Zhu, C.; Liu, A.; LIU, G.; Jang, G.; Meng, Y.; Fortunato, E.; Martins, R.; Shan, F. Low-Temperature, Nontoxic Water-Induced High-K Zirconium Oxide Dielectrics for Low-Voltage, High-Performance Oxide Thin-Film Transistors. *J. Mater. Chem. C* **2016**.

(94) Liu, A.; Liu, G.; Zhu, H.; Song, H.; Shin, B.; Fortunato, E.; Martins, R.; Shan, F. Water-Induced Scandium Oxide Dielectric for Low-Operating Voltage N- and P-Type Metal-Oxide Thin-Film Transistors. *Adv. Funct. Mater.* **2015**, *25* (46), 7180–7188.

(95) Liu, A.; Liu, G.; Zhu, H.; Shin, B.; Fortunato, E.; Martins, R.; Shan, F. Eco-Friendly Water-Induced Aluminum Oxide Dielectrics and Their Applications in Hybrid Metal Oxide/Polymer TFT. *RSC Adv.* **2015**, *5*, 86606–86613.

(96) Liu, A.; Liu, G. X.; Zhu, H. H.; Xu, F.; Fortunato, E.; Martins, R.; Shan, F. K. Fully Solution-Processed Low-Voltage Aqueous In 2 O 3 Thin-Film Transistors Using an Ultrathin ZrO X Dielectric. *ACS Appl. Mater. Interfaces* **2014**, *6* (20), 17364–17369.

(97) Kim, M.-G.; Kanatzidis, M. G.; Facchetti, A.; Marks, T. J. Low-Temperature Fabrication of High-Performance Metal Oxide Thin-Film Electronics via Combustion Processing SI. *Nat. Mater.* **2011**, *10* (5), 382–388.

(98) Arii, T.; Kishi, A. The Effect of Humidity on Thermal Process of Zinc Acetate. *Thermochim. Acta* **2003**, *400*, 175–185.

(99) Anderson, J. T.; Munsee, C. L.; Hung, C. M.; Phung, T. M.; Herman, G. S.; Johnson, D. C.; Wager, J. F.; Keszler, D. A. Solution-Processed HafSOx and ZircSOx Inorganic Thin-Film Dielectrics and Nanolaminates. *Adv. Funct. Mater.* **2007**, *17* (13), 2117–2124.

(100) Payne, D. J.; Egdell, R. G.; Walsh, A.; Watson, G. W.; Guo, J.; Glans, P. A.; Learmonth, T.; Smith, K. E. Electronic Origins of Structural Distortions in Post-Transition Metal Oxides: Experimental and Theoretical Evidence for a Revision of

the Lone Pair Model. *Phys. Rev. Lett.* **2006**, *96* (15), 1–4.

(101) Biesinger, M. C.; Lau, L. W. M.; Gerson, A. R.; Smart, R. S. C. Resolving Surface Chemical States in XPS Analysis of First Row Transition Metals, Oxides and Hydroxides: Sc, Ti, V, Cu and Zn. *Appl. Surf. Sci.* **2010**, *257* (3), 887–898.

(102) J. J. Donovan, T. N. T. An Imporved Atomic Number Background Correction for Quantitative Microanalysis. *JSMA* **1996**, *2* (1), 1–7.

(103) Qiang, W. U.; Yunbo, Y. U.; Hong, H. E. Mechanistic Study of Selective Catalytic Reduction of NO_X with C_2H_5OH and CH_3OCH_3 over Ag / Al_2O_3 by in Situ DRIFTS. **2006**, *27* (11), 2–6.

(104) Mulla, S. S.; Chaugule, S. S.; Yezerets, A.; Currier, N. W.; Delgass, W. N.; Ribeiro, F. H. Regeneration Mechanism of Pt / BaO / Al_2O_3 Lean NO_X Trap Catalyst with H_2. **2008**, *136* (x), 136–145.

(105) James, D.; Fourré, E.; Ishii, M.; Bowker, M. Catalytic Decomposition/regeneration of Pt/$Ba(NO_3)_2$ Catalysts: NO_x Storage and Reduction. *Appl. Catal. B Environ.* **2003**, *45* (2), 147–159.

(106) Chmielarz, L.; Dziembaj, R.; Grzybek, T.; Klinik, J.; Lojewski, T.; Olszewska, D.; Papp, H. Pillared Smectite Modified with Carbon and Manganese as Catalyst for SCR of NO_x with NH_3. Part I. General Characterization and Catalyst Screening. *Catal. Letters* **2000**, *68* (1–2), 95–100.

(107) Jiang, K.; Anderson, J. T.; Hoshino, K.; Li, D.; Wager, J. F.; Keszler, D. A. Low-Energy Path to Dense HfO2 Thin Films with Aqueous Precursor. *Chem. Mater.* **2011**, *23* (4), 945–952.

(108) Thompson, C.; Palasantzas, G.; Feng, Y. P.; Sinha, S. K.; Krim, J. X-Ray-Reflectivity Study of the Growth Kinetics of Vapor-Deposited Silver Films. *Phys. Rev. B* **1994**, *49* (7), 4902–4907.

(109) Schmitt, Johannes, Grunewald, Torsten, Decher, Gero, Pershan, Peter S., Kjare, Kristian and Löschre, M. Internal Structure of Layer-by-Layer Adsorbed Polyelectrolyte Films: A Neutron and X-Ray Reflectivity Study. *Macromolecules* **1993**, *26*, 7058–7063.

(110) H. You, H. K. K. X-Ray Reflectivity and Scanning-Tunneling-Microscope Study of Kinetic Roughening of Sputter-Deposited Gold Films during Growth. *Phys. Rev. B - Condens. Matter Mater. Phys.* **1993**, *70* (19), 2900–2903.

(111) Pal, B. N.; Dhar, B. M.; See, K. C.; Katz, H. E. Solution-Deposited Sodium Beta-Alumina Gate Dielectrics for Low-Voltage and Transparent Field-Effect Transistors. *Nat. Mater.* **2009**, *8* (11), 898–903.

(112) Figueiredo, V.; Elangovan, E.; Gonçalves, G.; Barquinha, P.; Pereira, L.; Franco, N.; Alves, E.; Martins, R.; Fortunato, E. Effect of Post-Annealing on the Properties of Copper Oxide Thin Films Obtained from the Oxidation of Evaporated Metallic Copper. *Appl. Surf. Sci.* **2008**, *254* (13), 3949–3954.

(113) Stowers, J.; Keszler, D. A. High Resolution, High Sensitivity Inorganic Resists. *Microelectron. Eng.* **2009**, *86* (4–6), 730–733.

(114) Perkins, C. K.; Mansergh, R. H.; Park, D.-H.; Nanayakkara, C. E.; Ramos, J. C.; Decker, S. R.; Huang, Y.; Chabal, Y. J.; Keszler, D. A. Aqueous Process to Limit Hydration of Thin-Film Inorganic Oxides. *Solid State Sci.* **2016**, *61*, 106–110.

(115) Oleksak, R. P.; Ruther, R. E.; Luo, F.; Fairley, K. C.; Decker, S. R.; Stickle, W. F.; Johnson, D. W.; Garfunkel, E. L.; Herman, G. S.; Keszler, D. A. Chemical and Structural Investigation of High-Resolution Patterning with HafSOx. *ACS Appl. Mater. Interfaces* **2014**, *6* (4), 2917–2921.

(116) Fairley, K. C.; Merrill, D. R.; Woods, K. N.; Ditto, J.; Xu, C.; Oleksak, R. P.; Gustafsson, T.; Johnson, D. W.; Garfunkel, E. L.; Herman, G. S.; Johnson, D. C.; Page, C. J. Non-Uniform Composition Profiles in Inorganic Thin Films from Aqueous Solutions. *ACS Appl. Mater. Interfaces* **2016**, *8* (1), 667–672.

(117) Anderson, J. T.; Wang, W.; Jiang, K.; Gustafsson, T.; Xu, C.; Gafunkel, E. L.; Keszler, D. A. Chemically Amplified Dehydration of Thin Oxide Films. *ACS Sustain. Chem. Eng.* **2015**, *3* (6), 1081–1085.

Chapter II

(1) Duan, C.; Tanner, P.; Makhov, V.; Kirm, M. Vacuum Ultraviolet Spectra and Crystal Field Analysis of $YAlO_3$ Doped with Nd^{3+} and Er^{3+}. Phys. Rev. B 2007, 75, 195130 1−12.

(2) Stanek, C. R.; McClellan, K. J.; Levy, M. R.; Grimes, R. W. Defect Behavior in Rare Earth $REAlO_3$ Scintillators. J. Appl. Phys. 2006, 99, 113518 1−7.

(3) Gruber, J. B.; Nash, K. L.; Yow, R. M.; Sardar, D. K.; Valiev, U. V.; Uzokov, A. A.; Burdick, G. W. Spectroscopic and Magnetic Susceptibility Analyses of the 7 FJ and 5 D4 Energy Levels of $Tb^{3+}(4f_8)$ in $TbAlO_3$. J. Lumin. 2008, 128, 1271−1284.

(4) Weber, J. K. R.; Abadie, J. G.; Key, T. S.; Hiera, K.; Nordine, P. C. Synthesis and Optical Properties of Rare-Earth−Aluminum Oxide Glasses. J. Am. Ceram. Soc. 2002, 11, 1309−1311.

(5) Cho, S. Y.; Kim, I. T.; Hong, K. S. Microwave Dielectric Properties and Applications of Rare-Earth Aluminates. J. Mater. Res. 1999, 14, 114−119.

(6) Suhane, A.; Cacciato, A.; Richard, O.; Arreghini, A.; Adelmann, C.; Swerts, J.; Rothschild, O.; Van den bosch, G.; Breuil, L.; Bender, H.; Jurczak, M.; Debusschere, I.; Kittl, J. A.; De Meyer, K.; Van Houdt, J. Rare-Earth Aluminates as a Charge Trapping Materials for NAND Flash Memories: Integration and Electrical Evaluation. Solid-State Electron. 2011, 65−66, 177−183.

(7) Wu, S. X.; Peng, H. Y.; Wu, T. Concurrent Nonvolatile Resistance and Capacitance Switching in $LaAlO_3$. Appl. Phys. Lett. 2011, 98, 093503 1−3.

(8) Zahid, M. B.; Degraeve, R.; Toledano-Luque, M.; Van Houdt, J. Characterization of Hexagonal Rare-Earth Aluminates for Application in Flash Memories. IEEE Int. Reliab. Phys. Symp. Proc. 2011, 815−818.

(9) Zhao, C.; Zhao, C. Z.; Lu, Q.; Yan, X.; Taylor, S.; Chalker, P. R. Hysteresis in Lanthanide Aluminum Oxides Observed by Fast Pulse CV Measurement. Materials 2014, 7, 6965−6981.

(10) Leskela, M.; Kukli, K.; Ritala, M. Rare-Earth Oxide Thin Films¨for Gate Dielectrics in Microelectronics. J. Alloys Compd. 2006, 418, 27−34.

(11) Lopes, J. M. J.; Roeckerath, M.; Heeg, T.; Littmark, U.; Schubert, J.; Mantl, S.; Jia, Y.; Schlom, D. G. La-Based Ternary RareEarth Oxides as Alternative High-κ Dielectrics. Microelectron. Eng. 2007, 84, 1890−1893.

(12) Bere, M. K.; Liu, Y.; Kyaw, L. M.; Ngoo, Y. J.; Singh, S. P.; Chor, E. F. Fabrication and Performances of InAlN/GaN-on-Si MOSHEMTs with $LaAlO_3$ Gate Dielectric Using Gate-First CMOS Compatible Process at Low Thermal Budget. ECS Trans. 2014, 61, 271−280.

(13) Wu, C. H.; Wang, S. J.; Huang, H. Y.; Chang, K. M.; Hsu, H. Y. Investigation of $LaAlO_3/ZrO_2$/a-InGaZnO Thin-Film Transistors Using Atmospheric Pressure Plasma Jet. Electron. Lett. 2014, 50, 706−708.

(14) Zheng, Z. W.; Cheng, C. H.; Chen, Y. C. Low Operation Voltage InGaZnO Thin Film Transistors with $LaAlO_3$ Gate Dielectric Incorporation. ECS J. Solid State Sci. Technol. 2013, 2, 179−181.

(15) Shoup, S. S.; Paranthaman, M.; Beach, D. B.; Specht, E. D.; Williams, R. K. Sol-gel Synthesis of LaAlO3; Epitaxial Growth of $LaAlO_3$ Thin Films on SrTiO3 (100). J. Mater. Res. 1997, 12, 1017− 1021.

(16) Shoup, S. S.; Paranthaman, M.; Goyal, A.; Specht, E. D.; Lee, D. F.; Kroeger, D. M.; Beach, D. B. Epitaxial Thin Film Growth of Lanthanum and Neodymium

Aluminate Films on Roll-Textured Nickel Using a Sol-Gel Method. J. Am. Ceram. Soc. 1998, 81, 3019− 3021.

(17) Huijben, M.; Brinkman, A.; Koster, G.; Rijnders, G.; Hilgenkamp, H.; Blank, D. H. A. Structure−Property Relation of $SrTiO_3/LaAlO_3$ Interfaces. Adv. Mater. 2009, 21, 1665−1677.

(18) Fortunato, E.; Barquinha, P.; Martins, R. Oxide Semiconductor Thin-Film Transistors: A Review of Recent Advances. Adv. Mater. 2012, 24, 2945−2986.

(19) Niinisto, L.; Nieminen, M.; Paivasaari, J.; Niinisto, J.; Putkonen, M.; Nieminen, M. Advanced Electronic and Optoelectronic Materials by Atomic Layer Deposition: An Overview with Special Emphasis on ACS Applied Materials & Interfaces Research Article DOI: 10.1021/am507271e ACS Appl. Mater. Interfaces 2015, 7, 1678−1684 1683 Recent Progress in Processing of High-K Dielectrics and Other Oxide Materials. Phys. Status Solidi A 2004, 201, 1443−1452.

(20) Jones, A. C.; Chalker, P. R. Some Recent Developments in the Chemical Vapor Deposition of Electroceramic Oxides. J. Phys. D: Appl. Phys. 2003, 36, 80−95.

(21) Christen, H. M.; Eres, G. Recent Advances in Pulsed-Laser Deposition of Complex Oxides. J. Phys.: Condens. Matter 2008, 20, 264005 1−16.

(22) Jia, T. T.; Cheng, X. H.; Chao, D.; Xu, D. W.; Wang, Z. J.; Xia, C.; Zhang, Y. W.; Yu, Y. H. Properties of LaAlO3 Thin Film on GaAs(100) Treated by In Situ NH3 Plasma. Nucl. Instrum. Methods Phys. Res, Sect B 2013, 307, 349−352.

(23) Liu, K. C.; Tzeng, W. H.; Chang, K. M.; Huang, J. J.; Lee, Y. J.; Yeh, P. H.; Chen, P. S.; Lee, H. Y.; Chen, F.; Tsai, M. J. Investigation of the Effect of Different Oxygen Partial Pressure to $LaAlO_3$ Thin Film Properties and Resistive Switching Characteristics. Thin Solid Films 2011, 520, 1246−1250.

(24) Wu, S.; Ren, L.; Qing, J.; Yu, F.; Yang, K.; Yang, M.; Wang, Y.; Meng, M.; Zhou, W.; Zhou, X.; Li, S. Bipolar Resistance Switching in Transparent $ITO/LaAlO_3/SrTiO_3$ Memristors. ACS Appl. Mater. Interfaces 2014, 6, 8575−8579.

(25) Lu, X. B.; Liu, Z. G.; Zhang, X.; Huang, R.; Zhou, H. W.; Wang, X. P.; Nguyen, B. C. Investigation of High-Quality Ultra-Thin $LaAlO_3$ Films as High-κ Gate Dielectrics. J. Phys. D: Appl. Phys. 2003, 36, 3047−3050.

(26) Vellianitis, G.; Apostolopoulos, G.; Mavrou, G.; Argyropoulos, K.; Dimoulas, A.; Hooker, J. C.; Conard, T.; Butcher, M. MBE Lanthanum-Based High-K Gate Dielectrics as Candidates for SiO2 Gate Oxide Replacement. Mater. Sci. Eng., B 2004, 109, 85−88.

(27) Li, A. D.; Shao, Q. Y.; Ling, H. Q.; Cheng, J. B.; Wu, D.; Liu, Z. G.; Ming, N. B.; Wang, C.; Zhou, H. W.; Nguyen, B. Y. Characteristics of $LaAlO_3$ Gate Dielectrics on Si Grown by Metalorganic Chemical Vapor Deposition. Appl. Phys. Lett. 2003, 83, 3540−3542.

(28) Lu, X.; Liu, Z.; Wang, Y.; Yang, Y.; Wang, X.; Zhou, H.; Nguyen, B. Structure and Dielectric Properties of Amorphous $LaAlO_3$ and $LaAlO_xN_y$ Films as Alternative Gate Dielectric Materials. J. Appl. Phys. 2003, 94, 1229−1234.

(29) Xiang, W.; Lü, H.; Yan, L.; Guo, H.; Liu, L.; Zhou, Y.; Yang, G.; Jiang, J.; Cheng, H.; Chen, Z. Characteristics of $LaAlO_3$/Si (100) Deposited under Various Oxygen Pressures. J. Appl. Phys. 2003, 93, 533−536.

(30) Chang, I. Y.; You, S.; Juan, P.; Wang, M.; Lee, J. Y. The Electrical and Interfacial Properties of Metal-High-κ Oxide Semiconductor Field-Effect Transistors With LaAlO3 Gate Dielectric. IEEE Electron Device Lett. 2009, 30, 161−164.

(31) Chung, W. F.; Chang, T. C.; Li, H. W.; Chen, S. C.; Chen, Y. C.; Tseng, T. Y.; Tai, Y. H. Environment-Dependent Thermal Instability of Sol-Gel Derived Amorphous Indium-Gallium-Zinc-Oxide Thin Film Transistors. Appl. Phys. Lett. 2011, 98, 152109 1−3.

(32) Ng, M. F.; Cima, M. J. Heteroepitaxial Growth of Lanthanum Aluminate Films Derived from Mixed Metal Nitrates. J. Mater. Res. 1997, 12, 1306−1314.

(33) Meyers, S. T.; Anderson, J. T.; Hong, D.; Hung, C. M.; Wager, J. F.; Keszler, D. A. Solution-Processed Aluminum Oxide Phosphate Thin-Film Dielectrics. Chem. Mater. 2007, 19, 4023−4029.

(34) Jiang, K.; Anderson, J. T.; Hoshino, K.; Li, D.; Wager, J. F.; Keszler, D. A. Low-Energy Path to Dense HfO_2 Thin Films with Aqueous Precursor. Chem. Mater. 2011, 23, 945−952.

(35) Anderson, J. T.; Munsee, C. L.; Hung, C. M.; Phung, T. M.; Herman, G. S.; Johnson, D. C.; Wager, J. F.; Keszler, D. A. SolutionProcessed HafSOx and ZircSOx Inorganic Thin-Film Dielectrics and Nanolaminates. Adv. Funct. Mater. 2007, 17, 2117−2124.

(36) Park, S. Y.; Kim, B. J.; Kim, K.; Kang, M. S.; Lim, K. H.; Lee, T. I; Myoung, J. M.; Baik, H. K.; Cho, J. H.; Kim, Y. S. Low-Temperature, Solution-Processed and Alkali Metal Doped ZnO for High-Performance Thin-Film Transistors. Adv. Mater. 2012, 24, 834−838.

(37) Meyers, S. T.; Anderson, J. T.; Hung, C. M.; Thompson, J.; Wager, J. F.; Keszler, D. A. Aqueous Inorganic Inks for LowTemperature Fabrication of ZnO TFTs. J. Am. Chem. Soc. 2008, 130, 17603−17609.

(38) Nadarajah, A.; Carnes, M. E.; Kast, M. G.; Johnson, D. W.; Boettcher, S. W. Aqueous Solution Processing of F-Doped SnO_2 Transparent Conducting Oxide Films Using a Reactive Tin(II) Hydroxide Nitrate Nanoscale Cluster. Chem. Mater. 2013, 25, 4080−4087.

(39) Smith, S. W.; Wang, W.; Keszler, D. A.; Conley, J. F. Solution Based Prompt Inorganic Condensation and Atomic Layer Deposition of Al_2O_3 Films: A Side-by-Side Comparison. J. Vac. Sci. Technol., A 2014, 32, 041501 1−7.

(40) Wang, W.; Wentz, K. M.; Hayes, S. E.; Johnson, D. W.; Keszler, D. A. Synthesis of the Hydroxide Cluster $[Al_{13}(\mu_3\text{-}OH)_6(\mu\text{-}OH)_{18}(H2O)_{24}]^{15+}$ From an Aqueous Solution. Inorg. Chem. 2011, 50, 4683−4685.

(41) Calvez, G.; Daiguebonne, C.; Guillou, O.; Le Dret, F. A New Series of Anhydrous Lanthanide-Based Octahedral Hexanuclear Complexes. Eur. J. Inorg. Chem. 2009, 3172−3178.

(42) Donovan, J.; Tingle, T. An Improved Mean Atomic Number Background Correction for Quantitative Microanalysis. J. Microsc. Soc. Am. 1996, 1−7.

(43) Rudolph, W. W.; Mason, R.; Pye, C. C. Aluminium(III) Hydration in Aqueous Solution. A Raman Spectroscopic Investigation and an Ab Initio Molecular Orbital Study of Aluminium(III) Water Clusters. Phys. Chem. Chem. Phys. 2000, 2, 5030−5040.

(44) Knoeckl, J. Vibrational Spectrometric and Electrochemical Lanthanum(III)-Nitrate Complexes in Aqueous. Anal. Chem. 1969, 41, 2069−2071.

(45) Kanno, H.; Hiraishi, J. Raman Study of Aqueous Rare-Earth Nitrate Solutions in Liquid and Glassy States. J. Phys. Chem. 1984, 88, 2787−2792.

(46) Klingenberg, B.; Vannice, M. A. Influence of Pretreatment on Lanthanum Nitrate, Carbonate, and Oxide Powders. Chem. Mater. 1996, 8, 2755−2768.

(47) Yuvaraj, S.; Fan-Yuan, L.; Tsong-Huei, C.; Chuin-Tih, Y. Thermal Decomposition of Metal Nitrates in Air and Hydrogen Environments. J. Phys. Chem. B 2003, 107, 1044−1047.

(48) Devine, R. A. B. Infrared and Electrical Properties of Amorphous Sputtered $(La_xAl_{1-x})_2O_3$ Films. J. Appl. Phys. 2003, 93, 9938−9942.

(49) Sze, S. M.; Ng, K. K. Physics of Semiconductor Devices, 3rd ed; Wiley-Interscience: Hoboken, NJ, 2007; pp 223−225.

(50) Schmidt, J.; Merkle, A.; Brendel, R.; Hoex, B.; van de Sanden, M. C. M.; Kessels, W. M. M. Surface Passivation of High-Efficiency Silicon Solar Cells by Atomic-Layer-Deposited Al_2O_3. Prog. Photovoltaics 2008, 16, 461−466.

(51) Hoex, B.; Schmidt, J.; Bock, R.; Altermatt, P. P.; van de Sanden, M. C. M.; Kessels, W. M. M. Excellent Passivation of Highly Doped PType Si Surfaces by the Negative-Charge-Dielectric Al_2O_3. Appl. Phys. Lett. 2007, 91, 112107 1−3.

(52) Zheng, Z. W.; Chen, Y. C. Improved Performances in LowVoltage-Driven InGaZnO Thin Film Transistors Using a SiO_2 Buffer Layer Insertion. Appl. Phys. A: Mater. Sci. Process. 2014, 115, 937−941.

(53) Wager, J. F.; Keszler, D. A.; Presley, R. E. Transparent Electronics; Springer: New York, 2008; pp 234−238.

Chapter III

(1) Heo, J.; Kim, S. B.; Gordon, R. G. Atomic Layer Deposited Zinc Tin Oxide Channel for Amorphous Oxide Thin Film Transistors. *Appl. Phys. Lett.* **2012**, *101* (11), 10–15.

(2) Kukli, K.; Ritala, M.; Pore, V.; Leskelä, M.; Sajavaara, T.; Hegde, R. I.; Gilmer, D. C.; Tobin, P. J.; Jones, a. C.; Aspinall, H. C. Atomic Layer Deposition and Properties of Lanthanum Oxide and Lanthanum-Aluminum-Oxide Films. *Chem. Vap. Depos.* **2006**, *12* (2–3), 158–164.

(3) Banger, K. K.; Yamashita, Y.; Mori, K.; Peterson, R. L.; Leedham, T.; Rickard, J.; Sirringhaus, H. Low-Temperature, High-Performance Solution-Processed Metal Oxide Thin-Film Transistors Formed by a "sol–gel on Chip" Process. *Nat. Mater.* **2011**, *10* (1), 45–50.

(4) Ko, J.; Kim, J.; Park, S. Y.; Lee, E.; Kim, K.; Lim, K.-H.; Kim, Y. S. Solution-Processed Amorphous Hafnium-Lanthanum Oxide Gate Insulator for Oxide Thin-Film Transistors. *J. Mater. Chem. C* **2014**, *2* (6), 1050.

(5) Mansergh, R. H.; Fullmer, L. B.; Park, D. H.; Nyman, M.; Keszler, D. A. Reaction Pathway: Aqueous Hexatantalate Clusters to High-Density Tantalum Oxide Nanofilms. *Chem. Mater.* **2016**, *28* (5), 1553–1558.

(6) Anderson, J. T.; Munsee, C. L.; Hung, C. M.; Phung, T. M.; Herman, G. S.; Johnson, D. C.; Wager, J. F.; Keszler, D. A. Solution-Processed HafSOx and ZircSOx Inorganic Thin-Film Dielectrics and Nanolaminates. *Adv. Funct. Mater.* **2007**, *17* (13), 2117–2124.

(7) Chang, J.; Chang, K. L.; Chi, C.; Zhang, J.; Wu, J. Water Induced Zinc Oxide Thin

Film Formation and Its Transistor Performance. *J. Mater. Chem. C* **2014**, *2*, 5397.

(8) Jiang, K.; Anderson, J. T.; Hoshino, K.; Li, D.; Wager, J. F.; Keszler, D. a. Low-Energy Path to Dense HfO2 Thin Films with Aqueous Precursor. *Chem. Mater.* **2011**, *23* (4), 945–952.

(9) Liu, A.; Liu, G.; Zhu, H.; Song, H.; Shin, B.; Fortunato, E.; Martins, R.; Shan, F. Water-Induced Scandium Oxide Dielectric for Low-Operating Voltage N- and P-Type Metal-Oxide Thin-Film Transistors. *Adv. Funct. Mater.* **2015**, *25* (46), 7180–7188.

(10) Liu, G.; Liu, A.; Zhu, H.; Shin, B.; Fortunato, E.; Martins, R.; Wang, Y.; Shan, F. Lowerature, Nontoxic Water-Induced Metal-Oxide Thin Films and Their Application in Thin-Film Transistors. *Adv. Funct. Mater.* **2015**, *25* (17), 2564–2572.

(11) Meyers, S. T.; Anderson, J. T.; Hong, D.; Hung, C. M.; Wager, J. F.; Keszler, D. a. Solution-Processed Aluminum Oxide Phosphate Thin-Film Dielectrics. *Chem. Mater.* **2007**, *19* (16), 4023–4029.

(12) Nadarajah, A.; Wu, M. Z. B.; Archila, K.; Kasti, M. G.; Smith, A. M.; Chiang, T. H.; Keszler, D. A.; Wager, J. F.; Boettcher, S. W. Amorphous In-Ga-Zn Oxide Semiconducting Thin Films with High Mobility from Electrochemically Generated Aqueous Nanocluster Inks. *Chem. Mater.* **2015**, *27* (16), 5587–5596.

(13) Plassmeyer, P. N.; Archila, K.; Wager, J. F.; Page, C. J. Lanthanum Aluminum Oxide Thin-Film Dielectrics from Aqueous Solution. *ACS Appl. Mater. Interfaces* **2015**, *7* (3), 1678–1684.

(14) Bakos, T.; Rashkeev, S. N.; Pantelides, S. T. H2O and O2 Molecules in Amorphous SiO_2: Defect Formation and Annihilation Mechanisms. *Phys. Rev. B - Condens. Matter Mater. Phys.* **2004**, *69* (19), 1–9.

(15) Bakos, T.; Rashkeev, S. N.; Pantelides, S. T. Reactions and Diffusion of Water and Oxygen Molecules in Amorphous SiO_2 *Phys. Rev. Lett.* **2002**, *88* (5), 55508.

(16) Arii, T.; Kishi, A. Humidity Controlled Thermal Analysis. The Effect of Humidity on Thermal Decomposition of Zinc Acetylacetonate Monohydrate. *J. Therm. Anal. Calorim.* **2006**, *83*, 253–260.

(17) Arii, T.; Kishi, A. The Effect of Humidity on Thermal Process of Zinc Acetate. *Thermochim. Acta* **2003**, *400*, 175–185.

(18) Mauger, S. A.; Steirer, K. X.; Boé, J.; Ostrowski, D. P.; Olson, D. C.; Hammond, S. R. Effects of Humidity during Formation of Zinc Oxide Electron Contact Layers from a Diethylzinc Precursor Solution. *Org. Electron. physics, Mater. Appl.* **2016**, *31*, 63–70.

(19) Anderson, J. T.; Wang, W.; Jiang, K.; Gustafsson, T.; Xu, C.; Gafunkel, E. L.;

Keszler, D. A. Chemically Amplified Dehydration of Thin Oxide Films. *ACS Sustain. Chem. Eng.* **2015**, *3* (6), 1081–1085.

(20) Perkins, C. K.; Mansergh, R. H.; Park, D.-H.; Nanayakkara, C. E.; Ramos, J. C.; Decker, S. R.; Huang, Y.; Chabal, Y. J.; Keszler, D. A. Aqueous Process to Limit Hydration of Thin-Film Inorganic Oxides. *Solid State Sci.* **2016**, *61*, 106–110.

(21) Chen, B. T. Investigation of the Solvent-Evaporation Effect on Spin Coating of Thin Films. *Polymer Engineering and Science*. 1983, pp 399–403.

(22) Fairley, K. C.; Merrill, D. R.; Woods, K. N.; Ditto, J.; Xu, C.; Oleksak, R. P.; Gustafsson, T.; Johnson, D. W.; Garfunkel, E. L.; Herman, G. S.; Johnson, D. C.; Page, C. J. Non-Uniform Composition Profiles in Inorganic Thin Films from Aqueous Solutions. *ACS Appl. Mater. Interfaces* **2016**, *8* (1), 667–672.

(23) Flack, W. W.; Soong, D. S.; Bell, A. T.; Hess, D. W. A Mathematical Model for Spin Coating of Polymer Resists. *J. Appl. Phys.* **1984**, *56* (4), 1199–1206.

(24) Shimoji, S. A New Analytical Model for Spin Coating Process with Solvent Evaporation. *Japanese J. Appl. Phys. Part 2-Letters* **1987**, *26* (6), L905–L907.

(25) Anderson, J. T.; Munsee, C. L.; Hung, C. M.; Phung, T. M.; Herman, G. S.; Johnson, D. C.; Wager, J. F.; Keszler, D. A. Solution-Processed HafSOx and ZircSOx Inorganic Thin-Film Dielectrics and Nanolaminates. *Adv. Funct. Mater.* **2007**, *17* (13), 2117–2124.

(26) Hammond, P. F.; Goslin, R. The Effect of Humidity Upon the Rate of Evaporation. *Ecology* **1933**, *14* (4), 411–413.

(27) Kampmeyer, P. M. The Temperature Dependence of Viscosity for Water and Mercury. *J. Appl. Phys.* **1952**, *23* (1), 99–102.

Chapter IV

(1) Niinistö, L.; Päiväsaari, J.; Niinistö, J.; Putkonen, M.; Nieminen, M. Advanced Electronic and Optoelectronic Materials by Atomic Layer Deposition: An Overview with Special Emphasis on Recent Progress in Processing of High-K Dielectrics and Other Oxide Materials. *Phys. Status Solidi A* **2004**, *201*, 1443–1452.

(2) Jones, A. C.; Aspinall, H. C.; Chalker, P. R.; Potter, R. J.; Kukli, K.; Rahtu, A.; Ritala, M.; Leskela, M. Some Recent Developments in the MOCVD and ALD of High-K Dielectric Oxides. *J. Mater. Chem.* **2004**, *14*, 3101–3112.

(3) Jones, A. C.; Chalker, P. R. Some Recent Developments in the Chemical Vapour Deposition of Electroceramic Oxides. *J. Phys. D. Appl. Phys.* **2003**, *36*, R80–R95.

(4) Christen, H. M.; Eres, G. Recent Advances in Pulsed-Laser Deposition of

Complex Oxides. *J. Phys. Condens. Matter* **2008**, *20*, 264005.

(5) Takata, R.; Neumann, A.; Weber, D.; Pham, D.-V.; Anselmann, R.; Kitamura, Y.; Kakimura, T.; Suzuki, S.; Minami, S.; Kodama, M. Scalability and Homogeneity of Slot Die-Coated Metal Oxide Semiconductor for TFTs. *J. Soc. Inf. Disp.* **2016**, *24*, 381–385.

(6) Thomas, S. R.; Pattanasattayavong, P.; Anthopoulos, T. D. Solution-Processable Metal Oxide Semiconductors for Thin-Film Transistor Applications. *Chem. Soc. Rev.* **2013**, *42*, 6910–6923.

(7) Hyun, S. K.; Kim, M. G.; Ha, Y. G.; Kanatzidis, M. G.; Marks, T. J.; Facchetti, A. Low-Temperature Solution-Processed Amorphous Indium Tin Oxide Field-Effect Transistors. *J. Am. Chem. Soc.* **2009**, *131*, 10826–10827.

(8) Banger, K. K.; Yamashita, Y.; Mori, K.; Peterson, R. L.; Leedham, T.; Rickard, J.; Sirringhaus, H. Low-Temperature, High-Performance Solution-Processed Metal Oxide Thin-Film Transistors Formed by a "Sol–Gel on Chip" Process. *Nat. Mater.* **2011**, *10*, 45–50.

(9) Aoki, Y.; Kunitake, T.; Nakao, A. Sol−Gel Fabrication of Dielectric HfO Nano-Films; Formation of Uniform, Void-Free Layers and Their Superior Electrical Properties. *Chem. Mater.* **2005**, *17*, 450–458.

(10) Kim, B. S.; Taek Jeong, Y.; Lee, D.; Choi, T.; Jung, S. H.; Whan Choi, J.; Yang, C.; Jo, K.; Lee, B. J.; Park, E.; Na Kim, D.; Kim, Y.; Shin, S. Solution-Processed Zinc-Indium-Tin Oxide Thin-Film Transistors for Flat-Panel Displays. *Appl. Phys. Lett.* **2013**, *103*, 2011–2016.

(11) Kim, H. S.; Byrne, P. D.; Facchetti, A.; Marks, T. J. High Performance Solution-Processed Indium Oxide Thin-Film Transistors. *J. Am. Chem. Soc.* **2008**, *130*, 12580–12581.

(12) Ong, B. S.; Li, C.; Li, Y.; Wu, Y.; Loutfy, R. Stable, Solution-Processed, High-Mobility ZnO Thin-Film Transistors. *J. Am. Chem. Soc.* **2007**, *129*, 2750–2751.

(13) Pal, B. N.; Dhar, B. M.; See, K. C.; Katz, H. E. Solution-Deposited Sodium Beta-Alumina Gate Dielectrics for Low-Voltage and Transparent Field-Effect Transistors. *Nat. Mater.* **2009**, *8*, 898–903.

(14) Zhu, L.; Gao, Y.; Li, X.; Sun, X. W.; Zhang, J. Development of High-K Hafnium–Aluminum Oxide Dielectric Films Using Sol–gel Process. *J. Mater. Res.* **2014**, *29*, 1620–1625.

(15) Schwartz, R. W.; Schneller, T.; Waser, R. Chemical Solution Deposition of Electronic Oxide Films. *Comptes Rendus Chim.* **2004**, *7*, 433–461.

(16) Brinker, C. J.; Scherer, G. W. *Sol-Gel Science: The Physics and Chemsistry of Sol-Gel Processing*; Academic Press: San Diego, CA, USA, **1990**.

(17) Bernal Ramos, K.; Saly, M. J.; Chabal, Y. J. Precursor Design and Reaction Mechanisms for the Atomic Layer Deposition of Metal Films. *Coord. Chem. Rev.* **2013**, *257*, 3271–3281.

(18) Pierson, H. O. *Handbook of Chemical Vapor Deposition: Principles, Technology and Applications*; 2nd Ed.; William Andrew Publishing: Norwich, **1999**.

(19) Chang, J.; Chang, K. L.; Chi, C.; Zhang, J.; Wu, J. Water Induced Zinc Oxide Thin Film Formation and Its Transistor Performance. *J. Mater. Chem. C* **2014**, *2*, 5397–5403.

(20) Hwang, Y. H.; Seo, J.-S.; Yun, J. M.; Park, H.; Yang, S.; Park, S.-H. K.; Bae, B.-S. An "Aqueous Route" for the Fabrication of Low-Temperature-Processable Oxide Flexible Transparent Thin-Film Transistors on Plastic Substrates. *NPG Asia Mater.* **2013**, *5*, e45.

(21) Liu, A.; Liu, G. X.; Zhu, H. H.; Xu, F.; Fortunato, E.; Martins, R.; Shan, F. K. Fully Solution-Processed Low-Voltage Aqueous In_2O_3 Thin-Film Transistors Using an Ultrathin ZrOx Dielectric. *ACS Appl. Mater. Interfaces* **2014**, *6*, 17364–17369.

(22) Liu, A.; Liu, G.; Zhu, H.; Meng, Y.; Song, H.; Shin, B.; Fortunato, E.; Martins, R.; Shan, F. A Water-Induced High-K Yttrium Oxide Dielectric for Fully-Solution-Processed Oxide Thin-Film Transistors. *Curr. Appl. Phys.* **2014**, *15*, S75–S81.

(23) Liu, A.; Liu, G.; Zhu, H.; Shin, B.; Fortunato, E.; Martins, R.; Shan, F. Eco-Friendly Water-Induced Aluminum Oxide Dielectrics and Their Applications in Hybrid Metal Oxide/Polymer TFT. *RSC Adv.* **2015**, *5*, 86606–86613.

(24) Liu, A.; Liu, G.; Zhu, H.; Song, H.; Shin, B.; Fortunato, E.; Martins, R.; Shan, F. Water-Induced Scandium Oxide Dielectric for Low-Operating Voltage N- and P-Type Metal-Oxide Thin-Film Transistors. *Adv. Funct. Mater.* **2015**, *25*, 7180–7188.

(25) Liu, G.; Liu, A.; Zhu, H.; Shin, B.; Fortunato, E.; Martins, R.; Wang, Y.; Shan, F. Low-Temperature, Nontoxic Water-Induced Metal-Oxide Thin Films and Their Application in Thin-Film Transistors. *Adv. Funct. Mater.* **2015**, *25*, 2564–2572.

(26) Rim, Y. S.; Chen, H.; Song, T.-B.; Bae, S.-H.; Yang, Y. Hexaaqua Metal Complexes for Low-Temperature Formation of Fully Metal Oxide Thin-Film Transistors. *Chem. Mater.* **2015**, *27*, 5808–5812.

(27) Xu, W.; Cao, H.; Liang, L.; Xu, J.-B. Aqueous Solution-Deposited Gallium Oxide Dielectric for Low-Temperature, Low-Operating-Voltage Indium Oxide Thin-Film Transistors: A Facile Route to Green Oxide Electronics. *ACS Appl. Mater. Interfaces* **2015**, *7*, 14720–14725.

(28) Anderson, J. T.; Munsee, C. L.; Hung, C. M.; Phung, T. M.; Herman, G. S.; Johnson, D. C.; Wager, J. F.; Keszler, D. A. Solution-Processed HafSOx and ZircSOx Inorganic Thin-Film Dielectrics and Nanolaminates. *Adv. Funct. Mater.* **2007**, *17*, 2117–2124.

(29) Meyers, S. T.; Anderson, J. T.; Hong, D.; Hung, C. M.; Wager, J. F.; Keszler, D. A. Solution-Processed Aluminum Oxide Phosphate Thin-Film Dielectrics. *Chem. Mater.* **2007**, *19*, 4023–4029.

(30) Jiang, K.; Anderson, J. T.; Hoshino, K.; Li, D.; Wager, J. F.; Keszler, D. A. Low-Energy Path to Dense HfO_2 Thin Films with Aqueous Precursor. *Chem. Mater.* **2011**, *23*, 945–952.

(31) Alemayehu, M.; Davis, J. E.; Jackson, M.; Lessig, B.; Smith, L.; Sumega, J. D.; Knutson, C.; Beekman, M.; Johnson, D. C.; Keszler, D. A. Tunable Dielectric Thin Films by Aqueous, Inorganic Solution-Based Processing. *Solid State Sci.* **2011**, *13*, 2037–2040.

(32) Carnes, M. E.; Knutson, C. C.; Nadarajah, A.; Jackson Jr., M. N.; Oliveri, A. F.; Norelli, K. M.; Crockett, B. M.; Bauers, S. R.; Moreno-Luna, H. A.; Taber, B. N.; Pacheco, D. J.; Olson, J. Z.; Brevick, K. R.; Sheehan, C. E.; Johnson, D. W.; Boettcher, S. W. Electrochemical Synthesis of Flat-$[Ga_{13-x}\,In_x\,(\mu_3\text{-}OH)_6\,(\mu\text{-}OH)_{18}\,(H_2O)_{24}\,(NO_3)_{15}]$ Clusters as Aqueous Precursors for Solution-Processed Semiconductors. *J. Mater. Chem. C* **2014**, *2*, 8492–8496.

(33) Plassmeyer, P. N.; Archila, K.; Wager, J. F.; Page, C. J. Lanthanum Aluminum Oxide Thin-Film Dielectrics from Aqueous Solution. *ACS Appl. Mater. Interfaces* **2015**, *7*, 1678–1684.

(34) Nadarajah, A.; Wu, M. Z. B.; Archila, K.; Kast, M. G.; Smith, A. M.; Chiang, T. H.; Keszler, D. A.; Wager, J. F.; Boettcher, S. W. Amorphous In–Ga–Zn Oxide Semiconducting Thin Films with High Mobility from Electrochemically Generated Aqueous Nanocluster Inks. *Chem. Mater.* **2015**, *27*, 5587–5596.

(35) Mansergh, R. H.; Fullmer, L. B.; Park, D. H.; Nyman, M.; Keszler, D. A. Reaction Pathway: Aqueous Hexatantalate Clusters to High-Density Tantalum Oxide Nanofilms. *Chem. Mater.* **2016**, *28*, 1553–1558.

(36) Fullmer, L. B.; Mansergh, R. H.; Zakharov, L. N.; Keszler, D. A.; Nyman, M. Nb_2O_5 and Ta_2O_5 Thin Films from Polyoxometalate Precursors: A Single Proton

Makes a Difference. *Cryst. Growth Des.* **2015**, *15*, 3885–3892.

(37) Hwang, Y. H.; Jeon, J.-H.; Bae, B.-S. Post-Humid Annealing of Low-Temperature Solution-Processed Indium Based Metal Oxide TFTs. *Electrochem. Solid-State Lett.* **2011**, *14*, H303–H305.

(38) Park, W.-T.; Son, I.; Park, H.-W.; Chung, K.-B.; Xu, Y.; Lee, T.; Noh, Y.-Y. Facile Routes To Improve Performance of Solution-Processed Amorphous Metal Oxide Thin Film Transistors by Water Vapor Annealing. *ACS Appl. Mater. Interfaces* **2015**, *7*, 13289–13294.

(39) Arii, T.; Kishi, A. The Effect of Humidity on Thermal Process of Zinc Acetate. *Thermochim. Acta* **2003**, *400*, 175–185.

(40) Arii, T.; Kishi, A. Humidity Controlled Thermal Analysis. The Effect of Humidity on Thermal Decomposition of Zinc Acetylacetonate Monohydrate. *J. Therm. Anal. Calorim.* **2006**, *83*, 253–260.

(41) Mauger, S. A.; Steirer, K. X.; Boé, J.; Ostrowski, D. P.; Olson, D. C.; Hammond, S. R. Effects of Humidity During Formation of Zinc Oxide Electron Contact Layers from a Diethylzinc Precursor Solution. *Org. Electron.* **2016**, *31*, 63–70.

(42) Cong, C.; Li, K.; Zhang, X. X.; Yu, T. Visualization of Arrangements of Carbon Atoms in Graphene Layers by Raman Mapping and Atomic-Resolution TEM. *Sci. Rep.* **2013**, *3*, 1195.

(43) Kim, K. H.; Akase, Z.; Suzuki, T.; Shindo, D. Charging Effects on SEM/SIM Contrast of Metal/Insulator System in Various Metallic Coating Conditions. *Mater. Trans.* **2010**, *51*, 1080–1083.

(44) Sze, Y.-K.; Irish, D. E. Vibrational Spectral Studies of Ion-Ion and Ion-Solvent Interactions. I. Zinc Nitrate in Water. *J. Solution Chem.* **1978**, *7*, 395–415.

(45) Xu, W.; Wang, H.; Xie, F.; Chen, J.; Cao, H.; Xu, J.-B. Facile and Environmentally Friendly Solution-Processed Aluminum Oxide Dielectric for Low-Temperature, High-Performance Oxide Thin-Film Transistors. *ACS Appl. Mater. Interfaces* **2015**, *7*, 5803–5810.

(46) Al-Abadleh, H. A.; Grassian, V. H. FT-IR Study of Water Adsorption on Aluminum Oxide Surfaces. *Langmuir* **2003**, *19*, 341–347.

(47) Nyquist, R. A.; Putzig, C. L.; Leugers, M. A.; Kagel, R. O. *The Handbook of Infrared and Raman Spectra of Inorganic Compounds and Organic Salts*; Academic Press: San Diego, CA, USA, **1997**.

(48) Klingenberg, B.; Vannice, M. A. Influence of Pretreatment on Lanthanum Nitrate,

Carbonate, and Oxide Powders. *Chem. Mater.* **1996**, *8*, 2755–2768.

(49) Małecki, A.; Małecka, B. Formation of N_2O During Thermal Decomposition of D-Metal Hydrates Nitrates. *Thermochim. Acta* **2006**, *446*, 113–116.

(50) Zhang, X.; He, H.; Gao, H.; Yu, Y. Experimental and Theoretical Studies of Surface Nitrate Species on Ag/Al_2O_3 Using DRIFTS and DFT. *Spectrochim. Acta - Part A Mol. Biomol. Spectrosc.* **2008**, *71*, 1446–1451.

(51) Norelli, K. M.; Plassmeyer, P. N.; Woods, K. N.; Glassy, B. A.; Knutson, C. C.; Beekman, M.; Page, C. J. Influence of Composition and Processing Parameters on the Properties of Solution-Processed Aluminum Phosphate Oxide (AlPO) Thin Tilms. *Solid State Sci.* **2016**, *55*, 8–12.

Chapter V

(1) Thomas, S. R.; Pattanasattayavong, P.; Anthopoulos, T. D. Solution-Processable Metal Oxide Semiconductors for Thin-Film Transistor Applications. *Chem. Soc. Rev.* **2013**, *42* (16), 6910–6923.

(2) Rim, Y. S.; Lim, H. S.; Kim, H. J. Low-Temperature Metal-Oxide Thin-Film Transistors Formed by Directly Photopatternable and Combustible Solution Synthesis. *ACS Appl. Mater. Interfaces* **2013**, *5* (9), 3565–3571.

(3) Park, J. S.; Maeng, W.-J.; Kim, H.-S.; Park, J.-S. Review of Recent Developments in Amorphous Oxide Semiconductor Thin-Film Transistor Devices. *Thin Solid Films* **2012**, *520* (6), 1679–1693.

(4) Bhuiyan, M. S.; Paranthaman, M.; Salama, K. Solution-Derived Textured Oxide Thin Films—a Review. *Supercond. Sci. Technol.* **2009**, *22*, 049801–049801.

(5) Ahn, B. Du; Jeon, H.; Sheng, J.; Park, J.; Park, J.-S. A Review on the Recent Developments of Solution Processes for Oxide Thin Film Transistors. *Semicond. Sci. Technol.* **2015**, *30* (6), 64001.

(6) Amri, A.; Jiang, Z. T.; Pryor, T.; Yin, C. Y.; Djordjevic, S. Developments in the Synthesis of Flat Plate Solar Selective Absorber Materials via Sol-Gel Methods: A Review. *Renew. Sustain. Energy Rev.* **2014**, *36*, 316–328.

(7) Banger, K. K.; Yamashita, Y.; Mori, K.; Peterson, R. L.; Leedham, T.; Rickard, J.; Sirringhaus, H. Low-Temperature, High-Performance Solution-Processed Metal Oxide Thin-Film Transistors Formed by a “sol–gel on Chip” Process. *Nat. Mater.* **2011**, *10* (1), 45–50.

(8) Fu, Q.; Chen, J.; Shi, C.; Ma, D. Room-Temperature Sol-Gel Derived Molybdenum Oxide Thin Films for Efficient and Stable Solution-Processed Organic Light-Emitting Diodes. *ACS Appl. Mater. Interfaces* **2013**, *5*, 6024–6029.

(9) Sugahara, T.; Hirose, Y.; Cong, S.; Koga, H.; Jiu, J.; Nogi, M.; Nagao, S.; Suganuma, K. Sol-Gel-Derived High-Performance Stacked Transparent Conductive Oxide Thin Films. *J. Am. Ceram. Soc.* **2014**, *97* (10), 3238–3243.

(10) Jeong, S.; Moon, J. Low-Temperature, Solution-Processed Metal Oxide Thin Film Transistors. *J. Mater. Chem.* **2012**, *22* (4), 1243–1250.

(11) Revenant, C.; Benwadih, M. Morphology of Sol-Gel Porous In-Ga-Zn-O Thin Films as a Function of Annealing Temperatures. *Thin Solid Films* **2016**, *616*, 643–648.

(12) Kim, M.-G.; Kanatzidis, M. G.; Facchetti, A.; Marks, T. J. Low-Temperature Fabrication of High-Performance Metal Oxide Thin-Film Electronics via Combustion Processing SI. *Nat. Mater.* **2011**, *10* (5), 382–388.

(13) Ko, J.; Kim, J.; Park, S. Y.; Lee, E.; Kim, K.; Lim, K.-H.; Kim, Y. S. Solution-Processed Amorphous Hafnium-Lanthanum Oxide Gate Insulator for Oxide Thin-Film Transistors. *J. Mater. Chem. C* **2014**, *2* (6), 1050.

(14) Street, R. A.; Ng, T. N.; Lujan, R. A.; Son, I.; Smith, M.; Kim, S.; Lee, T.; Moon, Y.; Cho, S. Sol − Gel Solution-Deposited InGaZnO Thin Film Transistors. **2014**.

(15) Jiang, K.; Anderson, J. T.; Hoshino, K.; Li, D.; Wager, J. F.; Keszler, D. A. Low-Energy Path to Dense HfO_2 Thin Films with Aqueous Precursor. *Chem. Mater.* **2011**, *23* (4), 945–952.

(16) Meyers, S. T.; Anderson, J. T.; Hong, D.; Hung, C. M.; Wager, J. F.; Keszler, D. A. Solution-Processed Aluminum Oxide Phosphate Thin-Film Dielectrics. *Chem. Mater.* **2007**, *19* (16), 4023–4029.

(17) Plassmeyer, P. N.; Archila, K.; Wager, J. F.; Page, C. J. Lanthanum Aluminum Oxide Thin-Film Dielectrics from Aqueous Solution. *ACS Appl. Mater. Interfaces* **2015**, *7* (3), 1678–1684.

(18) Esro, M.; Vourlias, G.; Somerton, C.; Milne, W. I.; Adamopoulos, G. High-Mobility ZnO Thin Film Transistors Based on Solution-Processed Hafnium Oxide Gate Dielectrics. *Adv. Funct. Mater.* **2015**, *25* (1), 134–141.

(19) Kast, M. G.; Enman, L. J.; Gurnon, N. J.; Nadarajah, A.; Boettcher, S. W. Solution-Deposited F : SnO_2/TiO_2 as a Base Stable Protective Layer and Anti-Reflective Coating for Micro-Textured Buried-Junction H_2 -Evolving Si Photocathodes. *ACS Appl. Mater. Interfaces* **2014**, *6*, 22830–22837.

(20) Mansergh, R. H.; Fullmer, L. B.; Park, D. H.; Nyman, M.; Keszler, D. A. Reaction Pathway: Aqueous Hexatantalate Clusters to High-Density Tantalum Oxide Nanofilms. *Chem. Mater.* **2016**, *28* (5), 1553–1558.

(21) Norelli, K. M.; Plassmeyer, P. N.; Woods, K. N.; Glassy, B. A.; Knutson, C. C.; Beekman, M.; Page, C. J. Influence of Composition and Processing Parameters on the Properties of Solution-Processed Aluminum Phosphate Oxide (AlPO) Thin Films. *Solid State Sci.* **2016**, *55*, 8–12.

(22) Fuh, C. S.; Sze, S. M.; Liu, P. T.; Teng, L. F.; Chou, Y. T. Role of Environmental and Annealing Conditions on the Passivation-Free in-Ga-Zn-O TFT. *Thin Solid Films* **2011**, *520* (5), 1489–1494.

(23) Perkins, C. K.; Mansergh, R. H.; Park, D.-H.; Nanayakkara, C. E.; Ramos, J. C.; Decker, S. R.; Huang, Y.; Chabal, Y. J.; Keszler, D. A. Aqueous Process to Limit Hydration of Thin-Film Inorganic Oxides. *Solid State Sci.* **2016**, *61*, 106–110.

(24) James, D.; Fourré, E.; Ishii, M.; Bowker, M. Catalytic Decomposition/regeneration of $Pt/Ba(NO_3)_2$ Catalysts: NO_x Storage and Reduction. *Appl. Catal. B Environ.* **2003**, *45* (2), 147–159.

(25) Rim, Y. S.; Chen, H.; Song, T. Bin; Bae, S. H.; Yang, Y. Hexaaqua Metal Complexes for Low-Temperature Formation of Fully Metal Oxide Thin-Film Transistors. *Chem. Mater.* **2015**, *27* (16), 5808–5812.

(26) Kanno, H.; Hiraishi, J. Raman Study of Aqueous Rare-Earth Nitrate Solutions in Liquid and Glassy States. *J. Phys. Chem.* **1984**, *88* (13), 2787–2792.

(27) Klingenberg, B.; Vannice, M. A. Influence of Pretreatment on Lanthanum Nitrate, Carbonate, and Oxide Powders. *Chem. Mater.* **1996**, *8* (12), 2755–2768.

(28) Knoeckl, J. . Vibrational Spectrometric and Electrochemical Lanthanum (Lll) = Nitrate Complexes in Aqueous. *Anal. Chem.* **1969**, *41* (14), 2069–2071.